

CERN-PH-EP-2012-210

Submitted to: JHEP

Search for dark matter candidates and large extra dimensions in events with a jet and missing transverse momentum with the ATLAS detector

The ATLAS Collaboration

Abstract

A search for new phenomena in events with a high-energy jet and large missing transverse momentum is performed using data from proton-proton collisions at $\sqrt{s} = 7$ TeV with the ATLAS experiment at the Large Hadron Collider. Four kinematic regions are explored using a dataset corresponding to an integrated luminosity of 4.7 fb^{-1} . No excess of events beyond expectations from Standard Model processes is observed, and limits are set on large extra dimensions and the pair production of dark matter particles.

Search for dark matter candidates and large extra dimensions in events with a jet and missing transverse momentum with the ATLAS detector

The ATLAS Collaboration



E-mail: Atlas.Publications@cern.ch

ABSTRACT: A search for new phenomena in events with a high-energy jet and large missing transverse momentum is performed using data from proton-proton collisions at $\sqrt{s} = 7$ TeV with the ATLAS experiment at the Large Hadron Collider. Four kinematic regions are explored using a dataset corresponding to an integrated luminosity of 4.7 fb^{-1} . No excess of events beyond expectations from Standard Model processes is observed, and limits are set on large extra dimensions and the pair production of dark matter particles.

KEYWORDS: Hadron-Hadron Scattering

Contents

1	Introduction	2
2	Data and simulated samples	4
3	Analysis strategy and physics object reconstruction	6
4	Event selection	8
5	Background estimation	9
5.1	Backgrounds from Z/W +jets	10
5.2	Multijet backgrounds	14
5.3	Non-collision backgrounds	15
5.4	Systematic uncertainties on background estimates	15
5.5	Background summary and additional checks	16
6	Results and interpretation	19
6.1	Large extra dimensions	21
6.2	WIMP pair production	23
7	Summary	30
8	Acknowledgements	31

1 Introduction

Event topologies with a single jet with large transverse energy and large missing transverse momentum, referred to as *monojets* in the following, are important final states for searches for new phenomena beyond the Standard Model (SM) at a hadron collider. The primary SM process that results in a true monojet final state is Z -boson production in association with a jet, where the Z boson decays to two neutrinos. A further important reducible contribution to this final state consists of events that include a W boson and a jet, where the charged lepton from the W -boson decay is not reconstructed.

Phenomenological scenarios beyond the Standard Model (BSM) that result in a monojet final state include supersymmetry [1–11] and large extra dimensions (LED) [12]. A model-independent treatment of the production of dark matter (DM) particles at the Large Hadron Collider (LHC) has been proposed recently, where DM particles are pair-produced in association with a jet [13–15]. In the following, a search for an excess of monojet events over SM expectations is performed. The results are interpreted in a framework of LED and DM particle pair production. They are based on a dataset of 4.7 fb^{-1} of proton-proton (pp) collisions at $\sqrt{s} = 7 \text{ TeV}$ recorded with ATLAS at the LHC and supersede those presented in the 2010 ATLAS monojet analysis that used 35 pb^{-1} of data [16]. Other monojet searches were performed in Run I and Run II at the Tevatron [17–19] and also by CMS with the 2010 [20] and 2011 [21] LHC datasets. None of these found evidence of new phenomena beyond the Standard Model.

Models of large extra spatial dimensions have been proposed to remove the hierarchy problem [22–25] by addressing the weakness of gravity relative to all other forces. One popular model of LED that is often used to interpret the results of monojet searches at particle colliders is that of Arkani-Hamed, Dimopoulos, Dvali (ADD) [12]. In this model, gravity propagates in the $(4 + n)$ -dimensional bulk of space-time, while the SM fields are confined to four dimensions. The large observed difference between the characteristic mass scale of gravity (the Planck mass) and the electroweak scale (as characterised by the W -boson mass) is the result of the four-dimensional interpretation of the Planck scale, $M_{\text{Pl}} = 1.2 \times 10^{19} \text{ GeV}$, which is related to the fundamental $(4 + n)$ -dimensional Planck scale (M_{D}) by $M_{\text{Pl}}^2 = 8\pi M_{\text{D}}^{2+n} R^n$, where n and R are the number and size of the extra dimensions, respectively. An appropriate choice of R for a given n results in a value of M_{D} close to the electroweak scale. The extra spatial dimensions are compactified, resulting in a Kaluza-Klein tower of massive graviton modes. At hadron colliders, these graviton modes can be produced in association with a jet. The production processes include $qg \rightarrow qG$, $gg \rightarrow gG$, and $q\bar{q} \rightarrow gG$, where G stands for the tower of gravitons, q for a quark, and g for a gluon. As gravitons do not interact with the detector, these processes give rise to a monojet signature [26].

Particle dark matter is a well-established paradigm to explain a range of astrophysical measurements (see for example ref. [27] for a recent review). Since none of the known SM particles are adequate DM candidates, the existence of a new particle is hypothesised, with properties suitable to explain the astrophysical measurements. One class of particle candidates of interest for searches at the LHC consists of weakly interacting massive

particles (WIMPs) [28]. These are expected to couple to SM particles through a generic weak interaction, which could be the known weak interaction of the SM or a new type of interaction. Such a new particle is a cold dark matter candidate, which can be produced at the LHC. It results in the correct relic density values for non-relativistic matter in the early universe [29], as measured by the WMAP satellite [30], if its mass lies in the range between a few GeV and a TeV and if it has electroweak-scale interaction cross sections. The fact that a new particle with such properties can be a thermal relic of the early universe in accordance with the WMAP measurements is often referred to as the WIMP miracle. Many new particle physics models designed to solve the hierarchy problem also predict WIMPs.

Because WIMPs do not interact with the detector material, their production leads to signatures with missing transverse momentum ($\mathbf{p}_T^{\text{miss}}$)¹, the magnitude of which is called E_T^{miss} . Searches involving E_T^{miss} at the LHC are therefore canonical WIMP searches, although the LHC experiments cannot establish whether a WIMP candidate is stable on cosmological time scales and hence a DM candidate. In some supersymmetric models, WIMPs are expected to be dominantly produced in cascade decays of heavier unstable supersymmetric particles along with high transverse momentum ($p_T = |\mathbf{p}_T|$) SM particles. In a more model-independent approach, WIMP pair production at colliders is proposed to yield detectable E_T^{miss} if the WIMP pair is tagged by a jet or photon from initial- or final-state radiation (ISR/FSR) [13, 31]. Even though this approach does not rely on a specific BSM scenario, it does have assumptions: WIMPs are pair-produced at the LHC and all new particles mediating the interaction between WIMPs and the SM are too heavy to be produced directly; they can thus be integrated out in an effective field theory approach. The resulting interaction is hence a contact interaction between the dark sector and the SM. It is worth noting that the DM particles are not explicitly assumed to interact via the weak force. They may also couple to the SM via a new force. Throughout this work, the terms WIMP and DM particle (candidate) are synonymous.

Name	Initial state	Type	Operator
D1	qq	scalar	$\frac{m_q}{M_*^3} \bar{\chi} \chi \bar{q} q$
D5	qq	vector	$\frac{1}{M_*^2} \bar{\chi} \gamma^\mu \chi \bar{q} \gamma_\mu q$
D8	qq	axial-vector	$\frac{1}{M_*^2} \bar{\chi} \gamma^\mu \gamma^5 \chi \bar{q} \gamma_\mu \gamma^5 q$
D9	qq	tensor	$\frac{1}{M_*^2} \bar{\chi} \sigma^{\mu\nu} \chi \bar{q} \sigma_{\mu\nu} q$
D11	gg	scalar	$\frac{1}{4M_*^3} \bar{\chi} \chi \alpha_s (G_{\mu\nu}^a)^2$

Table 1. Effective interactions coupling Dirac fermion WIMPs to Standard Model quarks or gluons, following the formalism of ref. [32]. The tensor operator D9 describes a magnetic-moment coupling. The factor of the strong coupling constant α_s in the definition of D11 accounts for this operator being induced at one-loop level. $G_{\mu\nu}$ is the colour field-strength tensor.

¹Letters in bold font are used for vector quantities.

It is assumed here that the DM particle is a Dirac fermion χ , where the only difference for Majorana fermions would be that certain interaction types are not allowed and that the cross section for each operator is larger by a factor of four. Five interactions are considered (table 1), namely D1, D5, D8, D9, D11, following the naming scheme of ref. [32]. D1, D5, D8, and D9 describe different bilinear quark couplings to WIMPs, $qq \rightarrow \chi\chi$, and D11 describes the process $gg \rightarrow \chi\chi$. The 14 operators for Dirac fermions in ref. [32] fall into four categories with characteristic $E_{\text{T}}^{\text{miss}}$ spectral shapes. D1, D5, D9, and D11 are a representative set of operators for these four categories, while D8 falls into the same category as D5 but is listed explicitly in table 1 because it is often used to convert LHC limits into limits on DM pair production. In the operator definitions in table 1, M_* is the suppression scale of the heavy mediator particles that are integrated out. The use of a contact interaction to produce WIMP pairs via heavy mediators is considered conservative because it rarely overestimates cross sections when applied to a specific BSM scenario. Cases where this approach is indeed optimistic are studied in refs. [15, 33]. The effective theory provides a useful framework for comparing LHC results to direct or indirect dark matter searches. Within this framework, interactions of SM and DM particles are described by only two parameters, the suppression scale M_* and the DM particle mass m_χ .

2 Data and simulated samples

The ATLAS detector [34, 35] at the LHC covers the pseudorapidity² range of $|\eta| < 4.9$ and all of ϕ . It consists of an inner tracking detector surrounded by a thin superconducting solenoid, electromagnetic and hadronic calorimeters, and an external muon spectrometer incorporating large superconducting toroidal magnets. A three-level trigger system is used to select interesting events for recording and subsequent offline analysis. Only data for which all subsystems described above were operational are used. Applying these requirements to pp collision data, taken at a centre-of-mass energy of $\sqrt{s} = 7$ TeV with stable beam conditions during the 2011 LHC run, results in a data sample with a time-integrated luminosity of 4.7 fb^{-1} , determined with an uncertainty of 3.9% [36, 37].

Monte Carlo (MC) simulations are used both as part of the background estimation and to model signal processes. Processes that dominate the background are Z - or W -boson production in association with jets, which are simulated with ALPGEN [38] using the parton distribution function (PDF) set CTEQ6L1 [39]. The $W \rightarrow \ell\nu$ plus jets and $Z \rightarrow \nu\bar{\nu}$ plus jets samples are simulated with up to six additional partons at leading order, while the process $Z/\gamma^* \rightarrow \ell^+\ell^-$ plus jets is simulated with up to five additional partons at leading order. Additional jets are generated via parton showering, which, together with fragmentation and hadronisation, is performed by HERWIG [40, 41]. The MLM [42] prescription is used for matching the matrix-element calculations to the parton shower

²ATLAS uses a right-handed coordinate system with its origin at the nominal interaction point (IP) in the centre of the detector and the z -axis along the beam pipe. The x -axis points from the IP to the centre of the LHC ring, and the y -axis points upward. Polar coordinates (r, ϕ) are used in the transverse (x, y) -plane, ϕ being the azimuthal angle around the beam pipe. The pseudorapidity is defined in terms of the polar angle θ as $\eta = -\ln \tan(\theta/2)$.

Process	Generator	Parton shower	Underlying event	PDF
Z/W +jets	ALPGEN	HERWIG	JIMMY	CTEQ6L1
$t\bar{t}$, single t	MC@NLO	HERWIG	JIMMY	CTEQ6.6
Di-boson	SHERPA	SHERPA	SHERPA	CTEQ6L1
ADD	PYTHIA	PYTHIA	PYTHIA	MSTW2008 LO** / CTEQ6.6
WIMPs	MADGRAPH5	PYTHIA	PYTHIA	CTEQ6L1

Table 2. Overview of the main simulated samples.

evolution. JIMMY [43] is used to simulate the underlying event. Additional Z/W plus jets samples generated with SHERPA [44] are used to estimate the uncertainties related to the event generator. Single top quark and pair production are simulated with MC@NLO [45], fixing the top-quark mass to 172.5 GeV, and using the next-to-leading-order (NLO) PDF set CTEQ6.6 [46]. Parton showering and hadronisation are performed with HERWIG, and JIMMY is again used for the underlying event. Di-boson (WW , WZ , ZZ) samples are generated with SHERPA. Backgrounds from QCD multijet production are estimated from data (see section 5.2). PYTHIA [47] simulations of this process, normalised to data, are used in figures for illustrative purposes only.

For graviton production in the ADD model, a low-energy effective field theory [26] with energy scale M_D is used to calculate the signal cross section considering the contribution of different graviton mass modes. Signal samples corresponding to a number of extra dimensions varying between two and six are considered, with the renormalisation and factorisation scales set per event to $\sqrt{\frac{1}{2}M_G^2 + p_T^2}$, where M_G is the mass of the graviton mode produced in the event and p_T denotes the transverse momentum of the recoiling parton. The samples are produced with an ADD implementation as a user model of PYTHIA, which is also used for parton showering and hadronisation. MSTW2008 LO** [48] PDF sets are used for the event simulation. The event yields for CTEQ6.6 PDFs are obtained by re-weighting these samples, and are used to estimate cross sections, as well as PDF systematic uncertainties. ADD cross sections are calculated at both leading order (LO) and NLO. The NLO calculations take into account QCD corrections to graviton production and have been produced for the kinematic regions explored here following ref. [49].

The effective field theory of WIMP pair production is implemented in MADGRAPH5 [50] (version 1.3.33), taken from ref. [32]. WIMP pair production plus one and two additional partons from ISR/FSR is simulated requiring at least one parton with a minimum transverse momentum of 80 GeV. Only initial states of gluons and the four lightest quarks are considered, assuming equal coupling strengths for all quark flavours to the WIMPs. The mass of charm quarks is most relevant for the cross sections of the operator D1 (see table 1) and it is set to 1.42 GeV. The generated events are interfaced to PYTHIA for parton showering and hadronisation. The MLM prescription is used for matching the matrix-element calculations of MADGRAPH5 to the parton shower evolution of PYTHIA. The CTEQ6L1 PDF set is used for the event simulation. The MADGRAPH5 default choice for the renormalisation and factorisation scales is used. The scales are set to the sum of $\sqrt{m^2 + p_T^2}$ for all pro-

duced particles, where m is the mass of particles. Events with WIMP masses between 10 and 1300 GeV are simulated for four different effective operators (D1, D5, D9, D11). In all cases, WIMPs are taken to be Dirac fermions, and the pair-production cross section is calculated at LO.

The background MC samples use a detector simulation [51] based on GEANT4 [52] and are reconstructed with the same algorithms as the data. The signal MC samples employ a mix of the detailed GEANT4 detector simulation and a simulation relying on parametrisations of calorimetric signals to shorten the CPU time required (ATLFAST-II [51]). Individual signal MC samples have been validated against the more detailed detector simulation relying fully on GEANT4. Effects of *event pile-up*—multiple pp interactions occurring in the same or neighbouring crossing of two proton bunches, called *pile-up* from now on—are included in the simulation. MC events are re-weighted to reproduce the distribution of the number of collisions per bunch crossing observed in the data.

3 Analysis strategy and physics object reconstruction

A search for a BSM excess is performed in monojet final states. Leptons are vetoed to suppress background contributions from Z/W plus jets. A second jet is allowed as long as it is not aligned with E_T^{miss} , which would be the case in multijet background events with a mis-measured jet. Events with more than two jets are vetoed.

These selection requirements define the basic *signal region* (SR), defined in detail in table 3 below. The data sample consisting of events passing the SR selections is sub-divided into overlapping kinematic regions by applying selection criteria on E_T^{miss} and p_T^{jet1} , the transverse momentum of the most energetic jet (leading jet) in the event. Events in these overlapping individual signal regions are then used to search for a BSM excess above the predicted SM backgrounds.

The main SM background contributions to the SR data samples are from Z/W +jets production and they are estimated from data by selecting events based on a set of selection requirements—orthogonal to those of the signal regions—that define a *control region* (CR). These CR requirements are based on selecting events with leptons (either exactly one or two leptons). Different physics processes are used to estimate background contributions to a SR: $W \rightarrow e\nu$ +jets, $W \rightarrow \mu\nu$ +jets, $Z \rightarrow e^+e^-$ +jets, and $Z \rightarrow \mu^+\mu^-$ +jets. To obtain data samples enriched by these processes, a set of selection criteria defines corresponding CR’s. Each set of CR requirements is further sub-divided into the same kinematic categories as the signal regions.

This analysis is based on reconstructed jets, electrons, muons, and E_T^{miss} . The definitions of electron and muon candidates and of E_T^{miss} are different in the SR and CR requirements. All electron candidates are required to have $p_T > 20$ GeV and $|\eta| < 2.47$, in order to be within the acceptance of the tracking system. For the signal-region requirements, which comprise an electron veto, relatively loose criteria are used to define an electron candidate (*SR-electron*), because a looser electron definition leads to a more stringent veto. SR-electrons are required to pass the *medium* electron shower shape and track selection criteria described in ref. [56]. No spatial isolation is required. For the control-region selection

requirements, used for background estimates from events with measured electrons, more stringent electron selection criteria (defining the *CR-electron*) are used in case exactly one electron is selected. This is to better suppress jet contamination in these control regions. A CR-electron is required to pass the *tight* [56] electron shower shape and track selection criteria in $W \rightarrow e\nu$ control regions. In addition, the following isolation criterion is imposed for CR-electrons to suppress events where a jet is mis-identified as an electron: the scalar sum of the transverse momentum of tracks with $\Delta R \equiv \sqrt{(\Delta\phi)^2 + (\Delta\eta)^2} < 0.2$ around the electron candidate, excluding the electron itself, has to be less than 10% of the electron's transverse energy (E_T). In control regions where exactly two electrons are required, the looser SR-electron definition without isolation requirements is used.

A muon candidate used in the definition of the signal regions (*SR-muon*) is reconstructed either by associating a stand-alone muon spectrometer track with an inner detector track, or from an inner detector track that is confirmed by a directional segment in the muon spectrometer [57]. SR-muons, which are used as veto in signal-region selections, are required to have $p_T > 7$ GeV and $|\eta| < 2.5$. They are also required to be isolated: the scalar p_T sum of tracks within $\Delta R = 0.2$ around the muon track, excluding the muon itself, must be less than 1.8 GeV. As for electrons, the muon selection criteria in control-region definitions are more stringent. A *CR-muon* candidate must have a stand-alone muon spectrometer track associated with an inner detector track. Those SR-muons that have only an inner detector track tagged by a segment in the muon spectrometer do not satisfy the CR selection criteria. Furthermore, CR-muons satisfy $p_T > 20$ GeV and $|\eta| < 2.4$, and have an impact parameter along z with respect to the reconstructed primary vertex of $|z_0| < 10$ mm to reject cosmic-ray muons. The CR-muons are also required to be isolated: the scalar p_T sum of tracks within $\Delta R = 0.2$ around the muon track, excluding the muon itself, must be less than 10% of the muon p_T .

In the signal regions, the measurement of E_T^{miss} is performed using all clusters of energy deposits in the calorimeter up to $|\eta|$ of 4.5. The calibration of these clusters takes into account the different response of the calorimeters to hadrons compared to electrons or photons, as well as dead material and out-of-cluster energy losses [58, 59]. In the control regions, two additional definitions of E_T^{miss} are used to account for the different treatment in the signal and control regions of electrons and muons. This is because the calorimetric definition of the nominal E_T^{miss} takes into account energy deposits of electrons whereas it does not account for transverse momentum carried away by muons. The two additional definitions of E_T^{miss} either exclude the electron contributions to the missing transverse momentum in events with electrons or include the muon contributions to the missing transverse momentum in events with muons:

- $E_T^{\text{miss},\cancel{e}}$: for control regions that involve electrons ($W \rightarrow e\nu + \text{jets}$, $Z \rightarrow e^+e^- + \text{jets}$, explained in more detail below), $E_T^{\text{miss},\cancel{e}}$ is obtained by adding the electron clusters to the missing transverse momentum vector thereby removing the electron contribution to the calculation of E_T^{miss} : $E_T^{\text{miss},\cancel{e}} = |\mathbf{p}_T^{\text{miss}} + \mathbf{p}_T^{\text{electrons}}|$. This yields missing transverse momentum which, as in invisible Z decays, does not take into account the decay products of the Z boson.

- $E_T^{\text{miss},\mu}$: the second alternative version of E_T^{miss} takes into account the muon contribution to E_T^{miss} and it is used in the exclusive $W \rightarrow \mu\nu + \text{jets}$ control regions. It is defined as the negative sum of the calorimeter-based $\mathbf{p}_T^{\text{miss}}$ and the transverse momentum of muons, which do not deposit much energy in the calorimeters: $E_T^{\text{miss},\mu} = |\mathbf{p}_T^{\text{miss}} - \mathbf{p}_T^{\text{muons}}|$.

With these three versions of missing transverse momentum, the kinematics of invisible $Z \rightarrow \nu\bar{\nu}$ decays can be mimicked in Z or W events with measured muons (E_T^{miss}) or electrons ($E_T^{\text{miss},e}$). On the other hand, for the selection of such control samples enriched with Z or W events, the missing transverse momentum taking into account all visible decay products of Z or W bosons can be used in events with measured muons ($E_T^{\text{miss},\mu}$) or electrons (E_T^{miss}).

Jet candidates are reconstructed using the anti- k_t clustering algorithm [53] with a radius parameter of 0.4. The inputs to this algorithm are clusters of energy deposits in calorimeter cells seeded by those with energies significantly above the measured noise [54]. Jet momenta are calculated by performing a four-vector sum over these cell energy clusters, treating each cluster as an (E, \mathbf{p}) four-vector with zero mass. The direction of \mathbf{p} is given by the line joining the nominal interaction point with the calorimeter cluster. The resulting jet energies are corrected to the hadronic scale using p_T and η dependent calibration factors based on MC simulations and validated by extensive test beam and collision data studies [55].

4 Event selection

All data passing detector quality requirements are considered for the analysis. Events must be accepted by an inclusive E_T^{miss} trigger [60, 61] that is found to be 98% efficient for events with E_T^{miss} above 120 GeV, and more than 99% for E_T^{miss} above 150 GeV. At 120 GeV, a small residual dependence on pile-up of the E_T^{miss} trigger efficiency is found. Over the full 2011 dataset, where the pile-up varied from an average of 3 interactions per bunch crossing at the beginning of the year to 17 at the end of the year, an efficiency variation of 1.5% is observed and a correction is applied to account for this variation. For E_T^{miss} above 220 GeV, there is no measurable efficiency variation. Events are further required to satisfy a set of pre-selection and kinematic criteria that are aimed at selecting monojet events from good-quality pp collisions, as well as reducing electroweak, multijet, non-collision, and detector-induced backgrounds. These criteria require the event to have a monojet topology characterised by one unbalanced high- p_T jet resulting in large E_T^{miss} :

- A reconstructed primary vertex with at least two associated tracks (with $p_T > 0.4$ GeV) is required [62]. This ensures that the recorded event is consistent with a proton-proton collision rather than a noise event.
- The highest- p_T jet must have a charge fraction $f_{\text{ch}} = \sum p_T^{\text{track,jet}} / p_T^{\text{jet}} > 0.02$, where $\sum p_T^{\text{track,jet}}$ is the scalar sum of the transverse momenta of tracks associated with the primary vertex within a cone of radius $\Delta R = 0.4$ around the jet axis, and p_T^{jet} is

the transverse momentum of the jet as determined from calorimeter measurements. Furthermore, events are rejected if they contain any jet with an electromagnetic fraction f_{em} (fraction of the jet energy measured in the electromagnetic calorimeter) of less than 0.1, or any jet in the pseudorapidity range $|\eta| < 2$ with $f_{\text{em}} > 0.95$ and a charge fraction $f_{\text{ch}} \leq 0.05$. These requirements suppress jets produced by cosmic rays or beam-background muons that interact in the hadronic calorimeter without corresponding signals in the electromagnetic calorimeter or the tracking detector.

- Additional selection criteria to reject events with significant detector noise and non-collision backgrounds are applied: events are rejected if any jet with $p_{\text{T}} > 20$ GeV and $|\eta| < 4.5$ does not pass all of the additional quality criteria described in ref. [63].
- The leading jet has to be within $|\eta| < 2$, and no more than two jets with $p_{\text{T}} > 30$ GeV and $|\eta| < 4.5$ are allowed. Back-to-back dijet events are suppressed by requiring the sub-leading jet not to point in the direction of $\mathbf{p}_{\text{T}}^{\text{miss}}$: $|\Delta\phi(\mathbf{p}_{\text{T}}^{\text{miss}}, \mathbf{p}_{\text{T}}^{\text{jet}2})| > 0.5$.
- An electronics failure affecting 20% of the data sample created a small dead region in the second and third layers of the electromagnetic calorimeter. Any event with the two leading jets inside the affected region and either of the two jets pointing in the direction of $E_{\text{T}}^{\text{miss}}$ is removed from the sample to avoid fake signals. This condition removes only a few percent of the affected subset of the data.
- Events are required to have no SR-electron or SR-muon. In the background control regions, electrons and muons are explicitly selected. The electron and muon selection criteria in the signal and control regions are given in section 3.

Although the results of this analysis are interpreted in terms of the ADD model and WIMP pair production, the event selection criteria have not been tuned to maximise the sensitivity to any particular BSM scenario. To maintain sensitivity to a wide range of BSM models, four sets of overlapping kinematic selection criteria, designated as SR1 to SR4, differing in the values of the requirements for $E_{\text{T}}^{\text{miss}}$ and leading jet p_{T} , are defined (table 3). Note that the requirement on the leading jet p_{T} is the same as that on $E_{\text{T}}^{\text{miss}}$ for all signal regions. In comparison with the previous ATLAS monojet search [16], the veto on additional jets is less stringent, allowing a second jet in the event thereby reducing systematic uncertainties from ISR/FSR (see section 6) and increasing signal selection efficiencies. The signal region with the lowest $E_{\text{T}}^{\text{miss}}$ requirement (SR1) is chosen such that the $E_{\text{T}}^{\text{miss}}$ trigger is nearly 100% efficient. The signal region with the highest $E_{\text{T}}^{\text{miss}}$ requirement (SR4) is chosen so that there remain enough events in data control samples to validate MC predictions and estimate SR backgrounds in a data-driven way.

5 Background estimation

A number of SM processes can pass the monojet kinematic selection criteria described above. These backgrounds include, in decreasing order of importance: Z and W boson plus jets production, single or pair production of top quarks, multijet production, cosmic-ray

Signal regions	SR1	SR2	SR3	SR4
Common requirements	Data quality + trigger + vertex + jet quality + $ \eta^{\text{jet1}} < 2.0 + \Delta\phi(\mathbf{p}_T^{\text{miss}}, \mathbf{p}_T^{\text{jet2}}) > 0.5 + N_{\text{jets}} \leq 2 +$ lepton veto			
$E_T^{\text{miss}}, p_T^{\text{jet1}} >$	120 GeV	220 GeV	350 GeV	500 GeV

Table 3. Definition of the four overlapping signal regions SR1–SR4. *Data quality, trigger, vertex,* and *jet quality* refer to the selection criteria discussed in the main text.

and beam-background muons³ (collectively referred to as *non-collision background* [64]), and di-boson production (WW , WZ , ZZ). The dominant Z/W plus jets backgrounds are estimated using control regions in the data with corrections that account for differences between the selection requirements of the signal and control regions (see section 5.1). The multijet and non-collision backgrounds are also estimated from data (see sections 5.2 and 5.3, respectively) while the di-boson and top-quark backgrounds are obtained from MC simulations.

5.1 Backgrounds from Z/W +jets

The dominant background process for this search is irreducible and consists of the production of Z bosons in association with jets, where the Z decays to two neutrinos. A substantial source of reducible background is SM W boson plus jets production where the W decays to a charged lepton (τ , e , or μ in decreasing order of importance) and a neutrino. This process leads to a monojet final state if the lepton is outside the detector acceptance, is missed because of reconstruction inefficiencies or if a hadronic τ decay is reconstructed as a single jet. The Z and W boson plus jets backgrounds, collectively referred to in the following as *electroweak backgrounds*, are determined in a data-driven way:

1. Control regions are defined by explicitly selecting electrons or muons while keeping the same jet and E_T^{miss} selection criteria as in the signal regions. In a first step, samples enriched with four processes containing electrons or muons are separately selected with dedicated selection requirements: $W \rightarrow e\nu$ +jets, $W \rightarrow \mu\nu$ +jets, $Z \rightarrow e^+e^-$ +jets, $Z \rightarrow \mu^+\mu^-$ +jets. In a second step, the jet and E_T^{miss} selection criteria as in the signal regions are imposed. Corrections are made for contamination of these control samples from processes other than Z or W decays.
2. Correction factors are then applied to account for differences in trigger and kinematic selection criteria between the control and signal regions. The control-to-signal region transfer factors, which are multiplied by the number of control-region events obtained in the previous step to yield the background estimate, are obtained using both data and simulation (see below).

³Originating either from protons going in the direction of the experiment and hitting the LHC collimation system or gas molecules in the beam-pipe near the ATLAS interaction point.

SR process	$Z \rightarrow \nu\bar{\nu}+\text{jets}$	$W \rightarrow \tau\nu+\text{jets}$ $W \rightarrow \mu\nu+\text{jets}$	$W \rightarrow e\nu+\text{jets}$	$Z \rightarrow \tau^+\tau^-+\text{jets}$ $Z \rightarrow \mu^+\mu^-+\text{jets}$
CR process	$W \rightarrow e\nu+\text{jets}$ $W \rightarrow \mu\nu+\text{jets}$ $Z \rightarrow e^+e^-+\text{jets}$ $Z \rightarrow \mu^+\mu^-+\text{jets}$	$W \rightarrow \mu\nu+\text{jets}$	$W \rightarrow e\nu+\text{jets}$	$Z \rightarrow \mu^+\mu^-+\text{jets}$

Table 4. Overview of processes in the control regions (CR) used to estimate background contributions to processes in the signal regions (SR).

In this approach, the modelling of the jet and E_T^{miss} kinematics of the electroweak backgrounds is obtained directly from data. Simulations are therefore used only for quantities related to the electron and muon selection criteria, and only through ratios where systematic uncertainties related to the jet and E_T^{miss} selection criteria of the control regions cancel. Theoretical uncertainties normally associated with MC estimates are significantly reduced; only distributions related to the electron and muon selection criteria have to be well modelled in the simulations. Further experimental uncertainties that impact the background prediction, such as the jet energy scale (JES) and resolution (JER) [55], the trigger efficiency, and the luminosity measurement [36, 37], are minimised by this approach.

The control regions are expected to have no contamination from BSM signals that would normally pass the monojet event selection criteria. They are chosen such that they are dominated by Z and W decays with reconstructed electrons or muons. The selection criteria follow closely those used in Z and W cross-section measurements [65]. The kinematic selection criteria on E_T^{miss} and jet p_T of the signal regions are also applied. Therefore, each CR is split into four subsets corresponding to the four signal regions. Four visible decay modes are used for the background estimates: $W \rightarrow e\nu+\text{jets}$, $W \rightarrow \mu\nu+\text{jets}$, $Z \rightarrow e^+e^-+\text{jets}$, $Z \rightarrow \mu^+\mu^-+\text{jets}$. Based on these, all contributions to the signal regions from Z and W decay modes are estimated with the same method (except for $Z \rightarrow e^+e^-+\text{jets}$, which is found to be negligible in the signal regions because both e^+ and e^- would have to be missed in the event selection). In total, six background processes in each signal region are predicted based on four control region processes, as detailed in table 4. Note that the $W \rightarrow \tau\nu+\text{jets}$ background in the signal regions, where the τ lepton decays hadronically, can safely be estimated from $W \rightarrow \mu\nu+\text{jets}$ in control regions, since the jet and E_T^{miss} kinematics are the same. In both cases the leading jet is from radiation and recoils against the neutrino from the W decay. The hadronic τ decay results in a jet that is either below the jet threshold of 30 GeV or above this threshold but still sub-dominant compared to the leading jet from radiation.

For control regions that include processes with electrons, an electron trigger is used that requires a correction to account for differences in efficiency and acceptance compared to the E_T^{miss} trigger used for the signal regions.⁴ This different treatment is required because

⁴Note that the *acceptance* is defined as the ratio of the number of events within the detector volume that pass analysis requirements to the number of originally simulated events. The *efficiency* is defined as

the energy deposited by electrons is included in the E_T^{miss} measurement at trigger level and results in the selection of a different kinematic region than that of the signal regions, which exclude electrons. Muons, however, do not deposit large amounts of energy in the calorimeters and are not explicitly included in the E_T^{miss} trigger. The specific selection criteria for the four control region processes are given in the following:

- $W \rightarrow e\nu+\text{jets}$: Events are selected using electron triggers with thresholds of 20 or 22 GeV depending on the data-taking period. The CR-electron definition is used (see section 3) and exactly one electron with a p_T of at least 25 GeV is required. Events with additional electrons or muons are discarded. All triggers used are fully efficient above the chosen p_T cut value. If an object is reconstructed as both an electron and a jet, the jet is removed from the reconstructed jet collection if $\Delta R(e, \text{jet}) < 0.2$ while the electron is kept. To further improve the W purity, $E_T^{\text{miss}} > 25$ GeV and $40 < m_T < 100$ GeV are required. m_T is the transverse mass and it is defined as $m_T = \sqrt{2 p_T E_T^{\text{miss}} (1 - \cos \Delta\phi(\mathbf{p}_T^{\text{lepton}}, \mathbf{p}_T^{\text{miss}}))}$, using the p_T of the lepton (electron or muon). $\Delta\phi$ is the angle between the lepton and the missing transverse momentum vector. As mentioned earlier, the same selection criteria on jet p_T and E_T^{miss} are applied in the control regions as in the signal regions (see table 3). However, when the $W \rightarrow e\nu+\text{jets}$ CR is used to estimate the contribution of $Z \rightarrow \nu\bar{\nu}+\text{jets}$ to each SR, a special CR is defined where E_T^{miss} is substituted by $E_T^{\text{miss},\cancel{\ell}}$ to mimic the kinematics of the decay of the Z boson to two undetected neutrinos. The standard calorimeter-based E_T^{miss} is used for the CR to estimate the $W \rightarrow e\nu+\text{jets}$ contribution to the SRs.
- $W \rightarrow \mu\nu+\text{jets}$: Events have to pass the same inclusive E_T^{miss} trigger that is used for the signal regions. Exactly one CR-muon (see section 3) is required, and events with additional electrons or muons are rejected. Cuts on the transverse mass and missing transverse momentum are applied to improve the purity for W 's: $m_T > 40$ GeV, $E_T^{\text{miss},\mu} > 25$ GeV. Note that the E_T^{miss} that includes the muon contribution, $E_T^{\text{miss},\mu}$, is used for the W -specific selection cuts. For each kinematic region listed in table 3, the standard calorimeter-based E_T^{miss} is used to define the CRs for the estimates of both $Z \rightarrow \nu\bar{\nu}+\text{jets}$ and $W \rightarrow \mu\nu+\text{jets}$ in the corresponding SR.
- $Z \rightarrow e^+e^-+\text{jets}$: Electron triggers are used in this channel. Exactly two opposite-sign electrons are required and events with additional electrons or muons are discarded. The selected electrons have to satisfy $p_T > 25$ (20) GeV for the leading (sub-leading) electron. Jet-electron overlap removal is performed as described above for $W \rightarrow e\nu+\text{jets}$. Finally, to enhance the fraction of Z 's, an invariant mass requirement of $66 < m_{e^+e^-} < 116$ GeV is applied. $E_T^{\text{miss},\cancel{\ell}}$ is used to define these CRs, which are used to estimate the $Z \rightarrow \nu\bar{\nu}+\text{jets}$ contribution to the SRs.
- $Z \rightarrow \mu^+\mu^-+\text{jets}$: The inclusive E_T^{miss} trigger is used in this channel. Exactly two opposite-sign CR-muons (defined in section 3) are required and events with additional

the ratio of the number of events within the detector volume at reconstruction level to that at the original simulation level.

electrons or muons are rejected. An invariant mass of $66 < m_{\mu^+\mu^-} < 116$ GeV is required to select Z candidates. The signal-region selection criteria are then applied on the calorimeter-based E_T^{miss} , for the $Z \rightarrow \nu\bar{\nu}+\text{jets}$, $Z \rightarrow \tau^+\tau^-+\text{jets}$, $Z \rightarrow \mu^+\mu^-+\text{jets}$ estimates.

Using the control regions defined above, the background contribution to the signal regions for each combination of CR and SR processes mentioned in Table 4 is derived using:

$$N_{\text{SR}}^{\text{predicted}} = (N_{\text{CR}}^{\text{Data}} - N_{\text{CR}}^{\text{Bkg}}) \cdot C \cdot T =$$

$$\left((N_{\text{CR}}^{\text{Data}} - N_{\text{CR}}^{\text{multijet}}) \cdot (1 - f_{\text{EW}}) \right) \times \frac{\epsilon_{E_T^{\text{miss}}}^{\text{trig}} \cdot \mathcal{L}_{E_T^{\text{miss}}}}{A_\ell \cdot \epsilon_\ell \cdot \epsilon_{Z/W} \cdot \epsilon_\ell^{\text{trig}} \cdot \mathcal{L}_\ell} \times \frac{N_{\text{SR}}^{\text{MC}}}{N_{\text{jet}/E_T^{\text{miss}}}^{\text{MC}}}. \quad (5.1)$$

Data in the control regions are corrected for contamination arising from other sources (summarised as $N_{\text{CR}}^{\text{Bkg}}$ in the first line). Correction factors (C) based on MC simulation and data are applied together with the transfer factor T to obtain the number of background events, $N_{\text{SR}}^{\text{predicted}}$, predicted in the signal region. The terms appearing in the second line of equation 5.1 are:

- $N_{\text{CR}}^{\text{Data}}$ and $N_{\text{CR}}^{\text{multijet}}$ are the number of data and multijet events in the control region, respectively. To estimate the multijet contamination of control regions by processes with identified electrons, the selection cuts, in particular the isolation cuts, are varied. The fake rate in those regions is extracted from data using real and fake electron efficiencies determined from samples enriched in electrons and jets. Using this estimate, the multijet contamination is predicted to account for 1-2% of the events in the $W \rightarrow e\nu+\text{jets}$ electron control region when predicting the $Z \rightarrow \nu\bar{\nu}+\text{jets}$ contribution to the SRs. For other control regions containing electrons or muons, the multijet contamination is found to be negligible using similar techniques.
- f_{EW} is the estimated fraction of events, after multijet corrections, due to contamination of the control region by other electroweak or other SM processes. This contamination is due to top-quark and di-boson decays as well as decays of Z or W bosons to leptons of a flavour other than the one selected for that control region. The contribution of this contamination is obtained from MC simulation and is about 2% for Z bosons, and 10% for W bosons. The top-quark and di-boson contribution is negligible. As explained above, using ratios of MC estimates (f_{EW} in this case) is advantageous as it leads to cancellations of systematic uncertainties.
- A_ℓ and ϵ_ℓ are the lepton acceptance obtained from simulation and the identification efficiency obtained from data [56, 57], respectively.
- $\epsilon_{Z/W}$ are the efficiencies for the Z or W boson selection criteria obtained from simulation. The factors A_ℓ , ϵ_ℓ , and $\epsilon_{Z/W}$ correct for the fact that leptons and Z/W bosons are required only in the control regions.

- $\epsilon_\ell^{\text{trig}}$ and \mathcal{L}_ℓ are the electron trigger efficiency (obtained from data) and the corresponding luminosity associated with this trigger for the relevant control region. For muon control regions these factors do not apply because the signal-region trigger is used in the definition of the CR.
- $\epsilon_{E_T^{\text{miss}}}^{\text{trig}}$ and $\mathcal{L}_{E_T^{\text{miss}}}$ are the E_T^{miss} trigger efficiency (obtained from data) and the corresponding luminosity, and are only relevant for electron control regions where the electron trigger efficiency and luminosity ($\epsilon_\ell^{\text{trig}}$ and \mathcal{L}_ℓ) need to be corrected, accounting for the different triggers used in the definition of the signal and control regions.
- The transfer factor $T = \frac{N_{\text{SR}}^{\text{MC}}}{N_{\text{jet}/E_T^{\text{miss}}}^{\text{MC}}}$ is the ratio of simulated background events in the signal region (for example $Z \rightarrow \nu\bar{\nu} + \text{jets}$) to simulated events of a control-region process (for example $W \rightarrow e\nu + \text{jets}$) with only jet and E_T^{miss} related selection requirements applied. This term translates the number of observed events in the CR in the data to the predicted number of events in the signal region. Depending on the control region and the signal-region background component being determined, this factor can account for ratios of branching fractions, ratios of $W + \text{jets}$ to $Z + \text{jets}$ cross sections, and phase-space differences between the control and signal regions for a given source of background.

The correction factors and electroweak background predictions in equation 5.1 are determined in bins of E_T^{miss} for the final background prediction, and in bins of the leading and sub-leading jet p_T for the jet- p_T plots in figure 2.

5.2 Multijet backgrounds

Multijet events where one or more jets are severely mismeasured constitute a background that is not well modelled in the simulation. In order to measure this background from data, a sample is selected by applying all signal-region selection criteria except for the jet vetoes: A) either a second jet with $|\Delta\phi(\mathbf{p}_T^{\text{miss}}, \mathbf{p}_T^{\text{jet}2})| < 0.5$ is required, B) or the third-jet veto is reversed by requiring three jets, $N_{\text{jet}} = 3$, and missing transverse momentum to be aligned with the third jet: $|\Delta\phi(\mathbf{p}_T^{\text{miss}}, \mathbf{p}_T^{\text{jet}3})| < 0.5$ and $|\Delta\phi(\mathbf{p}_T^{\text{miss}}, \mathbf{p}_T^{\text{jet}2})| > 0.5$. These two samples are used to predict the multijet background from the resulting di- or trijet events. Contributions to these event samples from top-quark, and Z or W production are subtracted. The MC simulation is used for the top-quark contribution. For Z and W , MC estimates normalised to data are used for the subtraction. The multijet background is then estimated by fitting a straight line to the second or third jet p_T distributions in events passing the two selection criteria (A) and B)) and then extrapolating the fit below a p_T of 30 GeV. For this value of the transverse momentum, the jets fall below the threshold and can pass the monojet selection criteria. Note that the number of trijet events where both sub-leading jets are mismeasured, and fall below the jet threshold, is negligible compared to the case where either the second or the third jet is lost. The resulting background estimates are given in table 6. They are at most 1% of the total background predicted for SR1–SR3, and are negligible for SR4.

5.3 Non-collision backgrounds

Non-collision backgrounds in the signal regions are estimated using a dedicated algorithm that identifies beam-background muons that go through the detector along the direction of the beams. The algorithm selects through-going muons based on timing information obtained from the muon chambers in the forward regions. It combines this information with calorimeter energy clusters by matching them in ϕ . Unpaired proton bunches, where the bunch from one of the proton beams is empty, are used to determine identification efficiencies of the algorithm for beam-background and cosmic-ray muons. These efficiencies ($\epsilon_{\text{tag}}^{\text{non-coll.}}$), typically 20–50%, are used together with the number of beam-background (*halo*) candidates found in the signal regions, to predict the level of non-collision background ($N_{\text{non-coll.}} = N_{\text{halo}}/\epsilon_{\text{tag}}^{\text{non-coll.}}$). More details of this background component are given in ref. [64]. It contributes mainly in SR1 and SR2 at less than 1%. The predictions are given in table 6.

5.4 Systematic uncertainties on background estimates

The dominant systematic uncertainties associated with the electroweak background estimates are on JES and $E_{\text{T}}^{\text{miss}}$, as well as theoretical uncertainties on the shape of W kinematic distributions and the ratio of Z and W plus jets production cross sections. The latter theoretical uncertainty is relevant because background predictions from W control regions are also used to estimate $Z \rightarrow \nu\bar{\nu}$ +jets contributions to the signal region. Additional systematic uncertainties are due to the muon momentum scale and resolution, the data-driven scale factors to equalise lepton trigger and reconstruction efficiencies in simulations and data, statistical uncertainties associated with the limited size of MC samples, the subtraction of the electroweak contamination (f_{EW}), and, in the electron control regions, the multijet contamination. The uncertainties from pile-up variations are found to be negligible, as are those from the electron energy scale, resolution, and JER.

The systematic uncertainties associated with the small multijet background are estimated to be 100%. They are obtained by changing the fit range for the p_{T} extrapolation and varying the scale factors for the Z and W background prediction by 10%. All variations are within a factor of two of the central predictions.

Systematic uncertainties on the non-collision background are 10%. This estimate corresponds to the average fraction of unpaired proton bunches that are used to determine $\epsilon_{\text{tag}}^{\text{non-coll.}}$, and that are close (separated by 25 ns in time) to an unpaired bunch in the opposite beam. Such configurations may lead to double counting in the efficiency estimate, and their total contribution is hence considered as an uncertainty.

The JES and JER uncertainties are evaluated using a combination of data-driven and MC-based techniques [55]. These methods take into account the variation of the uncertainty with jet p_{T} and η , and the presence of nearby jets. The $E_{\text{T}}^{\text{miss}}$ uncertainty is derived from the JES and JER uncertainties by propagating the relative jet-level variations to the calorimeter cluster based $E_{\text{T}}^{\text{miss}}$. Since ratios are used to extrapolate from the control regions to the signal regions, the effects of these uncertainties tend to cancel.

Source	SR1	SR2	SR3	SR4
JES/JER/ E_T^{miss}	1.0	2.6	4.9	5.8
MC Z/W modelling	2.9	2.9	2.9	3.0
MC statistical uncertainty	0.5	1.4	3.4	8.9
$1 - f_{\text{EW}}$	1.0	1.0	0.7	0.7
Muon scale and resolution	0.03	0.02	0.08	0.61
Lepton scale factors	0.4	0.5	0.6	0.7
Multijet BG in electron CR	0.1	0.1	0.3	0.6
Di-boson, top, multijet, non-collisions	0.8	0.7	1.1	0.3
Total systematic uncertainty	3.4	4.4	6.8	11.1
Total data statistical uncertainty	0.5	1.7	4.3	11.8

Table 5. Relative systematic uncertainties for all signal regions (in percent). Individual contributions are summed in quadrature to derive the total numbers. The MC statistical uncertainty is included in the total systematic uncertainty.

Theoretical uncertainties on Z and W production and the shape of W kinematic distributions are evaluated by comparing background estimates using kinematic Z/W distributions from different generators (ALPGEN and SHERPA). Uncertainties on f_{EW} are derived by comparing ALPGEN to PYTHIA [66], but also by taking into account JES and lepton-scale uncertainties. The full difference is taken as systematic uncertainty in all cases.

Systematic and statistical uncertainties on all background estimates are given in table 5. The contribution from lepton scale factors is the quadratic sum of electron and muon uncertainties. The uncertainties from di-boson, top-quark, multijet, and non-collision backgrounds are summed in quadrature. A 20% uncertainty is assigned for the di-boson and top-quark MC-based estimates. This value is dominated by the JES uncertainty (16%), but also takes into account uncertainties of the trigger efficiency, luminosity measurement, and lepton identification uncertainties.

5.5 Background summary and additional checks

An overview of all backgrounds is given in table 6 (cf. table 4 for the definition of the control regions). The final $Z \rightarrow \nu\bar{\nu} + \text{jets}$ predictions are estimated from a combination of the predictions of the four control regions. The combination is the error-weighted average calculated taking into account correlations of uncertainties. The $Z \rightarrow \nu\bar{\nu} + \text{jets}$ prediction is dominated by the W control-region estimates and based on the assumption that the ratio of $Z + \text{jets}$ to $W + \text{jets}$ cross sections is well modelled in the simulation. This assumption is supported by dedicated measurements [66], albeit for smaller jet momenta than the ones used in SR2 to SR4. The theoretical uncertainty on the ratio of Z to W cross sections is included in the uncertainty derived from comparisons of different MC generators discussed above.

The electroweak background estimate, which relies on an exclusive W or Z selection in the control regions, is compared to two alternative correlated methods. In the first of

	SR1	SR2	SR3	SR4
$Z \rightarrow \nu\bar{\nu}+\text{jets}$	63000 ± 2100	5300 ± 280	500 ± 40	58 ± 9
$W \rightarrow \tau\nu+\text{jets}$	31400 ± 1000	1853 ± 81	133 ± 13	13 ± 3
$W \rightarrow e\nu+\text{jets}$	14600 ± 500	679 ± 43	40 ± 8	5 ± 2
$W \rightarrow \mu\nu+\text{jets}$	11100 ± 600	704 ± 60	55 ± 6	6 ± 1
$t\bar{t}$ + single t	1240 ± 250	57 ± 12	4 ± 1	-
Multijets	1100 ± 900	64 ± 64	8_{-8}^{+9}	-
Non-coll. Background	575 ± 83	25 ± 13	-	-
$Z/\gamma^* \rightarrow \tau\tau+\text{jets}$	421 ± 25	15 ± 2	2 ± 1	-
Di-bosons	302 ± 61	29 ± 5	5 ± 1	1 ± 1
$Z/\gamma^* \rightarrow \mu\mu+\text{jets}$	204 ± 19	8 ± 4	-	-
Total Background	124000 ± 4000	8800 ± 400	750 ± 60	83 ± 14
Events in Data (4.7 fb^{-1})	124703	8631	785	77
$\sigma_{\text{vis}}^{\text{obs}}$ at 90% [pb]	1.63	0.13	0.026	0.0055
$\sigma_{\text{vis}}^{\text{exp}}$ at 90% [pb]	1.54	0.15	0.020	0.0064
$\sigma_{\text{vis}}^{\text{obs}}$ at 95% [pb]	1.92	0.17	0.030	0.0069
$\sigma_{\text{vis}}^{\text{exp}}$ at 95% [pb]	1.82	0.18	0.024	0.0079

Table 6. Overview of predicted SM background and observed events in data for 4.7 fb^{-1} for each of the four signal regions. The total uncertainty quoted is the quadratic sum of statistical and systematic uncertainties. Observed and expected 90% and 95% CL upper limits on the non-SM contribution to all signal regions are also given in terms of limits on visible cross sections ($\sigma_{\text{vis}} \equiv \sigma \times A \times \epsilon$). The 90% CL upper limits are given to facilitate comparisons with other experiments.

these, which was the main method used in the previous ATLAS monojet search [16], an inclusive control region is defined by only inverting the lepton veto while keeping all other selection criteria the same as in the signal regions. No additional Z - or W -specific invariant or transverse mass selection criteria are applied, thereby yielding a mixed control sample dominated by W and Z bosons. The resulting background predictions are found to be consistent with those of the default method. The second alternative modifies the lepton definition in the control regions. Instead of applying lepton selection criteria in control regions that are more stringent than those of the signal regions, a modified exclusive control region is defined. The selection criteria include less stringent lepton definitions where the lepton veto cuts of the signal region are simply inverted, and dedicated Z or W selection criteria are used. These background predictions are also found to be consistent with the default method.

Distributions from all four visible decay modes used to determine the background in SR1 are shown in figure 1. The distributions are obtained by applying the exclusive Z and W selection criteria plus SR1 kinematic cuts on $E_{\text{T}}^{\text{miss}}$ and jets, as well as vetoes on additional electrons or muons. It should be noted that shape differences in the $E_{\text{T}}^{\text{miss}}$

distributions between data and MC are irrelevant for an accurate background prediction in the signal regions, because the E_T^{miss} distribution obtained from control-region data is used directly to predict the backgrounds in the signal regions. Distributions of variables that are subject to MC-based efficiency or acceptance corrections, namely those involving electrons or muons, need to agree in shape between data and MC (see figure 1, where good shape agreement is found for the leading electron and muon p_T distributions).

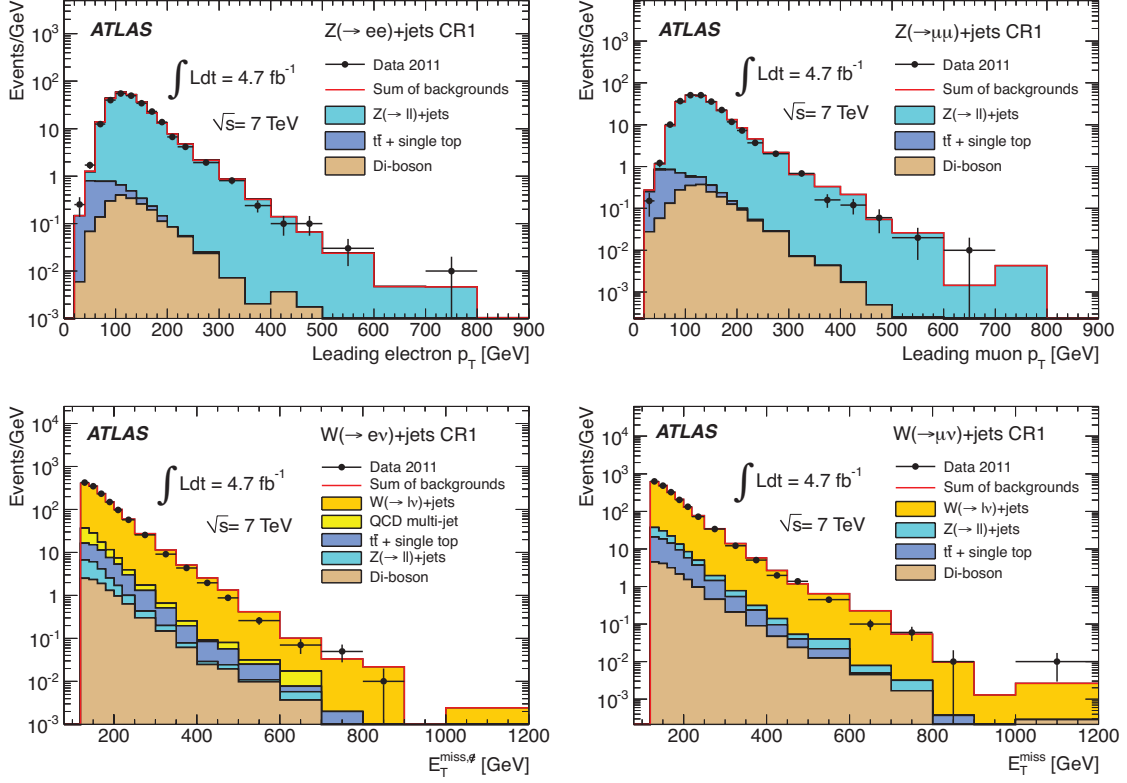


Figure 1. Kinematic distributions in the control regions corresponding to SR1 (labelled CR1) are shown. The upper row is the leading electron and muon p_T distribution for $Z \rightarrow e^+e^- + \text{jets}$ (left) and $Z \rightarrow \mu^+\mu^- + \text{jets}$ (right) and shows distributions after SR1 cuts on jets and E_T^{miss} . The lower row is the missing transverse momentum distribution $E_T^{\text{miss},\not{e}}$ for $W \rightarrow e\nu + \text{jets}$ (left) and E_T^{miss} for $W \rightarrow \mu\nu + \text{jets}$ (right) also after SR1 jet and E_T^{miss} cuts.

6 Results and interpretation

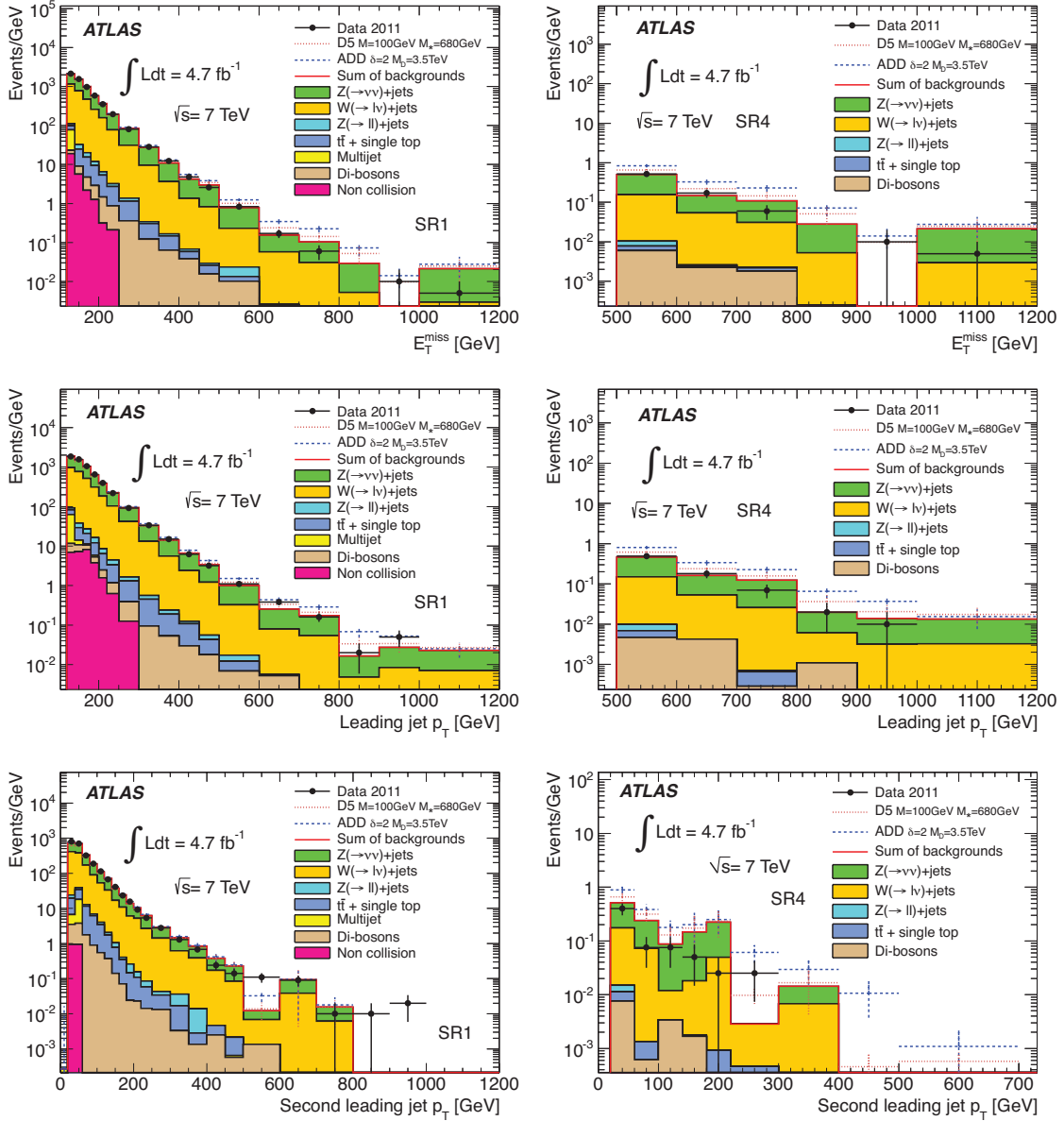


Figure 2. Kinematic distributions for signal regions SR1 on the left and SR4 on the right. Signal distributions for ADD and WIMP samples for cross sections equal to the excluded values are drawn as dashed lines on top of the predicted background distributions. The electroweak backgrounds (see equation 5.1) are determined in bins of the variable that is plotted.

The SM predictions are found to be consistent with the number of observed events in data for all signal regions considered. Comparisons of the SM predictions to the measured E_T^{miss} and leading and sub-leading jet p_T distributions are shown for SR1 and SR4 in figure 2. For illustration, the figures also contain simulated signal distributions for ADD

Sample	SR1 [%]	SR2 [%]	SR3 [%]	SR4 [%]
$Z \rightarrow \nu\bar{\nu}+\text{jets}$	1.706 ± 0.013	0.159 ± 0.004	0.0170 ± 0.0013	0.0027 ± 0.0005
ADD, $n = 2$	30.9 ± 0.2	9.2 ± 0.1	2.60 ± 0.07	0.74 ± 0.04
ADD, $n = 3$	33.2 ± 0.2	11.7 ± 0.1	3.92 ± 0.08	1.18 ± 0.05
ADD, $n = 4$	34.3 ± 0.2	13.8 ± 0.1	4.97 ± 0.09	1.67 ± 0.05
ADD, $n = 5$	35.1 ± 0.2	14.5 ± 0.1	5.50 ± 0.09	2.00 ± 0.06
ADD, $n = 6$	35.0 ± 0.2	15.0 ± 0.2	6.01 ± 0.10	2.23 ± 0.06
D1, $m_\chi = 10$ GeV	20.5 ± 0.3	3.3 ± 0.1	0.54 ± 0.01	0.09 ± 0.01
D1, $m_\chi = 1000$ GeV	32.2 ± 0.4	10.3 ± 0.2	2.88 ± 0.04	0.79 ± 0.02
D5, $m_\chi = 10$ GeV	30.4 ± 0.4	8.3 ± 0.2	2.04 ± 0.03	0.52 ± 0.01
D5, $m_\chi = 1000$ GeV	36.2 ± 0.4	12.6 ± 0.2	4.14 ± 0.05	1.24 ± 0.03
D9, $m_\chi = 10$ GeV	36.9 ± 0.5	12.9 ± 0.3	4.23 ± 0.15	1.31 ± 0.08
D9, $m_\chi = 1000$ GeV	37.6 ± 0.5	13.9 ± 0.3	4.70 ± 0.16	1.68 ± 0.09
D11, $m_\chi = 10$ GeV	30.3 ± 0.4	12.3 ± 0.3	4.57 ± 0.15	1.52 ± 0.09
D11, $m_\chi = 1000$ GeV	33.7 ± 0.5	17.0 ± 0.3	7.56 ± 0.20	3.27 ± 0.13

Table 7. Typical acceptances determined with MC simulations for the main background process $Z \rightarrow \nu\bar{\nu}+\text{jets}$ as well as for ADD and selected WIMP samples. For the $Z \rightarrow \nu\bar{\nu}+\text{jets}$ sample at least one parton with a minimum transverse momentum of 20 GeV is required, for the ADD and WIMP samples it is at least one parton with a momentum of 80 GeV. The values are given in percent and errors are statistical only.

and WIMP models added to the total background. Agreement both in the shape and the overall normalisation between SM predictions and data is observed in all cases. To facilitate comparisons with other experiments both 90% and the more conventional 95% confidence level (CL) upper limits are produced. These limits are on the visible cross section defined as cross section times acceptance and efficiency ($\sigma \times A \times \epsilon$) and they are based on the modified frequentist CL_s prescription [67]. The limits are derived by comparing the probabilities, based on Poisson distributions, that the observed number of events is compatible with the SM and the SM-plus-signal expectations. The mean values of the Poisson distributions are determined by the signal prediction, plus contributions from background processes extrapolated from the CRs to each SR. The number of events is integrated over the whole SR. Expected limits are obtained by repeating the analysis with pseudo-data obtained from Monte Carlo simulations. The distributions of the simulated probabilities for many pseudo-experiments allow $\pm 1\sigma$ bands to be plotted for the expected values. Systematic uncertainties (and their correlations) associated with SM backgrounds and the integrated luminosity are taken into account via nuisance parameters using a profile likelihood technique [68]. The nuisance parameters are assumed to be Gaussian distributed in the likelihood fit. The resulting visible cross-section limits, which apply for any source of BSM events, are summarised in table 6. Typical efficiencies of selection criteria related to jets and E_T^{miss} of $\epsilon \sim 83\%$ are found in simulated $Z \rightarrow \nu\bar{\nu}+\text{jets}$, WIMP or ADD samples. Typical acceptances are given in table 7. The negative search results are interpreted in

terms of limits on ADD and WIMP model parameters in the following sections.

6.1 Large extra dimensions

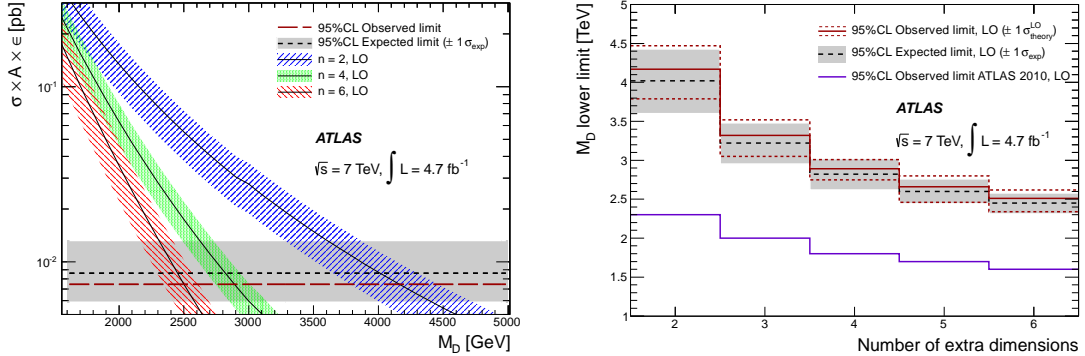


Figure 3. Left: Visible cross sections in SR4 as a function of M_D as predicted by the effective ADD theory, for $n = 2, 4, 6$ extra dimensions. The coloured bands correspond to the theoretical systematic uncertainties (PDF, ISR/FSR, scale). The horizontal lines are the expected and observed cross-section limits at 95% CL, taking into account experimental systematic uncertainties fully correlated between signal and background, as well as uncertainties on the luminosity estimate, trigger efficiency, and MC statistical uncertainties. The inclusion of signal uncertainties here increases the cross-section limits compared to those given in table 6, which exclude signal uncertainties. **Right:** 95% CL lower limits on M_D for different numbers of extra dimensions based on SR4. Observed and expected limits including all but the theoretical signal uncertainties are shown as solid and dashed lines, respectively. The grey $\pm 1\sigma$ band around the expected limit is the variation expected from statistical fluctuations and experimental systematic uncertainties on SM and signal processes. The impact of the theoretical uncertainties is shown by the red small-dashed $\pm 1\sigma$ limits. The previous ATLAS limit [16] is also shown for comparison.

Experimental and theoretical systematic uncertainties that affect the ADD signal are considered in order to set limits on the model parameters. The experimental uncertainties on JES, JER, and E_T^{miss} are considered to be fully correlated with those obtained for the background estimate. They range from 3–10% depending on the signal region and the number of extra dimensions. An additional 1% uncertainty on the trigger, and a 3.9% uncertainty on the luminosity are also considered for the signal simulation only. Theoretical uncertainties on the expected ADD signal are associated with the PDF set, ISR/FSR, and the factorisation and renormalisation scales. For the PDF uncertainties, the CTEQ6.6 error sets are used, converted from 90% to 68% CL. They range from 4–14% on the product of signal cross section and acceptance ($\sigma \times A$), depending on the number of extra dimensions. Uncertainties coming from the modelling of ISR/FSR are determined by varying the simulation parameters of PYTHIA within a range that is consistent with experimental data [69]. The resulting uncertainties vary from about 3–14%. The dominant theoretical systematic uncertainty affecting mostly the cross section rather than the acceptance is from the factorisation and renormalisation scales. Varying these scales

n	M_D [TeV]		R [pm]		Cross section truncation	
	LO	NLO	LO	NLO	LO	NLO
2	4.17	4.37	2.8×10^7	2.5×10^7	0.02%	0.01%
3	3.32	3.45	4.8×10^2	4.5×10^2	1.9%	1.3%
4	2.89	2.97	2.0	1.9	11.8%	9.9%
5	2.66	2.71	7.1×10^{-2}	7.0×10^{-2}	29.5%	27.2%
6	2.51	2.53	0.8×10^{-2}	0.8×10^{-2}	49.1%	47.9%

Table 8. 95% CL lower (upper) limits on M_D (R) for $n=2-6$ extra dimensions, using a dataset corresponding to 4.7 fb^{-1} at $\sqrt{s} = 7 \text{ TeV}$. These results are obtained using the selection criteria of SR4. All values correspond to the nominal observed limits excluding theoretical uncertainties in figure 3. The last two columns show the relative difference between the full cross sections and those of the truncated phase space ($\hat{s} < M_D^2$). The ADD cross sections are calculated at both LO and NLO, and the limits are derived from the full, not the truncated, phase space.

between twice and half their default values, following common practice, results in 20–30% uncertainties on $\sigma \times A$.⁵

The visible cross sections predicted by the ADD generator for SR4 are shown for $n = 2, 4, 6$ extra dimensions as a function of M_D on the left-hand side of figure 3. Theoretical systematic uncertainties are shown as coloured bands around the cross-section curves. The 95% CL expected and observed limits on the visible cross section $\sigma \times A \times \epsilon$ are shown as horizontal lines. The effect of restricting the simulated phase space to the kinematic region where the ADD effective field-theory implementation is valid is probed by evaluating the cross section after discarding events for which the parton centre-of-mass energy $\hat{s} > M_D^2$. The amount by which the truncated cross sections differ from the full ones provides a measure for the reliability of the effective field theory. This difference increases from SR1 to SR4 and with the number of extra dimensions. While the model with $n = 2$ extra dimensions is found to be insensitive to truncation effects for M_D values near the resulting limits for all signal regions, $n = 3, 4, 5$, and 6 extra dimensions show differences of 2%, 10%, 30%, and 50% between full and truncated cross sections for SR4 and M_D values close to the actual limits (table 8). This demonstrates that the high energy and integrated luminosity used in this search allow to probe kinematic regions where the effective field-theory model is not entirely valid.

The 95% CL lower limits on M_D versus n for the full phase space, not the truncated one, are shown for SR4 on the right-hand side of figure 3. The selection criteria of SR4 provide the best expected limits and are therefore used here. Limits from SR1, SR2, SR3 are typically 35%, 15%, 5% worse, respectively. The expected and observed limits in figure 3 are produced taking all but the theoretical uncertainties into account. The grey $\pm 1\sigma$ band around the expected limit shows the variation anticipated from statistical fluctuations and from experimental systematic uncertainties on background and signal processes. The

⁵Note that in ref. [16] the *squared* factorisation and renormalisation scales were varied between twice and half their default values.

impact of the theoretical uncertainties associated with PDFs, ISR/FSR, and factorisation and renormalisation scales is represented in the right-hand panel by dashed $\pm 1\sigma$ lines on either side of the observed limit. The resulting limit is taken as the observed line excluding theoretical uncertainties.⁶ All limits from SR4 are summarised in table 8, where the lower (upper) limits on M_D (R) are shown for cross sections calculated at LO and NLO. The K -factors (defined as $\sigma_{\text{NLO}}/\sigma_{\text{LO}}$) for $n = 2, 3, 4, 5, 6$ extra dimensions are 1.20, 1.20, 1.17, 1.13, 1.09, respectively, and have been derived for the selection criteria of SR4 by the authors of ref. [49]. M_D values below 4.17 (4.37) TeV for $n = 2$ and 2.51 (2.53) TeV for $n = 6$ are excluded at 95% CL at LO (NLO).

6.2 WIMP pair production

Systematic uncertainties on WIMP pair production are treated similarly to those of the ADD limits, except for the PDF and ISR/FSR uncertainties. The former are determined using CTEQ6M error sets for the relative uncertainty around the CTEQ6L1 central value. The ISR/FSR uncertainties are estimated differently in a way that is appropriate for the high- p_T ISR/FSR regime probed here: a WIMP pair recoils against a high- p_T ISR/FSR jet, whereas for ADD, additional low- p_T ISR/FSR jets dominate the uncertainty due to the impact of the jet veto.

The JES/JER/ E_T^{miss} experimental uncertainties lead to 1–20% uncertainties on the WIMP event yield depending on the signal region and the effective operator considered. Other experimental uncertainties affecting the WIMP event yield are associated with the trigger efficiency (1%) and the luminosity measurement (3.9%). The ISR/FSR uncertainties are estimated by varying the jet matching scale between MADGRAPH5 and PYTHIA by a factor of one half and two. Moreover, the α_s scale is varied in PYTHIA within a range that is consistent with experimental data [69]. The resulting uncertainties on $\sigma \times A$, added in quadrature, range from 3–5% for the matching scale and 4–6% for α_s depending on the signal region. A negligible dependence of the ISR/FSR uncertainties on the choice of effective operator is found. PDF uncertainties impact mostly the signal cross section and hardly the acceptance. They are found to depend on the effective operator chosen and not the particular signal region (since overall cross-section differences affect the signal regions in the same way). Uncertainties ranging from 4% and 5% for operators D9 and D5 to 16% and 18% for D11 and D1 are found. As for the ADD model, the dominating theoretical systematic uncertainty is from the factorisation and renormalisation scales. Varying these scales between twice and half their default value results in 30% signal uncertainties, independent of the effective operator choice or the signal region.

Figure 4 shows the 90% CL lower limits on the suppression scale M_* , for all operators probed as a function of WIMP mass m_χ . These limits on M_* are derived from the cross-section limits at a given mass m_χ . The values displayed are for the signal regions with the best expected limits, where those limits from SR3 and SR4 are typically within a few percent of each other, and those from SR2 (SR1) are 15–20% (40–50%) smaller than in SR3

⁶The previous ATLAS monojet search [16] has determined ADD parameter limits in a slightly different way. The effect of the signal cross section theoretical uncertainty was folded into the quoted limit and was not shown separately.

or SR4. The lower limits are based on simulation samples produced for m_χ between 10 and 1300 GeV. Extrapolations are shown down to $m_\chi = 1$ GeV. These are valid (and could be continued as constants to even smaller m_χ values entering the warm or hot dark-matter regime) since there is negligible change in cross section or kinematic distributions at the LHC for low-mass WIMPs. As before, the central values of observed and expected limits on M_* are displayed taking into account experimental but not theoretical uncertainties. The effect of $\pm 1\sigma$ variations on the expected limit due to statistical fluctuations and experimental uncertainties is shown as a grey band. The impact of the theoretical uncertainties is represented by dotted red $\pm 1\sigma$ lines on either side of the observed limit. The nominal observed limit line excluding theoretical uncertainties is the final result. All values of the lower limits on the suppression scale M_* at 90% and 95% CL are listed in table 9. For all operators, the lower limits are flat up to $m_\chi = 100$ GeV and worsen around $m_\chi = 200$ GeV. Note that the M_* limits for D1 are much smaller due to the inclusion of a factor m_q/M_* in the definition of the operator (see table 1).

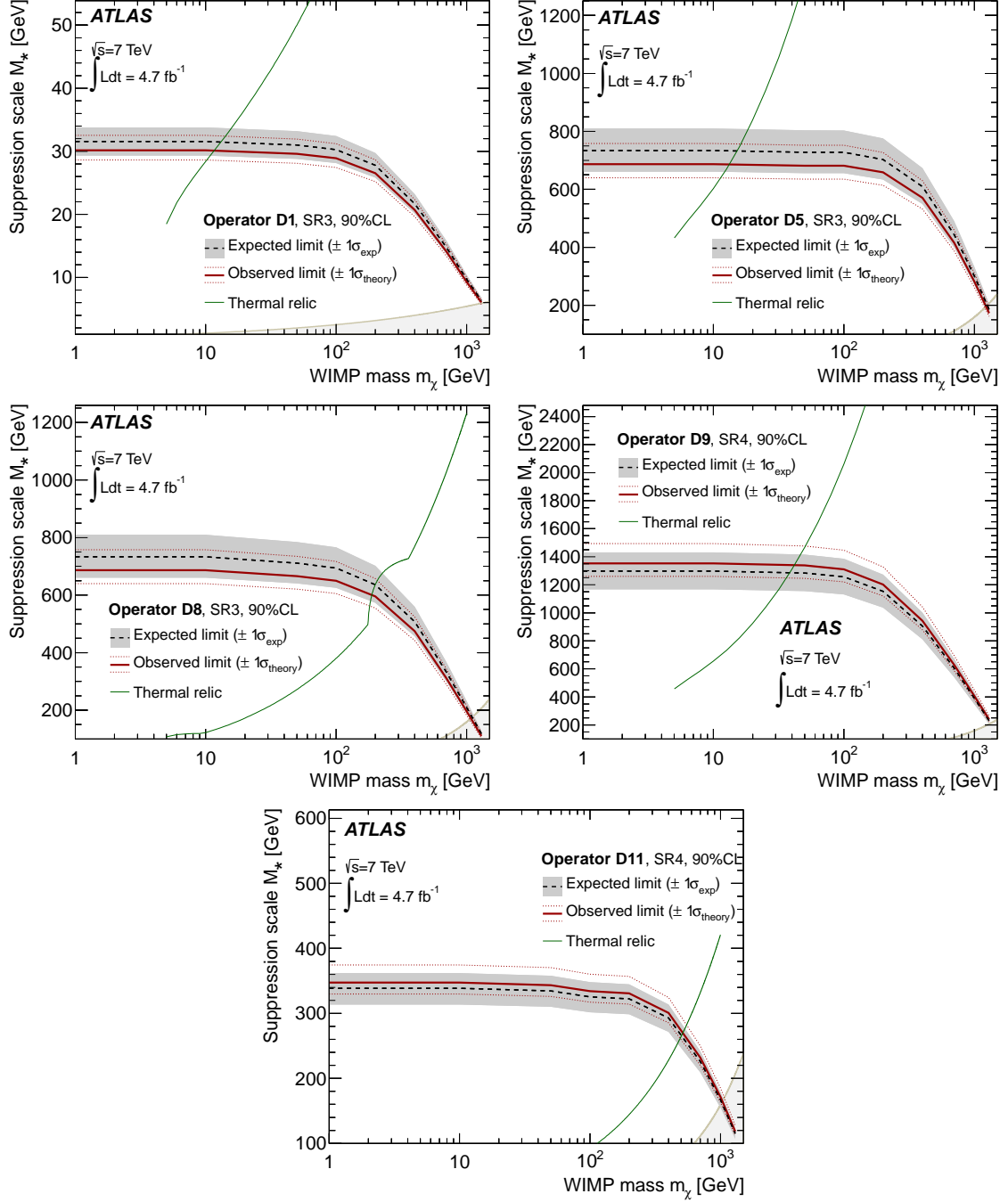


Figure 4. ATLAS lower limits at 90% CL on M_* for different masses of χ —the region below the limit lines is excluded. The 90% instead of the 95% CL lower limits are plotted because the former are used in the following figures 5 and 6. Observed and expected limits including all but the theoretical signal uncertainties are shown as dashed black and red solid lines, respectively. The grey $\pm 1\sigma$ band around the expected limit is the variation expected from statistical fluctuations and experimental systematic uncertainties on SM and signal processes. The impact of the theoretical uncertainties is shown by the thin red dotted $\pm 1\sigma$ limit lines around the observed limit. The M_* values at which WIMPs of a given mass would result in the required relic abundance are shown as rising green lines (taken from [32]), assuming annihilation in the early universe proceeded exclusively via the given operator. The shaded light-grey regions in the bottom right corners indicate where the effective field theory approach breaks down [32]. The plots for D1, D5, D8 are based on SR3, those for D9 and D11 on SR4.

m_χ	D1	D5	D8	D9	D11
1	30 (29)	687 (658)	687 (658)	1353 (1284)	347 (335)
5	30 (29)	687 (658)	687 (658)	1353 (1284)	347 (335)
10	30 (29)	687 (658)	687 (658)	1353 (1284)	347 (335)
50	30 (29)	682 (653)	666 (638)	1338 (1269)	343 (331)
100	29 (28)	681 (653)	650 (623)	1310 (1243)	334 (322)
200	27 (26)	658 (631)	595 (570)	1202 (1140)	331 (319)
400	21 (20)	571 (547)	475 (455)	943 (893)	301 (290)
700	14 (14)	416 (398)	311 (298)	629 (596)	232 (223)
1000	9 (9)	281 (269)	196 (188)	406 (384)	171 (165)
1300	6 (6)	173 (165)	110 (106)	240 (227)	118 (114)

Table 9. ATLAS 90% (95%) CL observed lower limits on the suppression scale M_* as a function of WIMP mass m_χ . All values are given in GeV and correspond to the nominal observed limit excluding theoretical uncertainties. The signal regions with the best expected limits are quoted in all cases, SR3 is used for D1, D5 and D8, SR4 for D9 and D11.

The light-grey shaded regions in figure 4 indicate where the effective field theory approach for WIMP pair production breaks down [32] (bottom-right corner in all plots).⁷ Except for some of the $m_\chi = 1300$ GeV points, the M_* limits set in this analysis are well above these bounds. No further measures are taken to ensure that the energy transfer in monojet events in this dataset remains in the valid region of the effective field theory. Such a region of validity cannot be defined without precise knowledge of the BSM physics, over which the effective operators integrate.

Figure 4 also includes *thermal relic* lines (taken from [32]) which correspond to a coupling, set by M_* , of WIMPs to quarks or gluons such that WIMPs have the correct relic abundance as measured by the WMAP satellite [30], in the absence of any other interaction than the one considered. Under the assumption that DM is entirely composed of thermal relics, ATLAS limits on M_* that are above the value required for the thermal relic density exclude the case where DM annihilates exclusively to SM particles via the corresponding operator. Should thermal relic WIMPs exist in these regions (above the thermal relic line), there would have to be other annihilation channels or annihilation via other operators in order to be consistent with the WMAP measurements.

In the effective operator approach, the ATLAS bounds on M_* for a given m_χ can be converted to bounds on WIMP-nucleon scattering cross sections, which are probed by direct dark matter detection experiments. These bounds describe scattering of WIMPs from nucleons at a very low momentum transfer of the order of a keV. Depending on the type of interaction, contributions to *spin-dependent* or *spin-independent* WIMP-nucleon interactions are expected. The translation of ATLAS limits to bounds on WIMP-nucleon

⁷Compared to ref. [32] the valid region of D1 shown here accounts for the factor of m_q in the definition of D1 (see table 1).

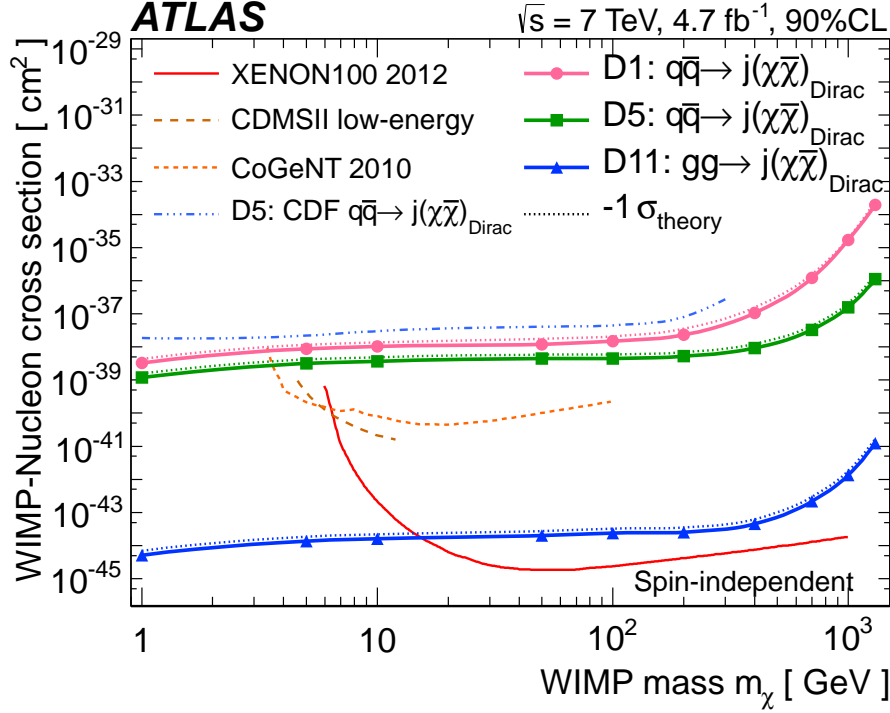


Figure 5. Inferred 90% CL ATLAS limits on spin-independent WIMP-nucleon scattering. Cross sections are shown versus WIMP mass m_χ . In all cases the thick solid lines are the observed limits excluding theoretical uncertainties; the observed limits corresponding to the WIMP-parton cross section obtained from the $-1\sigma_{\text{theory}}$ lines in figure 4 are shown as thin dotted lines. The latter limits are conservative because they also include theoretical uncertainties. The ATLAS limits for operators involving quarks are for the four light flavours assuming equal coupling strengths for all quark flavours to the WIMPs. For comparison, 90% CL limits from the XENON100 [70], CDMSII [71], CoGeNT [72], CDF [19], and CMS [21] experiments are shown.

scattering cross sections is done using equations (3) to (6) of ref. [32], and the results are shown in figures 5 and 6.⁸ As in ref. [32] uncertainties on hadronic matrix elements are neglected here. The spin-independent ATLAS limits in figure 5 are particularly relevant in the low m_χ region (< 10 GeV) where the XENON100 [70], CDMSII [71] or CoGeNT [72] limits suffer from a kinematic suppression. Should DM particles couple exclusively to gluons via D11, the collider limits would be competitive up to m_χ of about 20 GeV, and remain important over almost the full m_χ range covered. The spin-dependent limits in figure 6 are based on D8 and D9, where for D8 the M_* limits are calculated using the D5 acceptances (as they are identical) together with D8 production cross sections. Both the D8 and D9 cross-section limits are significantly smaller than those from direct-detection experiments.

As in figure 4, the collider limits can be interpreted in terms of the relic abundance

⁸There is a typographical error in equation (5) of ref. [32] (cross sections for D8 and D9). Instead of $9.18 \times 10^{-40} \text{cm}^2$ the pre-factor should be $4.7 \times 10^{-39} \text{cm}^2$.

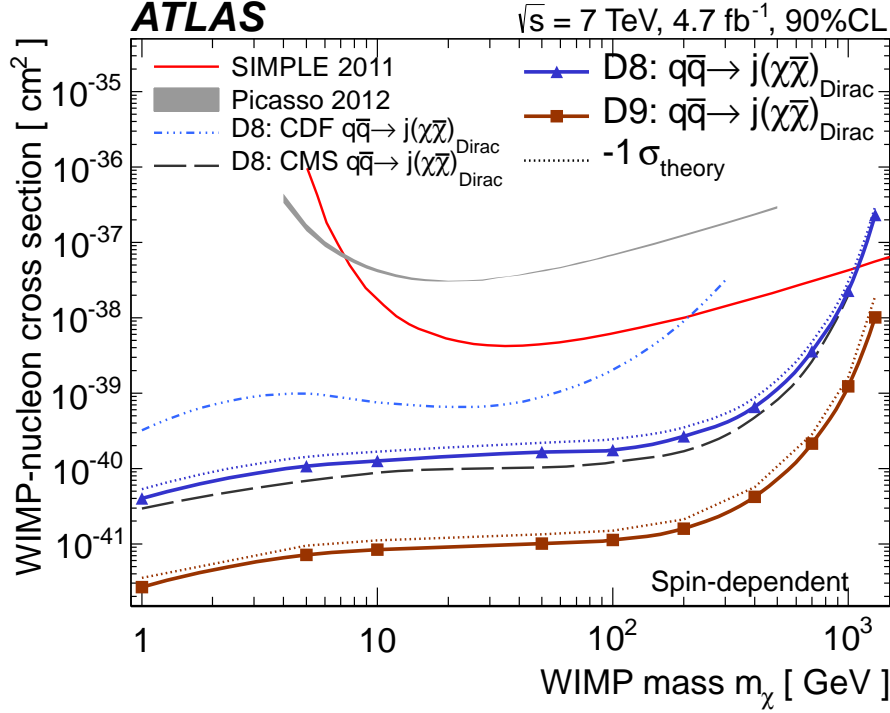


Figure 6. Inferred 90% CL ATLAS limits on spin-dependent WIMP-nucleon scattering. Cross sections are shown versus WIMP mass m_χ . In all cases the thick solid lines are the observed limits excluding theoretical uncertainties, the observed limits corresponding to the WIMP-parton cross section obtained from the $-1\sigma_{\text{theory}}$ lines in figure 4 are shown as thin dotted lines. The latter limits are conservative because they also include theoretical uncertainties. The ATLAS limits are for the four light flavours assuming equal coupling strengths for all quark flavours to the WIMPs. For comparison, 90% CL limits from the SIMPLE [73], Picasso [74], CDF [19], and CMS [21] experiments are shown.

of WIMPs [13, 15]. This is shown in figure 7 where the limits on vector and axial-vector interactions are translated into upper limits on the annihilation rate of WIMPs to the four light quark flavours. The annihilation rate is defined as the product of cross section σ and relative velocity v , averaged over the dark matter velocity distribution ($\langle\sigma v\rangle$). Equations (10) and (11) of ref. [15] are used to calculate the annihilation rates shown in figure 7. For comparison, limits on annihilation to $b\bar{b}$ from Galactic high-energy gamma-ray observations by the Fermi-LAT experiment [75] are also shown. The Fermi-LAT values are for Majorana fermions and are therefore scaled up by a factor of two for comparison with the ATLAS limits for Dirac fermions (see for example the description of equation (34) of ref. [76] for an explanation of the factor of two). Gamma-ray spectra and yields from WIMPs annihilating to $b\bar{b}$, where photons are produced in the hadronisation of the quarks, are expected to be very similar to those from WIMPs annihilating to lighter quarks [77, 78]. In this sense the ATLAS and Fermi-LAT limits can be compared to each other. The figure also demonstrates the complementarity between the two approaches. The Fermi-LAT experiment is equally

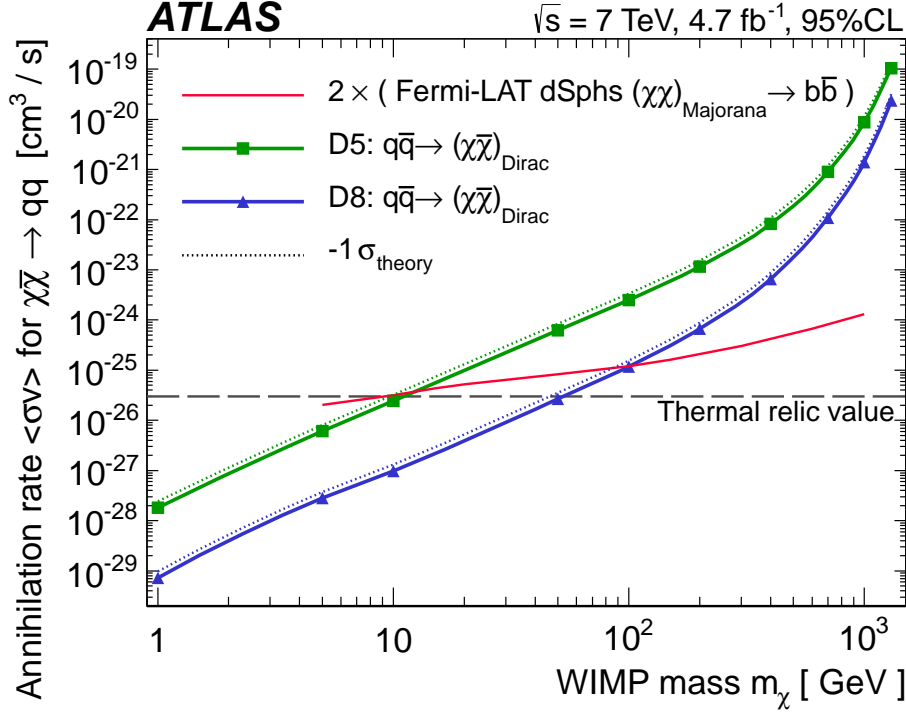


Figure 7. Inferred ATLAS 95% CL limits on WIMP annihilation rates $\langle\sigma v\rangle$ versus mass m_χ . $\langle\sigma v\rangle$ is calculated as in ref. [15]. The thick solid lines are the observed limits excluding theoretical uncertainties. The observed limits corresponding to the WIMP-parton cross section obtained from the $-1\sigma_{\text{theory}}$ lines in figure 4 are shown as thin dotted lines. The latter limits are conservative because they also include theoretical uncertainties. The ATLAS limits are for the four light quark flavours assuming equal coupling strengths for all quark flavours to the WIMPs. For comparison, high-energy gamma-ray limits from observations of Galactic satellite galaxies with the Fermi-LAT experiment [75] for Majorana WIMPs are shown. The Fermi-LAT limits are scaled up by a factor of two to make them comparable to the ATLAS Dirac WIMP limits. All limits shown here assume 100% branching fractions of WIMPs annihilating to quarks. The horizontal dashed line indicates the value required for WIMPs to make up the relic abundance set by the WMAP measurement.

sensitive to annihilation to light and heavy quarks, whereas ATLAS probes mostly WIMP couplings to lighter quarks and sets cross-section limits that are superior at WIMP masses below 10 GeV for vector couplings and below about 100 GeV for axial-vector couplings. At these low WIMP masses, the ATLAS limits are below the value needed for WIMPs to make up the cold dark matter abundance (labelled *Thermal relic value* in figure 7), assuming WIMPs have annihilated exclusively via the particular operator to SM quarks while they were in thermal equilibrium in the early universe. In this case WIMPs would result in relic densities that are too large and hence incompatible with the WMAP measurements. For masses of $m_\chi \geq 200$ GeV the ATLAS sensitivity worsens substantially compared to the Fermi-LAT one. This will improve when the LHC starts operation at higher centre-of-mass energies in the future.

The value of using an effective field theory approach to WIMP-SM particle coupling is that only two parameters, M_* and m_χ , are needed to describe WIMP pair production at the LHC, WIMP-nucleon scattering measured by direct-detection experiments, and WIMP annihilation measured by indirect-detection experiments. The complementarity between the different experimental approaches can hence be explored under a number of important assumptions: the effective field theory must be valid, WIMPs must interact with SM quarks or gluons exclusively via only one of the operators of the effective field theory (since a mix of operators with potential interference effects is not considered here), and the interactions must be flavour-universal for the four light quarks. In the future, should there be a WIMP signal in at least one of the experiments from these various fields, the effective-operator approach would allow important tests of the underlying physics by probing all the available experimental data.

7 Summary

A search for physics beyond the Standard Model is presented in events with a high-energy jet and missing transverse momentum. The search uses the full 2011 pp LHC dataset recorded with the ATLAS detector at a centre-of-mass energy of $\sqrt{s} = 7$ TeV. The data correspond to an integrated luminosity of 4.7 fb^{-1} .

Four overlapping signal regions are defined for the search. They require a high-energy jet and missing transverse momentum of at least 120, 220, 350 and 500 GeV, with at most one additional jet not aligned with the direction of E_T^{miss} (to suppress multijet background). In all cases the events are required to contain no identified electrons or muons. The dominant Standard Model backgrounds from Z and W plus jet production, where the boson decays to a final state that includes 1–2 neutrinos, are determined using data control regions with correction and transfer factors determined from data and simulations. This technique allows precise estimates of the SM contributions to monojet final states, which is reflected in a small total uncertainty of 3.2% for the background prediction in the high-statistics signal region SR1.

In each of the four signal regions, agreement is found between the Standard Model predictions and the data. Upper limits are set at 95% CL on the visible cross section of any non-SM contribution to the signal regions. These limits range from 1.92 pb in the first signal region to 7 fb in the fourth signal region. To allow comparisons with the results of other experiments, 90% CL limits are also provided. The cross-section upper limits are interpreted in terms of limits on the model parameters of two BSM physics scenarios. For ADD, a model of large extra spatial dimensions, lower limits are set on the $(4 + n)$ -dimensional Planck scale M_D of 4.17 (2.51) TeV for $n = 2$ (6) extra dimensions at LO and 4.37 (2.53) TeV at NLO. In a second scenario an effective field theory is used to derive limits on a mass suppression scale M_* for pair production of WIMP dark matter particles. Within this approach the ATLAS limits can be converted to limits on WIMP-nucleon scattering and WIMP annihilation cross sections. Assuming the effective field theory is valid, that WIMPs interact with SM quarks or gluons, and that they can be pair-produced at the LHC, some of the limits are competitive with or substantially better than limits set

by direct and indirect dark matter detection experiments, in particular at small WIMP masses of $m_\chi < 10$ GeV.

8 Acknowledgements

We would like to thank Tim Tait for providing the dark matter generator software and supporting us during its validation.

We thank CERN for the very successful operation of the LHC, as well as the support staff from our institutions without whom ATLAS could not be operated efficiently.

We acknowledge the support of ANPCyT, Argentina; YerPhI, Armenia; ARC, Australia; BMWF and FWF, Austria; ANAS, Azerbaijan; SSTC, Belarus; CNPq and FAPESP, Brazil; NSERC, NRC and CFI, Canada; CERN; CONICYT, Chile; CAS, MOST and NSFC, China; COLCIENCIAS, Colombia; MSMT CR, MPO CR and VSC CR, Czech Republic; DNRF, DNSRC and Lundbeck Foundation, Denmark; EPLANET and ERC, European Union; IN2P3-CNRS, CEA-DSM/IRFU, France; GNSF, Georgia; BMBF, DFG, HGF, MPG and AvH Foundation, Germany; GSRT, Greece; ISF, MINERVA, GIF, DIP and Benoziyo Center, Israel; INFN, Italy; MEXT and JSPS, Japan; CNRST, Morocco; FOM and NWO, Netherlands; BRF and RCN, Norway; MNiSW, Poland; GRICES and FCT, Portugal; MERYS (MECTS), Romania; MES of Russia and ROSATOM, Russian Federation; JINR; MSTD, Serbia; MSSR, Slovakia; ARRS and MVZT, Slovenia; DST/NRF, South Africa; MICINN, Spain; SRC and Wallenberg Foundation, Sweden; SER, SNSF and Cantons of Bern and Geneva, Switzerland; NSC, Taiwan; TAEK, Turkey; STFC, the Royal Society and Leverhulme Trust, United Kingdom; DOE and NSF, United States of America.

The crucial computing support from all WLCG partners is acknowledged gratefully, in particular from CERN and the ATLAS Tier-1 facilities at TRIUMF (Canada), NDGF (Denmark, Norway, Sweden), CC-IN2P3 (France), KIT/GridKA (Germany), INFN-CNAF (Italy), NL-T1 (Netherlands), PIC (Spain), ASGC (Taiwan), RAL (UK) and BNL (USA) and in the Tier-2 facilities worldwide.

References

- [1] H. Miyazawa, *Baryon Number Changing Currents*, [Prog. Theor. Phys. **36** \(6\) \(1966\) 1266–1276](#).
- [2] P. Ramond, *Dual Theory for Free Fermions*, [Phys. Rev. **D3** \(1971\) 2415–2418](#).
- [3] Y. A. Gol’fand and E. P. Likhtman, *Extension of the Algebra of Poincare Group Generators and Violation of p Invariance*, [JETP Lett. **13** \(1971\) 323–326](#).
- [4] A. Neveu and J. H. Schwarz, *Factorizable dual model of pions*, [Nucl. Phys. **B31** \(1971\) 86–112](#).
- [5] A. Neveu and J. H. Schwarz, *Quark Model of Dual Pions*, [Phys. Rev. **D4** \(1971\) 1109–1111](#).
- [6] J. Gervais and B. Sakita, *Field theory interpretation of supergauges in dual models*, [Nucl. Phys. **B34** \(1971\) 632–639](#).
- [7] D. V. Volkov and V. P. Akulov, *Is the Neutrino a Goldstone Particle?*, [Phys. Lett. **B46** \(1973\) 109–110](#).

- [8] J. Wess and B. Zumino, *A Lagrangian Model Invariant Under Supergauge Transformations*, *Phys. Lett.* **B49** (1974) 52.
- [9] J. Wess and B. Zumino, *Supergauge Transformations in Four-Dimensions*, *Nucl. Phys.* **B70** (1974) 39–50.
- [10] M. Carena, A. Freitas, and C. Wagner, *Light Stop Searches at the LHC in Events with One Hard Photon or Jet and Missing Energy*, *JHEP* **0810** (2008) 109, [arXiv:0808.2298 \[hep-ph\]](#).
- [11] B. C. Allanach, S. Grab, and H. E. Haber, *Supersymmetric Monojets at the Large Hadron Collider*, *JHEP* **1101** (2011) 138, [arXiv:1010.4261 \[hep-ph\]](#).
- [12] N. Arkani-Hamed, S. Dimopoulos, and G. Dvali, *The Hierarchy problem and new dimensions at a millimeter*, *Phys.Lett.* **B429** (1998) 263–272, [arXiv:hep-ph/9803315 \[hep-ph\]](#).
- [13] M. Beltran, D. Hooper, E. W. Kolb, Z. A. Krusberg, and T. M. Tait, *Maverick dark matter at colliders*, *JHEP* **1009** (2010) 037, [arXiv:1002.4137 \[hep-ph\]](#).
- [14] A. Rajaraman, W. Shepherd, T. M. Tait, and A. M. Wijangco, *LHC Bounds on Interactions of Dark Matter*, *Phys.Rev.* **D84** (2011) 095013, [arXiv:1108.1196 \[hep-ph\]](#).
- [15] P. J. Fox, R. Harnik, J. Kopp, and Y. Tsai, *Missing Energy Signatures of Dark Matter at the LHC*, *Phys.Rev.* **D85** (2012) 056011, [arXiv:1109.4398 \[hep-ph\]](#).
- [16] ATLAS Collaboration, *Search for new phenomena with the monojet and missing transverse momentum signature using the ATLAS detector in $\sqrt{s} = 7$ TeV proton-proton collisions*, *Phys.Lett.* **B705** (2011) 294–312, [arXiv:1106.5327 \[hep-ex\]](#).
- [17] D0 Collaboration, V. Abazov et al., *Search for large extra dimensions in the monojet + missing E_T channel at $D\bar{O}$* , *Phys.Rev.Lett.* **90** (2003) 251802, [arXiv:hep-ex/0302014 \[hep-ex\]](#).
- [18] CDF Collaboration, A. Abulencia et al., *Search for Large Extra Dimensions in the Production of Jets and Missing Transverse Energy in $p\bar{p}$ Collisions at $\sqrt{s} = 1.96$ TeV*, *Phys.Rev.Lett.* **97** (2006) 171802, [arXiv:hep-ex/0605101 \[hep-ex\]](#).
- [19] CDF Collaboration, T. Aaltonen et al., *Search for Dark Matter in Events with One Jet and Missing Transverse Energy in $p\bar{p}$ Collisions at $\sqrt{s}=1.96$ TeV*, *Physical Review Letters* **108** no. 21, (2012) 211804, [arXiv:1203.0742 \[hep-ex\]](#).
- [20] CMS Collaboration, *Search for New Physics with a Mono-Jet and Missing Transverse Energy in pp Collisions at $\sqrt{s} = 7$ TeV*, *Phys.Rev.Lett.* **107** (2011) 201804, [arXiv:1106.4775 \[hep-ex\]](#).
- [21] CMS Collaboration, *Search for dark matter and large extra dimensions in monojet events in pp collisions at $\sqrt{s} = 7$ TeV*, [arXiv:1206.5663 \[hep-ex\]](#).
- [22] S. Weinberg, *Implications of Dynamical Symmetry Breaking*, *Phys. Rev.* **D13** (1976) 974–996.
- [23] E. Gildener, *Gauge Symmetry Hierarchies*, *Phys. Rev.* **D14** (1976) 1667.
- [24] S. Weinberg, *Implications of Dynamical Symmetry Breaking: An Addendum*, *Phys. Rev.* **D19** (1979) 1277–1280.
- [25] L. Susskind, *Dynamics of Spontaneous Symmetry Breaking in the Weinberg- Salam Theory*, *Phys. Rev.* **D20** (1979) 2619–2625.

- [26] G. F. Giudice, R. Rattazzi, and J. D. Wells, *Quantum gravity and extra dimensions at high-energy colliders*, *Nucl.Phys.* **B544** (1999) 3–38, [arXiv:hep-ph/9811291](#) [[hep-ph](#)].
- [27] G. Bertone, D. Hooper, and J. Silk, *Particle dark matter: Evidence, candidates and constraints*, *Phys.Rept.* **405** (2005) 279–390, [arXiv:hep-ph/0404175](#) [[hep-ph](#)].
- [28] G. Steigman and M. S. Turner, *Cosmological Constraints on the Properties of Weakly Interacting Massive Particles*, *Nucl.Phys.* **B253** (1985) 375.
- [29] E. W. Kolb and M. S. Turner, *The Early universe*, *Front.Phys.* **69** (1990) 1–547.
- [30] WMAP Collaboration, E. Komatsu et al., *Seven-Year Wilkinson Microwave Anisotropy Probe (WMAP) Observations: Cosmological Interpretation*, *Astrophys.J.Suppl.* **192** (2011) 18, [arXiv:1001.4538](#) [[astro-ph.CO](#)].
- [31] A. Birkedal, K. Matchev, and M. Perelstein, *Dark matter at colliders: A Model independent approach*, *Phys.Rev.* **D70** (2004) 077701, [arXiv:hep-ph/0403004](#) [[hep-ph](#)].
- [32] J. Goodman, M. Ibe, A. Rajaraman, W. Shepherd, T. M. Tait, et al., *Constraints on Dark Matter from Colliders*, *Phys.Rev.* **D82** (2010) 116010, [arXiv:1008.1783](#) [[hep-ph](#)].
- [33] A. Friedland, M. L. Graesser, I. M. Shoemaker, and L. Vecchi, *Probing Nonstandard Standard Model Backgrounds with LHC Monojets*, *Phys.Lett.* **B714** (2012) 267–275, [arXiv:1111.5331](#) [[hep-ph](#)].
- [34] ATLAS Collaboration, *The ATLAS Experiment at the CERN Large Hadron Collider*, *JINST* **3** (2008) S08003.
- [35] ATLAS Collaboration, *Expected Performance of the ATLAS Experiment - Detector, Trigger and Physics*, [arXiv:0901.0512](#) [[hep-ex](#)].
- [36] ATLAS Collaboration, *Luminosity Determination in pp Collisions at $\sqrt{s} = 7$ TeV Using the ATLAS Detector at the LHC*, *Eur.Phys.J.* **C71** (2011) 1630, [arXiv:1101.2185](#) [[hep-ex](#)].
- [37] ATLAS Collaboration, *Luminosity Determination in pp Collisions at $\sqrt{s} = 7$ TeV Using the ATLAS Detector in 2011*, ATLAS-CONF-2011-116. <http://cdsweb.cern.ch/record/1376384>.
- [38] M. L. Mangano, M. Moretti, F. Piccinini, R. Pittau, and A. D. Polosa, *ALPGEN, a generator for hard multiparton processes in hadronic collisions*, *JHEP* **0307** (2003) 001, [arXiv:hep-ph/0206293](#) [[hep-ph](#)].
- [39] J. Pumplin, D. Stump, J. Huston, H. Lai, P. M. Nadolsky, et al., *New generation of parton distributions with uncertainties from global QCD analysis*, *JHEP* **0207** (2002) 012, [arXiv:hep-ph/0201195](#) [[hep-ph](#)].
- [40] G. Corcella, I. Knowles, G. Marchesini, S. Moretti, K. Odagiri, et al., *HERWIG 6: An Event generator for hadron emission reactions with interfering gluons (including supersymmetric processes)*, *JHEP* **0101** (2001) 010, [arXiv:hep-ph/0011363](#) [[hep-ph](#)].
- [41] G. Corcella, I. Knowles, G. Marchesini, S. Moretti, K. Odagiri, et al., *HERWIG 6.5 release note*, [arXiv:hep-ph/0210213](#) [[hep-ph](#)].
- [42] M. L. Mangano, M. Moretti, F. Piccinini, and M. Treccani, *Matching matrix elements and shower evolution for top-quark production in hadronic collisions*, *JHEP* **0701** (2007) 013, [arXiv:hep-ph/0611129](#) [[hep-ph](#)].
- [43] J. Butterworth, J. R. Forshaw, and M. Seymour, *Multiparton interactions in photoproduction at HERA*, *Z.Phys.* **C72** (1996) 637–646, [arXiv:hep-ph/9601371](#) [[hep-ph](#)].

- [44] T. Gleisberg, S. Hoeche, F. Krauss, M. Schonherr, S. Schumann, et al., *Event generation with SHERPA 1.1*, *JHEP* **0902** (2009) 007, [arXiv:0811.4622 \[hep-ph\]](#).
- [45] S. Frixione and B. R. Webber, *The MC@NLO 3.2 event generator*, [arXiv:hep-ph/0601192 \[hep-ph\]](#).
- [46] P. M. Nadolsky, H.-L. Lai, Q.-H. Cao, J. Huston, J. Pumplin, et al., *Implications of CTEQ global analysis for collider observables*, *Phys.Rev.* **D78** (2008) 013004, [arXiv:0802.0007 \[hep-ph\]](#).
- [47] T. Sjostrand, S. Mrenna, and P. Z. Skands, *PYTHIA 6.4 Physics and Manual*, *JHEP* **0605** (2006) 026, [arXiv:hep-ph/0603175 \[hep-ph\]](#).
- [48] A. D. Martin, W. J. Stirling, R. S. Thorne, and G. Watt, *Parton distributions for the LHC*, *Eur. Phys. J.* **C63** (2009) 189–285, [arXiv:0901.0002 \[hep-ph\]](#).
- [49] S. Karg, M. Kramer, Q. Li, and D. Zeppenfeld, *NLO QCD corrections to graviton production at hadron colliders*, *Phys.Rev.* **D81** (2010) 094036, [arXiv:0911.5095 \[hep-ph\]](#).
- [50] J. Alwall, M. Herquet, F. Maltoni, O. Mattelaer, and T. Stelzer, *MadGraph 5 : Going Beyond*, *JHEP* **1106** (2011) 128, [arXiv:1106.0522 \[hep-ph\]](#).
- [51] ATLAS Collaboration, *The ATLAS Simulation Infrastructure*, *Eur. Phys. J.* **C70** (2010) 823–874, [arXiv:1005.4568 \[physics.ins-det\]](#).
- [52] GEANT4 Collaboration, S. Agostinelli et al., *GEANT4: A simulation toolkit*, *Nucl. Instrum. Meth.* **A506** (2003) 250–303.
- [53] M. Cacciari, G. P. Salam, and G. Soyez, *The anti- k_t jet clustering algorithm*, *JHEP* **04** (2008) 063, [arXiv:0802.1189 \[hep-ph\]](#).
- [54] ATLAS Collaboration, *Calorimeter clustering algorithms: description and performance*, ATL-LARG-PUB-2008-002. <http://cdsweb.cern.ch/record/1099735>.
- [55] ATLAS Collaboration, *Jet energy measurement with the ATLAS detector in proton-proton collisions at $\sqrt{s} = 7$ TeV*, [arXiv:1112.6426 \[hep-ex\]](#).
- [56] ATLAS Collaboration, *Electron performance measurements with the ATLAS detector using the 2010 LHC proton-proton collision data*, *Eur.Phys.J.* **C72** (2012) 1909, [arXiv:1110.3174 \[hep-ex\]](#).
- [57] ATLAS Collaboration, *Measurement of the $W \rightarrow l\nu$ and $Z/\gamma^* \rightarrow ll$ production cross sections in proton-proton collisions at $\sqrt{s} = 7$ TeV with the ATLAS detector*, *JHEP* **1012** (2010) 060, [arXiv:1010.2130 \[hep-ex\]](#).
- [58] ATLAS Collaboration, *Local Hadron Calibration*, ATL-LARG-PUB-2009-001. <http://cdsweb.cern.ch/record/1112035>.
- [59] ATLAS Collaboration, *Performance of Missing Transverse Momentum Reconstruction in Proton-Proton Collisions at 7 TeV with ATLAS*, *Eur.Phys.J.* **C72** (2012) 1844, [arXiv:1108.5602 \[hep-ex\]](#).
- [60] ATLAS Collaboration, *The implementation of the ATLAS missing E_T triggers for the initial LHC operation*, ATL-DAQ-PUB-2011-001. <http://cdsweb.cern.ch/record/1331180>.
- [61] ATLAS Collaboration, *Performance of the ATLAS transverse energy triggers with initial LHC runs at $\sqrt{s} = 7$ TeV*, ATLAS-CONF-2011-072. <http://cdsweb.cern.ch/record/1351836>.

- [62] ATLAS Collaboration, *Performance of the ATLAS Inner Detector Track and Vertex Reconstruction in the High Pile-Up LHC Environment*, ATLAS-CONF-2012-042.
<http://cdsweb.cern.ch/record/1435196>.
- [63] ATLAS Collaboration, *Data-quality requirements and event cleaning for jets and missing transverse energy reconstruction with the ATLAS detector in proton-proton collisions at a center-of-mass energy of 7 TeV*, ATLAS-CONF-2010-038.
<http://cdsweb.cern.ch/record/1277678>.
- [64] ATLAS Collaboration, *Non-collision backgrounds as measured by the ATLAS detector during the 2010 proton-proton run*, ATLAS-CONF-2011-137.
<http://cdsweb.cern.ch/record/1383840>.
- [65] ATLAS Collaboration, *Measurement of the inclusive W^\pm and Z/γ^* cross sections in the electron and muon decay channels in pp collisions at $\sqrt{s} = 7$ TeV with the ATLAS detector*, *Phys. Rev. D* **85**, **072004** (2012), [arXiv:1109.5141](https://arxiv.org/abs/1109.5141) [[hep-ex](#)].
- [66] ATLAS Collaboration, *A measurement of the ratio of the W and Z cross sections with exactly one associated jet in pp collisions at $\sqrt{s} = 7$ TeV with ATLAS*, *Phys.Lett. B* **708** (2012) 221–240, [arXiv:1108.4908](https://arxiv.org/abs/1108.4908) [[hep-ex](#)].
- [67] A. L. Read, *Presentation of search results: The CL_s technique*, *J.Phys.G* **G28** (2002) 2693–2704.
- [68] G. Cowan, K. Cranmer, E. Gross, and O. Vitells, *Asymptotic formulae for likelihood-based tests of new physics*, *Eur.Phys.J. C* **71** (2011) 1554, [arXiv:1007.1727](https://arxiv.org/abs/1007.1727) [[physics.data-an](#)].
- [69] P. Z. Skands, *Tuning Monte Carlo Generators: The Perugia Tunes*, *Phys.Rev. D* **82** (2010) 074018, [arXiv:1005.3457](https://arxiv.org/abs/1005.3457) [[hep-ph](#)].
- [70] XENON100 Collaboration, E. Aprile et al., *Dark Matter Results from 225 Live Days of XENON100 Data*, [arXiv:1207.5988](https://arxiv.org/abs/1207.5988) [[astro-ph.CO](#)].
- [71] CDMS Collaboration, Z. Ahmed et al., *Results from a Low-Energy Analysis of the CDMS II Germanium Data*, *Phys. Rev. Lett.* **106** (2011) 131302.
<http://link.aps.org/doi/10.1103/PhysRevLett.106.131302>.
- [72] CoGeNT Collaboration, C. Aalseth et al., *Results from a Search for Light-Mass Dark Matter with a P-type Point Contact Germanium Detector*, *Phys.Rev.Lett.* **106** (2011) 131301, [arXiv:1002.4703](https://arxiv.org/abs/1002.4703) [[astro-ph.CO](#)].
- [73] M. Felizardo, T. Girard, T. Morlat, A. Fernandes, A. Ramos, et al., *Final Analysis and Results of the Phase II SIMPLE Dark Matter Search*, *Phys.Rev.Lett.* **108** (2012) 201302, [arXiv:1106.3014](https://arxiv.org/abs/1106.3014) [[astro-ph.CO](#)].
- [74] PICASSO Collaboration, S. Archambault et al., *Constraints on Low-Mass WIMP Interactions on ^{19}F from PICASSO*, *Phys.Lett. B* **711** (2012) 153–161, [arXiv:1202.1240](https://arxiv.org/abs/1202.1240) [[hep-ex](#)].
- [75] Fermi-LAT Collaboration, M. Ackermann et al., *Constraining Dark Matter Models from a Combined Analysis of Milky Way Satellites with the Fermi Large Area Telescope*, *Phys.Rev.Lett.* **107** (2011) 241302, [arXiv:1108.3546](https://arxiv.org/abs/1108.3546) [[astro-ph.HE](#)].
- [76] M. Cirelli et al., *PPPC 4 DM ID: A Poor Particle Physicist Cookbook for Dark Matter Indirect Detection*, *JCAP* **1103** (2011) 051, [arXiv:1012.4515](https://arxiv.org/abs/1012.4515) [[hep-ph](#)].
- [77] L. Bergstrom, P. Ullio, and J. H. Buckley, *Observability of gamma-rays from dark matter*

neutralino annihilations in the Milky Way halo, *Astropart.Phys.* **9** (1998) 137–162,
[arXiv:astro-ph/9712318](#) [[astro-ph](#)].

- [78] N. Fornengo, L. Pieri, and S. Scopel, *Neutralino annihilation into gamma-rays in the Milky Way and in external galaxies*, *Phys.Rev.* **D70** (2004) 103529,
[arXiv:hep-ph/0407342](#) [[hep-ph](#)].

The ATLAS Collaboration

G. Aad⁴⁸, T. Abajyan²¹, B. Abbott¹¹¹, J. Abdallah¹², S. Abdel Khalek¹¹⁵,
A.A. Abdelalim⁴⁹, O. Abdinov¹¹, R. Aben¹⁰⁵, B. Abi¹¹², M. Abolins⁸⁸, O.S. AbouZeid¹⁵⁸,
H. Abramowicz¹⁵³, H. Abreu¹³⁶, B.S. Acharya^{164a,164b}, L. Adamczyk³⁸, D.L. Adams²⁵,
T.N. Addy⁵⁶, J. Adelman¹⁷⁶, S. Adomeit⁹⁸, P. Adragna⁷⁵, T. Adye¹²⁹, S. Aefsky²³,
J.A. Aguilar-Saavedra^{124b,a}, M. Agustoni¹⁷, M. Aharrouche⁸¹, S.P. Ahlen²², F. Ahles⁴⁸,
A. Ahmad¹⁴⁸, M. Ahsan⁴¹, G. Aielli^{133a,133b}, T.P.A. Åkesson⁷⁹, G. Akimoto¹⁵⁵,
A.V. Akimov⁹⁴, M.S. Alam², M.A. Alam⁷⁶, J. Albert¹⁶⁹, S. Albrand⁵⁵, M. Aleksa³⁰,
I.N. Aleksandrov⁶⁴, F. Alessandria^{89a}, C. Alexa^{26a}, G. Alexander¹⁵³, G. Alexandre⁴⁹,
T. Alexopoulos¹⁰, M. Alhroob^{164a,164c}, M. Aliev¹⁶, G. Alimonti^{89a}, J. Alison¹²⁰,
B.M.M. Allbrooke¹⁸, P.P. Allport⁷³, S.E. Allwood-Spiers⁵³, J. Almond⁸²,
A. Aloisio^{102a,102b}, R. Alon¹⁷², A. Alonso⁷⁹, F. Alonso⁷⁰, A. Altheimer³⁵,
B. Alvarez Gonzalez⁸⁸, M.G. Alviggi^{102a,102b}, K. Amako⁶⁵, C. Amelung²³,
V.V. Ammosov^{128,*}, S.P. Amor Dos Santos^{124a}, A. Amorim^{124a,b}, N. Amram¹⁵³,
C. Anastopoulos³⁰, L.S. Ancu¹⁷, N. Andari¹¹⁵, T. Andeen³⁵, C.F. Anders^{58b},
G. Anders^{58a}, K.J. Anderson³¹, A. Andreazza^{89a,89b}, V. Andrei^{58a}, M-L. Andrieux⁵⁵,
X.S. Anduaga⁷⁰, S. Angelidakis⁹, P. Anger⁴⁴, A. Angerami³⁵, F. Anghinolfi³⁰,
A. Anisenkov¹⁰⁷, N. Anjos^{124a}, A. Annovi⁴⁷, A. Antonaki⁹, M. Antonelli⁴⁷, A. Antonov⁹⁶,
J. Antos^{144b}, F. Anulli^{132a}, M. Aoki¹⁰¹, S. Aoun⁸³, L. Aperio Bella⁵, R. Apolle^{118,c},
G. Arabidze⁸⁸, I. Aracena¹⁴³, Y. Arai⁶⁵, A.T.H. Arce⁴⁵, S. Arfaoui¹⁴⁸, J-F. Arguin⁹³,
S. Argyropoulos⁴², E. Arik^{19a,*}, M. Arik^{19a}, A.J. Armbruster⁸⁷, O. Arnaez⁸¹, V. Arnal⁸⁰,
C. Arnault¹¹⁵, A. Artamonov⁹⁵, G. Artoni^{132a,132b}, D. Arutinov²¹, S. Asai¹⁵⁵, S. Ask²⁸,
B. Åsman^{146a,146b}, L. Asquith⁶, K. Assamagan²⁵, A. Astbury¹⁶⁹, M. Atkinson¹⁶⁵,
B. Aubert⁵, E. Auge¹¹⁵, K. Augsten¹²⁷, M. Aurousseau^{145a}, G. Avolio³⁰, R. Avramidou¹⁰,
D. Axen¹⁶⁸, G. Azuelos^{93,d}, Y. Azuma¹⁵⁵, M.A. Baak³⁰, G. Baccaglioni^{89a},
C. Bacci^{134a,134b}, A.M. Bach¹⁵, H. Bachacou¹³⁶, K. Bachas³⁰, M. Backes⁴⁹,
M. Backhaus²¹, J. Backus Mayes¹⁴³, E. Badescu^{26a}, P. Bagnaia^{132a,132b}, S. Bahinipati³,
Y. Bai^{33a}, D.C. Bailey¹⁵⁸, T. Bain¹⁵⁸, J.T. Baines¹²⁹, O.K. Baker¹⁷⁶, M.D. Baker²⁵,
S. Baker⁷⁷, P. Balek¹²⁶, E. Banas³⁹, P. Banerjee⁹³, Sw. Banerjee¹⁷³, D. Banfi³⁰,
A. Bangert¹⁵⁰, V. Bansal¹⁶⁹, H.S. Bansil¹⁸, L. Barak¹⁷², S.P. Baranov⁹⁴,
A. Barbaro Galtieri¹⁵, T. Barber⁴⁸, E.L. Barberio⁸⁶, D. Barberis^{50a,50b}, M. Barbero²¹,
D.Y. Bardin⁶⁴, T. Barillari⁹⁹, M. Barisonzi¹⁷⁵, T. Barklow¹⁴³, N. Barlow²⁸,
B.M. Barnett¹²⁹, R.M. Barnett¹⁵, A. Baroncelli^{134a}, G. Barone⁴⁹, A.J. Barr¹¹⁸,
F. Barreiro⁸⁰, J. Barreiro Guimarães da Costa⁵⁷, P. Barrillon¹¹⁵, R. Bartoldus¹⁴³,
A.E. Barton⁷¹, V. Bartsch¹⁴⁹, A. Basye¹⁶⁵, R.L. Bates⁵³, L. Batkova^{144a}, J.R. Batley²⁸,
A. Battaglia¹⁷, M. Battistin³⁰, F. Bauer¹³⁶, H.S. Bawa^{143,e}, S. Beale⁹⁸, T. Beau⁷⁸,
P.H. Beauchemin¹⁶¹, R. Beccherle^{50a}, P. Bechtel²¹, H.P. Beck¹⁷, A.K. Becker¹⁷⁵,
S. Becker⁹⁸, M. Beckingham¹³⁸, K.H. Becks¹⁷⁵, A.J. Beddall^{19c}, A. Beddall^{19c},
S. Bedikian¹⁷⁶, V.A. Bednyakov⁶⁴, C.P. Bee⁸³, L.J. Beemster¹⁰⁵, M. Begej²⁵,
S. Behar Harpaz¹⁵², P.K. Behera⁶², M. Beimforde⁹⁹, C. Belanger-Champagne⁸⁵,
P.J. Bell⁴⁹, W.H. Bell⁴⁹, G. Bella¹⁵³, L. Bellagamba^{20a}, M. Bellomo³⁰, A. Belloni⁵⁷,
O. Beloborodova^{107,f}, K. Belotskiy⁹⁶, O. Beltramello³⁰, O. Benary¹⁵³,

D. Benchekroun^{135a}, K. Bendtz^{146a,146b}, N. Benekos¹⁶⁵, Y. Benhammou¹⁵³,
 E. Benhar Noccioli⁴⁹, J.A. Benitez Garcia^{159b}, D.P. Benjamin⁴⁵, M. Benoit¹¹⁵,
 J.R. Bensingher²³, K. Benslama¹³⁰, S. Bentvelsen¹⁰⁵, D. Berge³⁰,
 E. Bergeaas Kuutmann⁴², N. Berger⁵, F. Berghaus¹⁶⁹, E. Berglund¹⁰⁵, J. Beringer¹⁵,
 P. Bernat⁷⁷, R. Bernhard⁴⁸, C. Bernius²⁵, T. Berry⁷⁶, C. Bertella⁸³, A. Bertin^{20a,20b},
 F. Bertolucci^{122a,122b}, M.I. Besana^{89a,89b}, G.J. Besjes¹⁰⁴, N. Besson¹³⁶, S. Bethke⁹⁹,
 W. Bhimji⁴⁶, R.M. Bianchi³⁰, L. Bianchini²³, M. Bianco^{72a,72b}, O. Biebel⁹⁸,
 S.P. Bieniek⁷⁷, K. Bierwagen⁵⁴, J. Biesiada¹⁵, M. Biglietti^{134a}, H. Bilokon⁴⁷,
 M. Bindi^{20a,20b}, S. Binet¹¹⁵, A. Bingul^{19c}, C. Bini^{132a,132b}, C. Biscarat¹⁷⁸, B. Bittner⁹⁹,
 K.M. Black²², R.E. Blair⁶, J.-B. Blanchard¹³⁶, G. Blanchot³⁰, T. Blazek^{144a}, I. Bloch⁴²,
 C. Blocker²³, J. Blocki³⁹, A. Blondel⁴⁹, W. Blum⁸¹, U. Blumenschein⁵⁴, G.J. Bobbink¹⁰⁵,
 V.B. Bobrovnikov¹⁰⁷, S.S. Bocchetta⁷⁹, A. Bocci⁴⁵, C.R. Boddy¹¹⁸, M. Boehler⁴⁸,
 J. Boek¹⁷⁵, N. Boelaert³⁶, J.A. Bogaerts³⁰, A. Bogdanchikov¹⁰⁷, A. Bogouch^{90,*},
 C. Bohm^{146a}, J. Bohm¹²⁵, V. Boisvert⁷⁶, T. Bold³⁸, V. Boldea^{26a}, N.M. Bolnet¹³⁶,
 M. Bomben⁷⁸, M. Bona⁷⁵, M. Boonekamp¹³⁶, S. Bordoni⁷⁸, C. Borer¹⁷, A. Borisov¹²⁸,
 G. Borissov⁷¹, I. Borjanovic^{13a}, M. Borri⁸², S. Borroni⁸⁷, J. Bortfeldt⁹⁸,
 V. Bortolotto^{134a,134b}, K. Bos¹⁰⁵, D. Boscherini^{20a}, M. Bosman¹², H. Boterenbrood¹⁰⁵,
 J. Bouchami⁹³, J. Boudreau¹²³, E.V. Bouhova-Thacker⁷¹, D. Boumediene³⁴,
 C. Bourdarios¹¹⁵, N. Bousson⁸³, A. Boveia³¹, J. Boyd³⁰, I.R. Boyko⁶⁴,
 I. Bozovic-Jelisavcic^{13b}, J. Bracinik¹⁸, P. Branchini^{134a}, A. Brandt⁸, G. Brandt¹¹⁸,
 O. Brandt⁵⁴, U. Bratzler¹⁵⁶, B. Brau⁸⁴, J.E. Brau¹¹⁴, H.M. Braun^{175,*},
 S.F. Brazzale^{164a,164c}, B. Brelier¹⁵⁸, J. Bremer³⁰, K. Brendlinger¹²⁰, R. Brenner¹⁶⁶,
 S. Bressler¹⁷², D. Britton⁵³, F.M. Brochu²⁸, I. Brock²¹, R. Brock⁸⁸, F. Broggi^{89a},
 C. Bromberg⁸⁸, J. Bronner⁹⁹, G. Brooijmans³⁵, T. Brooks⁷⁶, W.K. Brooks^{32b},
 G. Brown⁸², H. Brown⁸, P.A. Bruckman de Renstrom³⁹, D. Bruncko^{144b}, R. Bruneliere⁴⁸,
 S. Brunet⁶⁰, A. Bruni^{20a}, G. Bruni^{20a}, M. Bruschi^{20a}, T. Buanes¹⁴, Q. Buat⁵⁵, F. Bucci⁴⁹,
 J. Buchanan¹¹⁸, P. Buchholz¹⁴¹, R.M. Buckingham¹¹⁸, A.G. Buckley⁴⁶, S.I. Buda^{26a},
 I.A. Budagov⁶⁴, B. Budick¹⁰⁸, V. Büscher⁸¹, L. Bugge¹¹⁷, O. Bulekov⁹⁶, A.C. Bundock⁷³,
 M. Bunse⁴³, T. Buran¹¹⁷, H. Burckhart³⁰, S. Burdin⁷³, T. Burgess¹⁴, S. Burke¹²⁹,
 E. Busato³⁴, P. Bussey⁵³, C.P. Buszello¹⁶⁶, B. Butler¹⁴³, J.M. Butler²², C.M. Buttar⁵³,
 J.M. Butterworth⁷⁷, W. Buttinger²⁸, M. Byszewski³⁰, S. Cabrera Urbán¹⁶⁷,
 D. Caforio^{20a,20b}, O. Cakir^{4a}, P. Calafiura¹⁵, G. Calderini⁷⁸, P. Calfayan⁹⁸, R. Calkins¹⁰⁶,
 L.P. Caloba^{24a}, R. Caloi^{132a,132b}, D. Calvet³⁴, S. Calvet³⁴, R. Camacho Toro³⁴,
 P. Camarri^{133a,133b}, D. Cameron¹¹⁷, L.M. Caminada¹⁵, R. Caminal Armadans¹²,
 S. Campana³⁰, M. Campanelli⁷⁷, V. Canale^{102a,102b}, F. Canelli^{31,g}, A. Canepa^{159a},
 J. Cantero⁸⁰, R. Cantrill⁷⁶, L. Capasso^{102a,102b}, M.D.M. Capeans Garrido³⁰, I. Caprini^{26a},
 M. Caprini^{26a}, D. Capriotti⁹⁹, M. Capua^{37a,37b}, R. Caputo⁸¹, R. Cardarelli^{133a},
 T. Carli³⁰, G. Carlino^{102a}, L. Carminati^{89a,89b}, B. Caron⁸⁵, S. Caron¹⁰⁴, E. Carquin^{32b},
 G.D. Carrillo-Montoya^{145b}, A.A. Carter⁷⁵, J.R. Carter²⁸, J. Carvalho^{124a,h}, D. Casadei¹⁰⁸,
 M.P. Casado¹², M. Cascella^{122a,122b}, C. Caso^{50a,50b,*}, A.M. Castaneda Hernandez^{173,i},
 E. Castaneda-Miranda¹⁷³, V. Castillo Gimenez¹⁶⁷, N.F. Castro^{124a}, G. Cataldi^{72a},
 P. Catastini⁵⁷, A. Catinaccio³⁰, J.R. Catmore³⁰, A. Cattai³⁰, G. Cattani^{133a,133b},
 S. Caughron⁸⁸, V. Cavaliere¹⁶⁵, P. Cavalleri⁷⁸, D. Cavalli^{89a}, M. Cavalli-Sforza¹²,

V. Cavasinni^{122a,122b}, F. Ceradini^{134a,134b}, A.S. Cerqueira^{24b}, A. Cerri³⁰, L. Cerrito⁷⁵,
F. Cerutti⁴⁷, S.A. Cetin^{19b}, A. Chafaq^{135a}, D. Chakraborty¹⁰⁶, I. Chalupkova¹²⁶,
K. Chan³, P. Chang¹⁶⁵, B. Chapleau⁸⁵, J.D. Chapman²⁸, J.W. Chapman⁸⁷,
E. Chareyre⁷⁸, D.G. Charlton¹⁸, V. Chavda⁸², C.A. Chavez Barajas³⁰, S. Cheatham⁸⁵,
S. Chekanov⁶, S.V. Chekulaev^{159a}, G.A. Chelkov⁶⁴, M.A. Chelstowska¹⁰⁴, C. Chen⁶³,
H. Chen²⁵, S. Chen^{33c}, X. Chen¹⁷³, Y. Chen³⁵, Y. Cheng³¹, A. Cheplakov⁶⁴,
R. Cherkaoui El Moursli^{135e}, V. Chernyatin²⁵, E. Cheu⁷, S.L. Cheung¹⁵⁸, L. Chevalier¹³⁶,
G. Chiefari^{102a,102b}, L. Chikovani^{51a,*}, J.T. Childers³⁰, A. Chilingarov⁷¹, G. Chiodini^{72a},
A.S. Chisholm¹⁸, R.T. Chislett⁷⁷, A. Chitan^{26a}, M.V. Chizhov⁶⁴, G. Choudalakis³¹,
S. Chouridou¹³⁷, I.A. Christidi⁷⁷, A. Christov⁴⁸, D. Chromek-Burckhart³⁰, M.L. Chu¹⁵¹,
J. Chudoba¹²⁵, G. Ciapetti^{132a,132b}, A.K. Ciftci^{4a}, R. Ciftci^{4a}, D. Cinca³⁴, V. Cindro⁷⁴,
C. Ciocca^{20a,20b}, A. Ciocio¹⁵, M. Cirilli⁸⁷, P. Cirkovic^{13b}, Z.H. Citron¹⁷², M. Citterio^{89a},
M. Ciubancan^{26a}, A. Clark⁴⁹, P.J. Clark⁴⁶, R.N. Clarke¹⁵, W. Cleland¹²³, J.C. Clemens⁸³,
B. Clement⁵⁵, C. Clement^{146a,146b}, Y. Coadou⁸³, M. Cobal^{164a,164c}, A. Cocco¹³⁸,
J. Cochran⁶³, L. Coffey²³, J.G. Cogan¹⁴³, J. Coggeshall¹⁶⁵, E. Cogneras¹⁷⁸, J. Colas⁵,
S. Cole¹⁰⁶, A.P. Colijn¹⁰⁵, N.J. Collins¹⁸, C. Collins-Tooth⁵³, J. Collot⁵⁵,
T. Colombo^{119a,119b}, G. Colon⁸⁴, G. Compostella⁹⁹, P. Conde Muiño^{124a}, E. Coniavitis¹⁶⁶,
M.C. Conidi¹², S.M. Consonni^{89a,89b}, V. Consorti⁴⁸, S. Constantinescu^{26a},
C. Conta^{119a,119b}, G. Conti⁵⁷, F. Conventi^{102a,j}, M. Cooke¹⁵, B.D. Cooper⁷⁷,
A.M. Cooper-Sarkar¹¹⁸, K. Copic¹⁵, T. Cornelissen¹⁷⁵, M. Corradi^{20a}, F. Corriveau^{85,k},
A. Cortes-Gonzalez¹⁶⁵, G. Cortiana⁹⁹, G. Costa^{89a}, M.J. Costa¹⁶⁷, D. Costanzo¹³⁹,
D. Côté³⁰, L. Courneyea¹⁶⁹, G. Cowan⁷⁶, C. Cowden²⁸, B.E. Cox⁸², K. Cranmer¹⁰⁸,
F. Crescioli^{122a,122b}, M. Cristinziani²¹, G. Crosetti^{37a,37b}, S. Crépe-Renaudin⁵⁵,
C.-M. Cuciuc^{26a}, C. Cuenca Almenar¹⁷⁶, T. Cuhadar Donszelmann¹³⁹, M. Curatolo⁴⁷,
C.J. Curtis¹⁸, C. Cuthbert¹⁵⁰, P. Cwetanski⁶⁰, H. Czirr¹⁴¹, P. Czodrowski⁴⁴,
Z. Czynzula¹⁷⁶, S. D'Auria⁵³, M. D'Onofrio⁷³, A. D'Orazio^{132a,132b},
M.J. Da Cunha Sargedas De Sousa^{124a}, C. Da Via⁸², W. Dabrowski³⁸, A. Dafinca¹¹⁸,
T. Dai⁸⁷, C. Dallapiccola⁸⁴, M. Dam³⁶, M. Dameri^{50a,50b}, D.S. Damiani¹³⁷,
H.O. Danielsson³⁰, V. Dao⁴⁹, G. Darbo^{50a}, G.L. Darlea^{26b}, J.A. Dassoulas⁴², W. Davey²¹,
T. Davidek¹²⁶, N. Davidson⁸⁶, R. Davidson⁷¹, E. Davies^{118,c}, M. Davies⁹³, O. Davignon⁷⁸,
A.R. Davison⁷⁷, Y. Davygora^{58a}, E. Dawe¹⁴², I. Dawson¹³⁹,
R.K. Daya-Ishmukhametova²³, K. De⁸, R. de Asmundis^{102a}, S. De Castro^{20a,20b},
S. De Cecco⁷⁸, J. de Graat⁹⁸, N. De Groot¹⁰⁴, P. de Jong¹⁰⁵, C. De La Taille¹¹⁵,
H. De la Torre⁸⁰, F. De Lorenzi⁶³, L. de Mora⁷¹, L. De Nooij¹⁰⁵, D. De Pedis^{132a},
A. De Salvo^{132a}, U. De Sanctis^{164a,164c}, A. De Santo¹⁴⁹, J.B. De Vivie De Regie¹¹⁵,
G. De Zorzi^{132a,132b}, W.J. Dearnaley⁷¹, R. Debbe²⁵, C. Debenedetti⁴⁶, B. Dechenaux⁵⁵,
D.V. Dedovich⁶⁴, J. Degenhardt¹²⁰, J. Del Peso⁸⁰, T. Del Prete^{122a,122b}, T. Delemontex⁵⁵,
M. Deliyergiyev⁷⁴, A. Dell'Acqua³⁰, L. Dell'Asta²², M. Della Pietra^{102a,j},
D. della Volpe^{102a,102b}, M. Delmastro⁵, P.A. Delsart⁵⁵, C. Deluca¹⁰⁵, S. Demers¹⁷⁶,
M. Demichev⁶⁴, B. Demirkoz^{12,l}, S.P. Denisov¹²⁸, D. Derendarz³⁹, J.E. Derkaoui^{135d},
F. Derue⁷⁸, P. Dervan⁷³, K. Desch²¹, E. Devetak¹⁴⁸, P.O. Deviveiros¹⁰⁵, A. Dewhurst¹²⁹,
B. DeWilde¹⁴⁸, S. Dhaliwal¹⁵⁸, R. Dhullipudi^{25,m}, A. Di Ciaccio^{133a,133b}, L. Di Ciaccio⁵,
C. Di Donato^{102a,102b}, A. Di Girolamo³⁰, B. Di Girolamo³⁰, S. Di Luise^{134a,134b},

A. Di Mattia¹⁷³, B. Di Micco³⁰, R. Di Nardo⁴⁷, A. Di Simone^{133a,133b}, R. Di Sipio^{20a,20b},
 M.A. Diaz^{32a}, E.B. Diehl⁸⁷, J. Dietrich⁴², T.A. Dietzsch^{58a}, S. Diglio⁸⁶,
 K. Dindar Yagci⁴⁰, J. Dingfelder²¹, F. Dinut^{26a}, C. Dionisi^{132a,132b}, P. Dita^{26a}, S. Dita^{26a},
 F. Dittus³⁰, F. Djama⁸³, T. Djobava^{51b}, M.A.B. do Vale^{24c}, A. Do Valle Wemans^{124a,n},
 T.K.O. Doan⁵, M. Dobbs⁸⁵, D. Dobos³⁰, E. Dobson^{30,o}, J. Dodd³⁵, C. Doglioni⁴⁹,
 T. Doherty⁵³, Y. Doi^{65,*}, J. Dolejsi¹²⁶, I. Dolenc⁷⁴, Z. Dolezal¹²⁶, B.A. Dolgoshein^{96,*},
 T. Dohmae¹⁵⁵, M. Donadelli^{24d}, J. Donini³⁴, J. Dopke³⁰, A. Doria^{102a}, A. Dos Anjos¹⁷³,
 A. Dotti^{122a,122b}, M.T. Dova⁷⁰, A.D. Doxiadis¹⁰⁵, A.T. Doyle⁵³, N. Dressnandt¹²⁰,
 M. Dris¹⁰, J. Dubbert⁹⁹, S. Dube¹⁵, E. Duchovni¹⁷², G. Duckeck⁹⁸, D. Duda¹⁷⁵,
 A. Dudarev³⁰, F. Dudziak⁶³, M. Dührssen³⁰, I.P. Duerdoth⁸², L. Duflot¹¹⁵,
 M-A. Dufour⁸⁵, L. Duguid⁷⁶, M. Dunford^{58a}, H. Duran Yildiz^{4a}, R. Duxfield¹³⁹,
 M. Dwuznik³⁸, M. Düren⁵², W.L. Ebenstein⁴⁵, J. Ebke⁹⁸, S. Eckweiler⁸¹, K. Edmonds⁸¹,
 W. Edson², C.A. Edwards⁷⁶, N.C. Edwards⁵³, W. Ehrenfeld⁴², T. Eifert¹⁴³, G. Eigen¹⁴,
 K. Einsweiler¹⁵, E. Eisenhandler⁷⁵, T. Ekelof¹⁶⁶, M. El Kacimi^{135c}, M. Ellert¹⁶⁶, S. Elles⁵,
 F. Ellinghaus⁸¹, K. Ellis⁷⁵, N. Ellis³⁰, J. Elmsheuser⁹⁸, M. Elsing³⁰, D. Emeliyanov¹²⁹,
 R. Engelmann¹⁴⁸, A. Engl⁹⁸, B. Epp⁶¹, J. Erdmann⁵⁴, A. Ereditato¹⁷, D. Eriksson^{146a},
 J. Ernst², M. Ernst²⁵, J. Ernwein¹³⁶, D. Errede¹⁶⁵, S. Errede¹⁶⁵, E. Ertel⁸¹,
 M. Escalier¹¹⁵, H. Esch⁴³, C. Escobar¹²³, X. Espinal Curull¹², B. Esposito⁴⁷,
 F. Etienne⁸³, A.I. Etienvre¹³⁶, E. Etzion¹⁵³, D. Evangelakou⁵⁴, H. Evans⁶⁰,
 L. Fabbri^{20a,20b}, C. Fabre³⁰, R.M. Fakhruddinov¹²⁸, S. Falciano^{132a}, Y. Fang¹⁷³,
 M. Fanti^{89a,89b}, A. Farbin⁸, A. Farilla^{134a}, J. Farley¹⁴⁸, T. Farooque¹⁵⁸, S. Farrell¹⁶³,
 S.M. Farrington¹⁷⁰, P. Farthouat³⁰, F. Fassi¹⁶⁷, P. Fassnacht³⁰, D. Fassouliotis⁹,
 B. Fatholahzadeh¹⁵⁸, A. Favareto^{89a,89b}, L. Fayard¹¹⁵, S. Fazio^{37a,37b}, R. Febbraro³⁴,
 P. Federic^{144a}, O.L. Fedin¹²¹, W. Fedorko⁸⁸, M. Fehling-Kaschek⁴⁸, L. Felgioni⁸³,
 C. Feng^{33d}, E.J. Feng⁶, A.B. Fenyuk¹²⁸, J. Ferencei^{144b}, W. Fernando⁶, S. Ferrag⁵³,
 J. Ferrando⁵³, V. Ferrara⁴², A. Ferrari¹⁶⁶, P. Ferrari¹⁰⁵, R. Ferrari^{119a},
 D.E. Ferreira de Lima⁵³, A. Ferrer¹⁶⁷, D. Ferrere⁴⁹, C. Ferretti⁸⁷,
 A. Ferretto Parodi^{50a,50b}, M. Fiascaris³¹, F. Fiedler⁸¹, A. Filipčič⁷⁴, F. Filthaut¹⁰⁴,
 M. Fincke-Keeler¹⁶⁹, M.C.N. Fiolhais^{124a,h}, L. Fiorini¹⁶⁷, A. Firan⁴⁰, G. Fischer⁴²,
 M.J. Fisher¹⁰⁹, M. Flechl⁴⁸, I. Fleck¹⁴¹, J. Fleckner⁸¹, P. Fleischmann¹⁷⁴,
 S. Fleischmann¹⁷⁵, T. Flick¹⁷⁵, A. Floderus⁷⁹, L.R. Flores Castillo¹⁷³, M.J. Flowerdew⁹⁹,
 T. Fonseca Martin¹⁷, A. Formica¹³⁶, A. Forti⁸², D. Fortin^{159a}, D. Fournier¹¹⁵,
 A.J. Fowler⁴⁵, H. Fox⁷¹, P. Francavilla¹², M. Franchini^{20a,20b}, S. Franchino^{119a,119b},
 D. Francis³⁰, T. Frank¹⁷², M. Franklin⁵⁷, S. Franz³⁰, M. Fraternali^{119a,119b}, S. Fratina¹²⁰,
 S.T. French²⁸, C. Friedrich⁴², F. Friedrich⁴⁴, R. Froeschl³⁰, D. Froidevaux³⁰, J.A. Frost²⁸,
 C. Fukunaga¹⁵⁶, E. Fullana Torregrosa³⁰, B.G. Fulsom¹⁴³, J. Fuster¹⁶⁷, C. Gabaldon³⁰,
 O. Gabizon¹⁷², T. Gadfort²⁵, S. Gadomski⁴⁹, G. Gagliardi^{50a,50b}, P. Gagnon⁶⁰,
 C. Galea⁹⁸, B. Galhardo^{124a}, E.J. Gallas¹¹⁸, V. Gallo¹⁷, B.J. Gallop¹²⁹, P. Gallus¹²⁵,
 K.K. Gan¹⁰⁹, Y.S. Gao^{143,e}, A. Gaponenko¹⁵, F. Garberson¹⁷⁶, M. Garcia-Sciveres¹⁵,
 C. García¹⁶⁷, J.E. García Navarro¹⁶⁷, R.W. Gardner³¹, N. Garelli³⁰, H. Garitaonandia¹⁰⁵,
 V. Garonne³⁰, C. Gatti⁴⁷, G. Gaudio^{119a}, B. Gaur¹⁴¹, L. Gauthier¹³⁶, P. Gauzzi^{132a,132b},
 I.L. Gavrilenko⁹⁴, C. Gay¹⁶⁸, G. Gaycken²¹, E.N. Gazis¹⁰, P. Ge^{33d}, Z. Gece¹⁶⁸,
 C.N.P. Gee¹²⁹, D.A.A. Geerts¹⁰⁵, Ch. Geich-Gimbel²¹, K. Gellerstedt^{146a,146b},

C. Gemme^{50a}, A. Gemmell⁵³, M.H. Genest⁵⁵, S. Gentile^{132a,132b}, M. George⁵⁴,
 S. George⁷⁶, P. Gerlach¹⁷⁵, A. Gershon¹⁵³, C. Geweniger^{58a}, H. Ghazlane^{135b},
 N. Ghodbane³⁴, B. Giacobbe^{20a}, S. Giagu^{132a,132b}, V. Giakoumopoulou⁹,
 V. Giangiobbe¹², F. Gianotti³⁰, B. Gibbard²⁵, A. Gibson¹⁵⁸, S.M. Gibson³⁰,
 M. Gilchriese¹⁵, D. Gillberg²⁹, A.R. Gillman¹²⁹, D.M. Gingrich^{3,d}, J. Ginzburg¹⁵³,
 N. Giokaris⁹, M.P. Giordani^{164c}, R. Giordano^{102a,102b}, F.M. Giorgi¹⁶, P. Giovannini⁹⁹,
 P.F. Giraud¹³⁶, D. Giugni^{89a}, M. Giunta⁹³, B.K. Gjelsten¹¹⁷, L.K. Gladilin⁹⁷,
 C. Glasman⁸⁰, J. Glatzer²¹, A. Glazov⁴², K.W. Glitza¹⁷⁵, G.L. Glonti⁶⁴, J.R. Goddard⁷⁵,
 J. Godfrey¹⁴², J. Godlewski³⁰, M. Goebel⁴², T. Göpfert⁴⁴, C. Goeringer⁸¹, C. Gössling⁴³,
 S. Goldfarb⁸⁷, T. Golling¹⁷⁶, A. Gomes^{124a,b}, L.S. Gomez Fajardo⁴², R. Gonçalo⁷⁶,
 J. Goncalves Pinto Firmino Da Costa⁴², L. Gonella²¹, S. González de la Hoz¹⁶⁷,
 G. Gonzalez Parra¹², M.L. Gonzalez Silva²⁷, S. Gonzalez-Sevilla⁴⁹, J.J. Goodson¹⁴⁸,
 L. Goossens³⁰, P.A. Gorbounov⁹⁵, H.A. Gordon²⁵, I. Gorelov¹⁰³, G. Gorfine¹⁷⁵,
 B. Gorini³⁰, E. Gorini^{72a,72b}, A. Gorišek⁷⁴, E. Gornicki³⁹, A.T. Goshaw⁶, M. Gosselink¹⁰⁵,
 M.I. Gostkin⁶⁴, I. Gough Eschrich¹⁶³, M. Gouighri^{135a}, D. Goujdami^{135c}, M.P. Goulette⁴⁹,
 A.G. Goussiou¹³⁸, C. Goy⁵, S. Gozpinar²³, I. Grabowska-Bold³⁸, P. Grafström^{20a,20b},
 K.-J. Grahn⁴², E. Gramstad¹¹⁷, F. Grancagnolo^{72a}, S. Grancagnolo¹⁶, V. Grassi¹⁴⁸,
 V. Gratchev¹²¹, N. Grau³⁵, H.M. Gray³⁰, J.A. Gray¹⁴⁸, E. Graziani^{134a},
 O.G. Grebenyuk¹²¹, T. Greenshaw⁷³, Z.D. Greenwood^{25,m}, K. Gregersen³⁶, I.M. Gregor⁴²,
 P. Grenier¹⁴³, J. Griffiths⁸, N. Grigalashvili⁶⁴, A.A. Grillo¹³⁷, S. Grinstein¹², Ph. Gris³⁴,
 Y.V. Grishkevich⁹⁷, J.-F. Grivaz¹¹⁵, E. Gross¹⁷², J. Grosse-Knetter⁵⁴, J. Groth-Jensen¹⁷²,
 K. Grybel¹⁴¹, D. Guest¹⁷⁶, C. Guicheney³⁴, E. Guido^{50a,50b}, S. Guindon⁵⁴, U. Gul⁵³,
 J. Gunther¹²⁵, B. Guo¹⁵⁸, J. Guo³⁵, P. Gutierrez¹¹¹, N. Guttman¹⁵³, O. Gutzwiller¹⁷³,
 C. Guyot¹³⁶, C. Gwenlan¹¹⁸, C.B. Gwilliam⁷³, A. Haas¹⁰⁸, S. Haas³⁰, C. Haber¹⁵,
 H.K. Hadavand⁸, D.R. Hadley¹⁸, P. Haefner²¹, F. Hahn³⁰, Z. Hajduk³⁹, H. Hakobyan¹⁷⁷,
 D. Hall¹¹⁸, K. Hamacher¹⁷⁵, P. Hamal¹¹³, K. Hamano⁸⁶, M. Hamer⁵⁴, A. Hamilton^{145b,p},
 S. Hamilton¹⁶¹, L. Han^{33b}, K. Hanagaki¹¹⁶, K. Hanawa¹⁶⁰, M. Hance¹⁵, C. Handel⁸¹,
 P. Hanke^{58a}, J.R. Hansen³⁶, J.B. Hansen³⁶, J.D. Hansen³⁶, P.H. Hansen³⁶, P. Hansson¹⁴³,
 K. Hara¹⁶⁰, T. Harenberg¹⁷⁵, S. Harkusha⁹⁰, D. Harper⁸⁷, R.D. Harrington⁴⁶,
 O.M. Harris¹³⁸, J. Hartert⁴⁸, F. Hartjes¹⁰⁵, T. Haruyama⁶⁵, A. Harvey⁵⁶, S. Hasegawa¹⁰¹,
 Y. Hasegawa¹⁴⁰, S. Hassani¹³⁶, S. Haug¹⁷, M. Hauschild³⁰, R. Hauser⁸⁸, M. Havranek²¹,
 C.M. Hawkes¹⁸, R.J. Hawkins³⁰, A.D. Hawkins⁷⁹, T. Hayakawa⁶⁶, T. Hayashi¹⁶⁰,
 D. Hayden⁷⁶, C.P. Hays¹¹⁸, H.S. Hayward⁷³, S.J. Haywood¹²⁹, S.J. Head¹⁸, V. Hedberg⁷⁹,
 L. Heelan⁸, S. Heim⁸⁸, B. Heinemann¹⁵, S. Heisterkamp³⁶, L. Helary²², C. Heller⁹⁸,
 M. Heller³⁰, S. Hellman^{146a,146b}, D. Hellmich²¹, C. Helsens¹², R.C.W. Henderson⁷¹,
 M. Henke^{58a}, A. Henrichs¹⁷⁶, A.M. Henriques Correia³⁰, S. Henrot-Versille¹¹⁵,
 C. Hensel⁵⁴, T. Henß¹⁷⁵, C.M. Hernandez⁸, Y. Hernández Jiménez¹⁶⁷, R. Herrberg¹⁶,
 G. Herten⁴⁸, R. Hertenberger⁹⁸, L. Hervas³⁰, G.G. Hesketh⁷⁷, N.P. Hessey¹⁰⁵,
 E. Higón-Rodriguez¹⁶⁷, J.C. Hill²⁸, K.H. Hiller⁴², S. Hillert²¹, S.J. Hillier¹⁸,
 I. Hinchliffe¹⁵, E. Hines¹²⁰, M. Hirose¹¹⁶, F. Hirsch⁴³, D. Hirschbuehl¹⁷⁵, J. Hobbs¹⁴⁸,
 N. Hod¹⁵³, M.C. Hodgkinson¹³⁹, P. Hodgson¹³⁹, A. Hoecker³⁰, M.R. Hoferkamp¹⁰³,
 J. Hoffman⁴⁰, D. Hoffmann⁸³, M. Hohlfeld⁸¹, M. Holder¹⁴¹, S.O. Holmgren^{146a},
 T. Holy¹²⁷, J.L. Holzbauer⁸⁸, T.M. Hong¹²⁰, L. Hooft van Huysduynen¹⁰⁸, S. Horner⁴⁸,

J-Y. Hostachy⁵⁵, S. Hou¹⁵¹, A. Hoummada^{135a}, J. Howard¹¹⁸, J. Howarth⁸², I. Hristova¹⁶,
 J. Hrivnac¹¹⁵, T. Hryn'ova⁵, P.J. Hsu⁸¹, S.-C. Hsu¹⁵, D. Hu³⁵, Z. Hubacek¹²⁷,
 F. Hubaut⁸³, F. Huegging²¹, A. Huettmann⁴², T.B. Huffman¹¹⁸, E.W. Hughes³⁵,
 G. Hughes⁷¹, M. Huhtinen³⁰, M. Hurwitz¹⁵, N. Huseynov^{64,q}, J. Huston⁸⁸, J. Huth⁵⁷,
 G. Iacobucci⁴⁹, G. Iakovidis¹⁰, M. Ibbotson⁸², I. Ibragimov¹⁴¹, L. Iconomidou-Fayard¹¹⁵,
 J. Idarraga¹¹⁵, P. Iengo^{102a}, O. Igonkina¹⁰⁵, Y. Ikegami⁶⁵, M. Ikeno⁶⁵, D. Iliadis¹⁵⁴,
 N. Ilic¹⁵⁸, T. Ince⁹⁹, P. Ioannou⁹, M. Iodice^{134a}, K. Iordanidou⁹, V. Ippolito^{132a,132b},
 A. Irles Quiles¹⁶⁷, C. Isaksson¹⁶⁶, M. Ishino⁶⁷, M. Ishitsuka¹⁵⁷, R. Ishmukhametov¹⁰⁹,
 C. Issever¹¹⁸, S. Istin^{19a}, A.V. Ivashin¹²⁸, W. Iwanski³⁹, H. Iwasaki⁶⁵, J.M. Izen⁴¹,
 V. Izzo^{102a}, B. Jackson¹²⁰, J.N. Jackson⁷³, P. Jackson¹, M.R. Jaekel³⁰, V. Jain⁶⁰,
 K. Jakobs⁴⁸, S. Jakobsen³⁶, T. Jakoubek¹²⁵, J. Jakubek¹²⁷, D.O. Jamin¹⁵¹, D.K. Jana¹¹¹,
 E. Jansen⁷⁷, H. Jansen³⁰, J. Janssen²¹, A. Jantsch⁹⁹, M. Janus⁴⁸, G. Jarlskog⁷⁹,
 L. Jeanty⁵⁷, I. Jen-La Plante³¹, D. Jennens⁸⁶, P. Jenni³⁰, A.E. Loevschall-Jensen³⁶,
 P. Jež³⁶, S. Jézéquel⁵, M.K. Jha^{20a}, H. Ji¹⁷³, W. Ji⁸¹, J. Jia¹⁴⁸, Y. Jiang^{33b},
 M. Jimenez Belenguer⁴², S. Jin^{33a}, O. Jinnouchi¹⁵⁷, M.D. Joergensen³⁶, D. Joffe⁴⁰,
 M. Johansen^{146a,146b}, K.E. Johansson^{146a}, P. Johansson¹³⁹, S. Johnert⁴², K.A. Johns⁷,
 K. Jon-And^{146a,146b}, G. Jones¹⁷⁰, R.W.L. Jones⁷¹, T.J. Jones⁷³, C. Joram³⁰,
 P.M. Jorge^{124a}, K.D. Joshi⁸², J. Jovicevic¹⁴⁷, T. Jovin^{13b}, X. Ju¹⁷³, C.A. Jung⁴³,
 R.M. Jungst³⁰, V. Juraneck¹²⁵, P. Jussel⁶¹, A. Juste Rozas¹², S. Kabana¹⁷, M. Kaci¹⁶⁷,
 A. Kaczmarek³⁹, P. Kadlecik³⁶, M. Kado¹¹⁵, H. Kagan¹⁰⁹, M. Kagan⁵⁷,
 E. Kajomovitz¹⁵², S. Kalinin¹⁷⁵, L.V. Kalinovskaya⁶⁴, S. Kama⁴⁰, N. Kanaya¹⁵⁵,
 M. Kaneda³⁰, S. Kaneti²⁸, T. Kanno¹⁵⁷, V.A. Kantserov⁹⁶, J. Kanzaki⁶⁵, B. Kaplan¹⁰⁸,
 A. Kapliy³¹, J. Kaplon³⁰, D. Kar⁵³, M. Karagounis²¹, K. Karakostas¹⁰, M. Karnevskiy⁴²,
 V. Kartvelishvili⁷¹, A.N. Karyukhin¹²⁸, L. Kashif¹⁷³, G. Kasieczka^{58b}, R.D. Kass¹⁰⁹,
 A. Kastanas¹⁴, M. Kataoka⁵, Y. Kataoka¹⁵⁵, E. Katsoufis¹⁰, J. Katzy⁴², V. Kaushik⁷,
 K. Kawagoe⁶⁹, T. Kawamoto¹⁵⁵, G. Kawamura⁸¹, M.S. Kayl¹⁰⁵, S. Kazama¹⁵⁵,
 V.A. Kazanin¹⁰⁷, M.Y. Kazarinov⁶⁴, R. Keeler¹⁶⁹, P.T. Keener¹²⁰, R. Kehoe⁴⁰, M. Keil⁵⁴,
 G.D. Kekelidze⁶⁴, J.S. Keller¹³⁸, M. Kenyon⁵³, O. Kepka¹²⁵, N. Kerschen³⁰,
 B.P. Kerševan⁷⁴, S. Kersten¹⁷⁵, K. Kessoku¹⁵⁵, J. Keung¹⁵⁸, F. Khalil-zada¹¹,
 H. Khandanyan^{146a,146b}, A. Khanov¹¹², D. Kharchenko⁶⁴, A. Khodinov⁹⁶, A. Khomich^{58a},
 T.J. Khoo²⁸, G. Khoriauli²¹, A. Khoroshilov¹⁷⁵, V. Khovanskiy⁹⁵, E. Khramov⁶⁴,
 J. Khubua^{51b}, H. Kim^{146a,146b}, S.H. Kim¹⁶⁰, N. Kimura¹⁷¹, O. Kind¹⁶, B.T. King⁷³,
 M. King⁶⁶, R.S.B. King¹¹⁸, J. Kirk¹²⁹, A.E. Kiryunin⁹⁹, T. Kishimoto⁶⁶,
 D. Kisielewska³⁸, T. Kitamura⁶⁶, T. Kittelmann¹²³, K. Kiuchi¹⁶⁰, E. Kladiva^{144b},
 M. Klein⁷³, U. Klein⁷³, K. Kleinknecht⁸¹, M. Klemetti⁸⁵, A. Klier¹⁷², P. Klimek^{146a,146b},
 A. Klimentov²⁵, R. Klingenberg⁴³, J.A. Klinger⁸², E.B. Klinkby³⁶, T. Klioutchnikova³⁰,
 P.F. Klok¹⁰⁴, S. Klous¹⁰⁵, E.-E. Kluge^{58a}, T. Kluge⁷³, P. Kluit¹⁰⁵, S. Kluth⁹⁹,
 E. Kneringer⁶¹, E.B.F.G. Knoops⁸³, A. Knue⁵⁴, B.R. Ko⁴⁵, T. Kobayashi¹⁵⁵, M. Kobel⁴⁴,
 M. Kocian¹⁴³, P. Kodys¹²⁶, K. Köneke³⁰, A.C. König¹⁰⁴, S. Koenig⁸¹, L. Köpke⁸¹,
 F. Koetsveld¹⁰⁴, P. Koevesarki²¹, T. Koffas²⁹, E. Koffeman¹⁰⁵, L.A. Kogan¹¹⁸,
 S. Kohlmann¹⁷⁵, F. Kohn⁵⁴, Z. Kohout¹²⁷, T. Kohriki⁶⁵, T. Koi¹⁴³, G.M. Kolachev^{107,*},
 H. Kolanoski¹⁶, V. Kolesnikov⁶⁴, I. Koletsou^{89a}, J. Koll⁸⁸, A.A. Komar⁹⁴, Y. Komori¹⁵⁵,
 T. Kondo⁶⁵, T. Kono^{42,r}, A.I. Kononov⁴⁸, R. Konoplich^{108,s}, N. Konstantinidis⁷⁷,

R. Kopeliansky¹⁵², S. Koperny³⁸, K. Korcyl³⁹, K. Kordas¹⁵⁴, A. Korn¹¹⁸, A. Korol¹⁰⁷,
 I. Korolkov¹², E.V. Korolkova¹³⁹, V.A. Korotkov¹²⁸, O. Kortner⁹⁹, S. Kortner⁹⁹,
 V.V. Kostyukhin²¹, S. Kotov⁹⁹, V.M. Kotov⁶⁴, A. Kotwal⁴⁵, C. Kourkoumelis⁹,
 V. Kouskoura¹⁵⁴, A. Koutsman^{159a}, R. Kowalewski¹⁶⁹, T.Z. Kowalski³⁸, W. Kozanecki¹³⁶,
 A.S. Kozhin¹²⁸, V. Kral¹²⁷, V.A. Kramarenko⁹⁷, G. Kramberger⁷⁴, M.W. Krasny⁷⁸,
 A. Krasznahorkay¹⁰⁸, J.K. Kraus²¹, S. Kreiss¹⁰⁸, F. Krejci¹²⁷, J. Kretzschmar⁷³,
 N. Krieger⁵⁴, P. Krieger¹⁵⁸, K. Kroeninger⁵⁴, H. Kroha⁹⁹, J. Kroll¹²⁰, J. Kroseberg²¹,
 J. Krstic^{13a}, U. Kruchonak⁶⁴, H. Krüger²¹, T. Kruker¹⁷, N. Krumnack⁶³,
 Z.V. Krumshteyn⁶⁴, M.K. Kruse⁴⁵, T. Kubota⁸⁶, S. Kудay^{4a}, S. Kuehn⁴⁸, A. Kugel^{58c},
 T. Kuhl⁴², D. Kuhn⁶¹, V. Kukhtin⁶⁴, Y. Kulchitsky⁹⁰, S. Kuleshov^{32b}, C. Kummer⁹⁸,
 M. Kuna⁷⁸, J. Kunkle¹²⁰, A. Kupco¹²⁵, H. Kurashige⁶⁶, M. Kurata¹⁶⁰, Y.A. Kurochkin⁹⁰,
 V. Kus¹²⁵, E.S. Kuwertz¹⁴⁷, M. Kuze¹⁵⁷, J. Kvita¹⁴², R. Kwee¹⁶, A. La Rosa⁴⁹,
 L. La Rotonda^{37a,37b}, L. Labarga⁸⁰, J. Labbe⁵, S. Lablak^{135a}, C. Lacasta¹⁶⁷,
 F. Lacava^{132a,132b}, J. Lacey²⁹, H. Lacker¹⁶, D. Lacour⁷⁸, V.R. Lacuesta¹⁶⁷, E. Ladygin⁶⁴,
 R. Lafaye⁵, B. Laforge⁷⁸, T. Lagouri¹⁷⁶, S. Lai⁴⁸, E. Laisne⁵⁵, L. Lambourne⁷⁷,
 C.L. Lampen⁷, W. Lampl⁷, E. Lancon¹³⁶, U. Landgraf⁴⁸, M.P.J. Landon⁷⁵, V.S. Lang^{58a},
 C. Lange⁴², A.J. Lankford¹⁶³, F. Lanni²⁵, K. Lantzsch¹⁷⁵, S. Laplace⁷⁸, C. Lapoire²¹,
 J.F. Laporte¹³⁶, T. Lari^{89a}, A. Lerner¹¹⁸, M. Lassnig³⁰, P. Laurelli⁴⁷, V. Lavorini^{37a,37b},
 W. Lavrijsen¹⁵, P. Laycock⁷³, O. Le Dortz⁷⁸, E. Le Guirriec⁸³, E. Le Menedeu¹²,
 T. LeCompte⁶, F. Ledroit-Guillon⁵⁵, H. Lee¹⁰⁵, J.S.H. Lee¹¹⁶, S.C. Lee¹⁵¹, L. Lee¹⁷⁶,
 M. Lefebvre¹⁶⁹, M. Legendre¹³⁶, F. Legger⁹⁸, C. Leggett¹⁵, M. Lehmacher²¹,
 G. Lehmann Miotto³⁰, X. Lei⁷, M.A.L. Leite^{24d}, R. Leitner¹²⁶, D. Lellouch¹⁷²,
 B. Lemmer⁵⁴, V. Lendermann^{58a}, K.J.C. Leney^{145b}, T. Lenz¹⁰⁵, G. Lenzen¹⁷⁵, B. Lenzi³⁰,
 K. Leonhardt⁴⁴, S. Leontsinis¹⁰, F. Lepold^{58a}, C. Leroy⁹³, J-R. Lessard¹⁶⁹, C.G. Lester²⁸,
 C.M. Lester¹²⁰, J. Levêque⁵, D. Levin⁸⁷, L.J. Levinson¹⁷², A. Lewis¹¹⁸, G.H. Lewis¹⁰⁸,
 A.M. Leyko²¹, M. Leyton¹⁶, B. Li^{33b}, B. Li⁸³, H. Li¹⁴⁸, H.L. Li³¹, S. Li^{33b,t}, X. Li⁸⁷,
 Z. Liang^{118,u}, H. Liao³⁴, B. Liberti^{133a}, P. Lichard³⁰, M. Lichtnecker⁹⁸, K. Lie¹⁶⁵,
 W. Liebig¹⁴, C. Limbach²¹, A. Limosani⁸⁶, M. Limper⁶², S.C. Lin^{151,v}, F. Linde¹⁰⁵,
 J.T. Linnemann⁸⁸, E. Lipeles¹²⁰, A. Lipniacka¹⁴, T.M. Liss¹⁶⁵, D. Lissauer²⁵, A. Lister⁴⁹,
 A.M. Litke¹³⁷, C. Liu²⁹, D. Liu¹⁵¹, H. Liu⁸⁷, J.B. Liu⁸⁷, L. Liu⁸⁷, M. Liu^{33b}, Y. Liu^{33b},
 M. Livan^{119a,119b}, S.S.A. Livermore¹¹⁸, A. Lleres⁵⁵, J. Llorente Merino⁸⁰, S.L. Lloyd⁷⁵,
 E. Lobodzinska⁴², P. Loch⁷, W.S. Lockman¹³⁷, T. Loddenkoetter²¹, F.K. Loebinger⁸²,
 A. Loginov¹⁷⁶, C.W. Loh¹⁶⁸, T. Lohse¹⁶, K. Lohwasser⁴⁸, M. Lokajicek¹²⁵,
 V.P. Lombardo⁵, R.E. Long⁷¹, L. Lopes^{124a}, D. Lopez Mateos⁵⁷, J. Lorenz⁹⁸,
 N. Lorenzo Martinez¹¹⁵, M. Losada¹⁶², P. Loscutoff¹⁵, F. Lo Sterzo^{132a,132b},
 M.J. Losty^{159a,*}, X. Lou⁴¹, A. Lounis¹¹⁵, K.F. Loureiro¹⁶², J. Love⁶, P.A. Love⁷¹,
 A.J. Lowe^{143,e}, F. Lu^{33a}, H.J. Lubatti¹³⁸, C. Luci^{132a,132b}, A. Lucotte⁵⁵, A. Ludwig⁴⁴,
 D. Ludwig⁴², I. Ludwig⁴⁸, J. Ludwig⁴⁸, F. Luehring⁶⁰, G. Luijckx¹⁰⁵, W. Lukas⁶¹,
 L. Luminari^{132a}, E. Lund¹¹⁷, B. Lund-Jensen¹⁴⁷, B. Lundberg⁷⁹, J. Lundberg^{146a,146b},
 O. Lundberg^{146a,146b}, J. Lundquist³⁶, M. Lungwitz⁸¹, D. Lynn²⁵, E. Lytken⁷⁹, H. Ma²⁵,
 L.L. Ma¹⁷³, G. Maccarrone⁴⁷, A. Macchiolo⁹⁹, B. Maček⁷⁴, J. Machado Miguens^{124a},
 D. Macina³⁰, R. Mackeprang³⁶, R.J. Madaras¹⁵, H.J. Maddocks⁷¹, W.F. Mader⁴⁴,
 R. Maenner^{58c}, T. Maeno²⁵, P. Mättig¹⁷⁵, S. Mättig⁴², L. Magnoni¹⁶³, E. Magradze⁵⁴,

K. Mahboubi⁴⁸, J. Mahlstedt¹⁰⁵, S. Mahmoud⁷³, G. Mahout¹⁸, C. Maiani¹³⁶,
 C. Maidantchik^{24a}, A. Maio^{124a,b}, S. Majewski²⁵, Y. Makida⁶⁵, N. Makovec¹¹⁵, P. Mal¹³⁶,
 B. Malaescu³⁰, Pa. Malecki³⁹, P. Malecki³⁹, V.P. Maleev¹²¹, F. Malek⁵⁵, U. Mallik⁶²,
 D. Malon⁶, C. Malone¹⁴³, S. Maltezos¹⁰, V. Malyshev¹⁰⁷, S. Malyukov³⁰,
 R. Mameghani⁹⁸, J. Mamuzic^{13b}, A. Manabe⁶⁵, L. Mandelli^{89a}, I. Mandić⁷⁴,
 R. Mandrysch¹⁶, J. Maneira^{124a}, A. Manfredini⁹⁹, L. Manhaes de Andrade Filho^{24b},
 J.A. Manjarres Ramos¹³⁶, A. Mann⁵⁴, P.M. Manning¹³⁷, A. Manousakis-Katsikakis⁹,
 B. Mansoulie¹³⁶, A. Mapelli³⁰, L. Mapelli³⁰, L. March¹⁶⁷, J.F. Marchand²⁹,
 F. Marchese^{133a,133b}, G. Marchiori⁷⁸, M. Marcisovsky¹²⁵, C.P. Marino¹⁶⁹,
 F. Marroquin^{24a}, Z. Marshall³⁰, L.F. Marti¹⁷, S. Marti-Garcia¹⁶⁷, B. Martin³⁰,
 B. Martin⁸⁸, J.P. Martin⁹³, T.A. Martin¹⁸, V.J. Martin⁴⁶, B. Martin dit Latour⁴⁹,
 S. Martin-Haugh¹⁴⁹, M. Martinez¹², V. Martinez Outschoorn⁵⁷, A.C. Martyniuk¹⁶⁹,
 M. Marx⁸², F. Marzano^{132a}, A. Marzin¹¹¹, L. Masetti⁸¹, T. Mashimo¹⁵⁵,
 R. Mashinistov⁹⁴, J. Masik⁸², A.L. Maslennikov¹⁰⁷, I. Massa^{20a,20b}, G. Massaro¹⁰⁵,
 N. Massol⁵, P. Mastrandrea¹⁴⁸, A. Mastroberardino^{37a,37b}, T. Masubuchi¹⁵⁵,
 P. Matricon¹¹⁵, H. Matsunaga¹⁵⁵, T. Matsushita⁶⁶, C. Mattravers^{118,c}, J. Maurer⁸³,
 S.J. Maxfield⁷³, A. Mayne¹³⁹, R. Mazini¹⁵¹, M. Mazur²¹, L. Mazzaferro^{133a,133b},
 M. Mazzanti^{89a}, J. Mc Donald⁸⁵, S.P. Mc Kee⁸⁷, A. McCarn¹⁶⁵, R.L. McCarthy¹⁴⁸,
 T.G. McCarthy²⁹, N.A. McCubbin¹²⁹, K.W. McFarlane^{56,*}, J.A. Mcfayden¹³⁹,
 G. Mchedlidze^{51b}, T. Mclaughlan¹⁸, S.J. McMahon¹²⁹, R.A. McPherson^{169,k}, A. Meade⁸⁴,
 J. Mechnich¹⁰⁵, M. Mechtel¹⁷⁵, M. Medinnis⁴², S. Meehan³¹, R. Meera-Lebbai¹¹¹,
 T. Meguro¹¹⁶, S. Mehlhase³⁶, A. Mehta⁷³, K. Meier^{58a}, B. Meirose⁷⁹, C. Melachrinou³¹,
 B.R. Mellado Garcia¹⁷³, F. Meloni^{89a,89b}, L. Mendoza Navas¹⁶², Z. Meng^{151,w},
 A. Mengarelli^{20a,20b}, S. Menke⁹⁹, E. Meoni¹⁶¹, K.M. Mercurio⁵⁷, P. Mermoud⁴⁹,
 L. Merola^{102a,102b}, C. Meroni^{89a}, F.S. Merritt³¹, H. Merritt¹⁰⁹, A. Messina^{30,x},
 J. Metcalfe²⁵, A.S. Mete¹⁶³, C. Meyer⁸¹, C. Meyer³¹, J-P. Meyer¹³⁶, J. Meyer¹⁷⁴,
 J. Meyer⁵⁴, S. Michal³⁰, L. Micu^{26a}, R.P. Middleton¹²⁹, S. Migas⁷³, L. Mijović¹³⁶,
 G. Mikenberg¹⁷², M. Mikestikova¹²⁵, M. Mikuž⁷⁴, D.W. Miller³¹, R.J. Miller⁸⁸,
 W.J. Mills¹⁶⁸, C. Mills⁵⁷, A. Milov¹⁷², D.A. Milstead^{146a,146b}, D. Milstein¹⁷²,
 A.A. Minaenko¹²⁸, M. Miñano Moya¹⁶⁷, I.A. Minashvili⁶⁴, A.I. Mincer¹⁰⁸, B. Mindur³⁸,
 M. Mineev⁶⁴, Y. Ming¹⁷³, L.M. Mir¹², G. Mirabelli^{132a}, J. Mitrevski¹³⁷, V.A. Mitsou¹⁶⁷,
 S. Mitsui⁶⁵, P.S. Miyagawa¹³⁹, J.U. Mjörnmark⁷⁹, T. Moa^{146a,146b}, V. Moeller²⁸,
 K. Mönig⁴², N. Möser²¹, S. Mohapatra¹⁴⁸, W. Mohr⁴⁸, R. Moles-Valls¹⁶⁷, A. Molfetas³⁰,
 J. Monk⁷⁷, E. Monnier⁸³, J. Montejo Berlingen¹², F. Monticelli⁷⁰, S. Monzani^{20a,20b},
 R.W. Moore³, G.F. Moorhead⁸⁶, C. Mora Herrera⁴⁹, A. Moraes⁵³, N. Morange¹³⁶,
 J. Morel⁵⁴, G. Morello^{37a,37b}, D. Moreno⁸¹, M. Moreno Llácer¹⁶⁷, P. Morettini^{50a},
 M. Morgenstern⁴⁴, M. Morii⁵⁷, A.K. Morley³⁰, G. Mornacchi³⁰, J.D. Morris⁷⁵,
 L. Morvaj¹⁰¹, H.G. Moser⁹⁹, M. Mosidze^{51b}, J. Moss¹⁰⁹, R. Mount¹⁴³, E. Mountricha^{10,y},
 S.V. Mouraviev^{94,*}, E.J.W. Moyses⁸⁴, F. Mueller^{58a}, J. Mueller¹²³, K. Mueller²¹,
 T.A. Müller⁹⁸, T. Mueller⁸¹, D. Muenstermann³⁰, Y. Munwes¹⁵³, W.J. Murray¹²⁹,
 I. Mussche¹⁰⁵, E. Musto^{102a,102b}, A.G. Myagkov¹²⁸, M. Myska¹²⁵, O. Nackenhorst⁵⁴,
 J. Nadal¹², K. Nagai¹⁶⁰, R. Nagai¹⁵⁷, K. Nagano⁶⁵, A. Nagarkar¹⁰⁹, Y. Nagasaka⁵⁹,
 M. Nagel⁹⁹, A.M. Nairz³⁰, Y. Nakahama³⁰, K. Nakamura¹⁵⁵, T. Nakamura¹⁵⁵,

I. Nakano¹¹⁰, G. Nanava²¹, A. Napier¹⁶¹, R. Narayan^{58b}, M. Nash^{77,c}, T. Nattermann²¹,
 T. Naumann⁴², G. Navarro¹⁶², H.A. Neal⁸⁷, P.Yu. Nechaeva⁹⁴, T.J. Neep⁸²,
 A. Negri^{119a,119b}, G. Negri³⁰, M. Negrini^{20a}, S. Nektarijevic⁴⁹, A. Nelson¹⁶³,
 T.K. Nelson¹⁴³, S. Nemecek¹²⁵, P. Nemethy¹⁰⁸, A.A. Nepomuceno^{24a}, M. Nessi^{30,z},
 M.S. Neubauer¹⁶⁵, M. Neumann¹⁷⁵, A. Neusiedl⁸¹, R.M. Neves¹⁰⁸, P. Nevski²⁵,
 F.M. Newcomer¹²⁰, P.R. Newman¹⁸, V. Nguyen Thi Hong¹³⁶, R.B. Nickerson¹¹⁸,
 R. Nicolaidou¹³⁶, B. Nicquevert³⁰, F. Niedercorn¹¹⁵, J. Nielsen¹³⁷, N. Nikiforou³⁵,
 A. Nikiforov¹⁶, V. Nikolaenko¹²⁸, I. Nikolic-Audit⁷⁸, K. Nikolics⁴⁹, K. Nikolopoulos¹⁸,
 H. Nilsen⁴⁸, P. Nilsson⁸, Y. Ninomiya¹⁵⁵, A. Nisati^{132a}, R. Nisius⁹⁹, T. Nobe¹⁵⁷,
 L. Nodulman⁶, M. Nomachi¹¹⁶, I. Nomidis¹⁵⁴, S. Norberg¹¹¹, M. Nordberg³⁰,
 P.R. Norton¹²⁹, J. Novakova¹²⁶, M. Nozaki⁶⁵, L. Nozka¹¹³, I.M. Nugent^{159a},
 A.-E. Nuncio-Quiroz²¹, G. Nunes Hanninger⁸⁶, T. Nunnemann⁹⁸, E. Nurse⁷⁷,
 B.J. O'Brien⁴⁶, D.C. O'Neil¹⁴², V. O'Shea⁵³, L.B. Oakes⁹⁸, F.G. Oakham^{29,d},
 H. Oberlack⁹⁹, J. Ocariz⁷⁸, A. Ochi⁶⁶, S. Oda⁶⁹, S. Odaka⁶⁵, J. Odier⁸³, H. Ogren⁶⁰,
 A. Oh⁸², S.H. Oh⁴⁵, C.C. Ohm³⁰, T. Ohshima¹⁰¹, W. Okamura¹¹⁶, H. Okawa²⁵,
 Y. Okumura³¹, T. Okuyama¹⁵⁵, A. Olariu^{26a}, A.G. Olchevski⁶⁴, S.A. Olivares Pino^{32a},
 M. Oliveira^{124a,h}, D. Oliveira Damazio²⁵, E. Oliver Garcia¹⁶⁷, D. Olivito¹²⁰,
 A. Olszewski³⁹, J. Olszowska³⁹, A. Onofre^{124a,aa}, P.U.E. Onyisi³¹, C.J. Oram^{159a},
 M.J. Oreglia³¹, Y. Oren¹⁵³, D. Orestano^{134a,134b}, N. Orlando^{72a,72b}, I. Orlov¹⁰⁷,
 C. Oropeza Barrera⁵³, R.S. Orr¹⁵⁸, B. Osculati^{50a,50b}, R. Ospanov¹²⁰, C. Osuna¹²,
 G. Otero y Garzon²⁷, J.P. Ottersbach¹⁰⁵, M. Ouchrif^{135d}, E.A. Ouellette¹⁶⁹,
 F. Ould-Saada¹¹⁷, A. Ouraou¹³⁶, Q. Ouyang^{33a}, A. Ovcharova¹⁵, M. Owen⁸², S. Owen¹³⁹,
 V.E. Ozcan^{19a}, N. Ozturk⁸, A. Pacheco Pages¹², C. Padilla Aranda¹², S. Pagan Griso¹⁵,
 E. Paganis¹³⁹, C. Pahl⁹⁹, F. Paige²⁵, P. Pais⁸⁴, K. Pajchel¹¹⁷, G. Palacino^{159b},
 C.P. Paleari⁷, S. Palestini³⁰, D. Pallin³⁴, A. Palma^{124a}, J.D. Palmer¹⁸, Y.B. Pan¹⁷³,
 E. Panagiotopoulou¹⁰, J.G. Panduro Vazquez⁷⁶, P. Pani¹⁰⁵, N. Panikashvili⁸⁷,
 S. Panitkin²⁵, D. Pantea^{26a}, A. Papadelis^{146a}, Th.D. Papadopoulou¹⁰, A. Paramonov⁶,
 D. Paredes Hernandez³⁴, W. Park^{25,ab}, M.A. Parker²⁸, F. Parodi^{50a,50b}, J.A. Parsons³⁵,
 U. Parzefall⁴⁸, S. Pashapour⁵⁴, E. Pasqualucci^{132a}, S. Passaggio^{50a}, A. Passeri^{134a},
 F. Pastore^{134a,134b,*}, Fr. Pastore⁷⁶, G. Pásztor^{49,ac}, S. Patariaia¹⁷⁵, N. Patel¹⁵⁰,
 J.R. Pater⁸², S. Patricelli^{102a,102b}, T. Pauly³⁰, M. Pecsny^{144a}, S. Pedraza Lopez¹⁶⁷,
 M.I. Pedraza Morales¹⁷³, S.V. Peleganchuk¹⁰⁷, D. Pelikan¹⁶⁶, H. Peng^{33b}, B. Penning³¹,
 A. Penson³⁵, J. Penwell⁶⁰, M. Perantoni^{24a}, K. Perez^{35,ad}, T. Perez Cavalcanti⁴²,
 E. Perez Codina^{159a}, M.T. Pérez García-Estañ¹⁶⁷, V. Perez Reale³⁵, L. Perini^{89a,89b},
 H. Pernegger³⁰, R. Perrino^{72a}, P. Perrodo⁵, V.D. Peshekhonov⁶⁴, K. Peters³⁰,
 B.A. Petersen³⁰, J. Petersen³⁰, T.C. Petersen³⁶, E. Petit⁵, A. Petridis¹⁵⁴, C. Petridou¹⁵⁴,
 E. Petrolo^{132a}, F. Petrucci^{134a,134b}, D. Petschull⁴², M. Petteni¹⁴², R. Pezoa^{32b}, A. Phan⁸⁶,
 P.W. Phillips¹²⁹, G. Piacquadio³⁰, A. Picazio⁴⁹, E. Piccaro⁷⁵, M. Piccinini^{20a,20b},
 S.M. Piec⁴², R. Piegai²⁷, D.T. Pignotti¹⁰⁹, J.E. Pilcher³¹, A.D. Pilkington⁸²,
 J. Pina^{124a,b}, M. Pinamonti^{164a,164c}, A. Pinder¹¹⁸, J.L. Pinfeld³, B. Pinto^{124a},
 C. Pizio^{89a,89b}, M. Plamondon¹⁶⁹, M.-A. Pleier²⁵, E. Plotnikova⁶⁴, A. Poblaguev²⁵,
 S. Poddar^{58a}, F. Podlyski³⁴, R. Poettgen⁸¹, L. Poggioli¹¹⁵, D. Pohl²¹, M. Pohl⁴⁹,
 G. Polesello^{119a}, A. Policicchio^{37a,37b}, A. Polini^{20a}, J. Poll⁷⁵, V. Polychronakos²⁵,

D. Pomeroy²³, K. Pommès³⁰, L. Pontecorvo^{132a}, B.G. Pope⁸⁸, G.A. Popenciu^{26a},
 D.S. Popovic^{13a}, A. Poppleton³⁰, X. Portell Bueso³⁰, G.E. Pospelov⁹⁹, S. Pospisil¹²⁷,
 I.N. Potrap⁹⁹, C.J. Potter¹⁴⁹, C.T. Potter¹¹⁴, G. Poulard³⁰, J. Poveda⁶⁰,
 V. Pozdnyakov⁶⁴, R. Prabhu⁷⁷, P. Pralavorio⁸³, A. Pranko¹⁵, S. Prasad³⁰, R. Pravahan²⁵,
 S. Prell⁶³, K. Pretzl¹⁷, D. Price⁶⁰, J. Price⁷³, L.E. Price⁶, D. Prieur¹²³, M. Primavera^{72a},
 K. Prokofiev¹⁰⁸, F. Prokoshin^{32b}, S. Protopopescu²⁵, J. Proudfoot⁶, X. Prudent⁴⁴,
 M. Przybycien³⁸, H. Przysieznik⁵, S. Psoroulas²¹, E. Ptacek¹¹⁴, E. Pueschel⁸⁴,
 J. Purdham⁸⁷, M. Purohit^{25,ab}, P. Puzo¹¹⁵, Y. Pylypchenko⁶², J. Qian⁸⁷, A. Quadt⁵⁴,
 D.R. Quarrie¹⁵, W.B. Quayle¹⁷³, F. Quinonez^{32a}, M. Raas¹⁰⁴, V. Radeka²⁵, V. Radescu⁴²,
 P. Radloff¹¹⁴, F. Ragusa^{89a,89b}, G. Rahal¹⁷⁸, A.M. Rahimi¹⁰⁹, D. Rahm²⁵,
 S. Rajagopalan²⁵, M. Rammensee⁴⁸, M. Rammes¹⁴¹, A.S. Randle-Conde⁴⁰,
 K. Randrianarivony²⁹, F. Rauscher⁹⁸, T.C. Rave⁴⁸, M. Raymond³⁰, A.L. Read¹¹⁷,
 D.M. Rebuffi^{119a,119b}, A. Redelbach¹⁷⁴, G. Redlinger²⁵, R. Reece¹²⁰, K. Reeves⁴¹,
 A. Reinsch¹¹⁴, I. Reisinger⁴³, C. Rembser³⁰, Z.L. Ren¹⁵¹, A. Renaud¹¹⁵, M. Rescigno^{132a},
 S. Resconi^{89a}, B. Resende¹³⁶, P. Reznicek⁹⁸, R. Rezvani¹⁵⁸, R. Richter⁹⁹,
 E. Richter-Was^{5,ae}, M. Ridel⁷⁸, M. Rijpstra¹⁰⁵, M. Rijssenbeek¹⁴⁸, A. Rimoldi^{119a,119b},
 L. Rinaldi^{20a}, R.R. Rios⁴⁰, I. Riu¹², G. Rivoltella^{89a,89b}, F. Rizatdinova¹¹², E. Rizvi⁷⁵,
 S.H. Robertson^{85,k}, A. Robichaud-Veronneau¹¹⁸, D. Robinson²⁸, J.E.M. Robinson⁸²,
 A. Robson⁵³, J.G. Rocha de Lima¹⁰⁶, C. Roda^{122a,122b}, D. Roda Dos Santos³⁰, A. Roe⁵⁴,
 S. Roe³⁰, O. Røhne¹¹⁷, S. Rolli¹⁶¹, A. Romaniouk⁹⁶, M. Romano^{20a,20b}, G. Romeo²⁷,
 E. Romero Adam¹⁶⁷, N. Rompotis¹³⁸, L. Roos⁷⁸, E. Ros¹⁶⁷, S. Rosati^{132a}, K. Rosbach⁴⁹,
 A. Rose¹⁴⁹, M. Rose⁷⁶, G.A. Rosenbaum¹⁵⁸, E.I. Rosenberg⁶³, P.L. Rosendahl¹⁴,
 O. Rosenthal¹⁴¹, L. Rosselet⁴⁹, V. Rossetti¹², E. Rossi^{132a,132b}, L.P. Rossi^{50a},
 M. Rotaru^{26a}, I. Roth¹⁷², J. Rothberg¹³⁸, D. Rousseau¹¹⁵, C.R. Royon¹³⁶, A. Rozanov⁸³,
 Y. Rozen¹⁵², X. Ruan^{33a,af}, F. Rubbo¹², I. Rubinskiy⁴², N. Ruckstuhl¹⁰⁵, V.I. Rud⁹⁷,
 C. Rudolph⁴⁴, G. Rudolph⁶¹, F. Rühr⁷, A. Ruiz-Martinez⁶³, L. Rumyantsev⁶⁴,
 Z. Rurikova⁴⁸, N.A. Rusakovich⁶⁴, A. Ruschke⁹⁸, J.P. Rutherford⁷, P. Ruzicka¹²⁵,
 Y.F. Ryabov¹²¹, M. Rybar¹²⁶, G. Rybkin¹¹⁵, N.C. Ryder¹¹⁸, A.F. Saavedra¹⁵⁰,
 I. Sadeh¹⁵³, H.F.W. Sadrozinski¹³⁷, R. Sadykov⁶⁴, F. Safai Tehrani^{132a}, H. Sakamoto¹⁵⁵,
 G. Salamanna⁷⁵, A. Salamon^{133a}, M. Saleem¹¹¹, D. Salek³⁰, D. Salihagic⁹⁹,
 A. Salnikov¹⁴³, J. Salt¹⁶⁷, B.M. Salvachua Ferrando⁶, D. Salvatore^{37a,37b}, F. Salvatore¹⁴⁹,
 A. Salvucci¹⁰⁴, A. Salzburger³⁰, D. Sampsonidis¹⁵⁴, B.H. Samset¹¹⁷, A. Sanchez^{102a,102b},
 V. Sanchez Martinez¹⁶⁷, H. Sandaker¹⁴, H.G. Sander⁸¹, M.P. Sanders⁹⁸, M. Sandhoff¹⁷⁵,
 T. Sandoval²⁸, C. Sandoval¹⁶², R. Sandstroem⁹⁹, D.P.C. Sankey¹²⁹, A. Sansoni⁴⁷,
 C. Santamarina Rios⁸⁵, C. Santoni³⁴, R. Santonico^{133a,133b}, H. Santos^{124a},
 I. Santoyo Castillo¹⁴⁹, J.G. Saraiva^{124a}, T. Sarangi¹⁷³, E. Sarkisyan-Grinbaum⁸,
 F. Sarri^{122a,122b}, G. Sartisohn¹⁷⁵, O. Sasaki⁶⁵, Y. Sasaki¹⁵⁵, N. Sasao⁶⁷,
 I. Satsounkevitch⁹⁰, G. Sauvage^{5,*}, E. Sauvan⁵, J.B. Sauvan¹¹⁵, P. Savard^{158,d},
 V. Savinov¹²³, D.O. Savu³⁰, L. Sawyer^{25,m}, D.H. Saxon⁵³, J. Saxon¹²⁰, C. Sbarra^{20a},
 A. Sbrizzi^{20a,20b}, D.A. Scannicchio¹⁶³, M. Scarcella¹⁵⁰, J. Schaarschmidt¹¹⁵, P. Schacht⁹⁹,
 D. Schaefer¹²⁰, U. Schäfer⁸¹, A. Schaelicke⁴⁶, S. Schaepe²¹, S. Schaezel^{58b},
 A.C. Schaffer¹¹⁵, D. Schaile⁹⁸, R.D. Schamberger¹⁴⁸, A.G. Schamov¹⁰⁷, V. Scharf^{58a},
 V.A. Schegelsky¹²¹, D. Scheirich⁸⁷, M. Schernau¹⁶³, M.I. Scherzer³⁵, C. Schiavi^{50a,50b},

J. Schieck⁹⁸, M. Schioppa^{37a,37b}, S. Schlenker³⁰, E. Schmidt⁴⁸, K. Schmieden²¹,
 C. Schmitt⁸¹, S. Schmitt^{58b}, B. Schneider¹⁷, U. Schnoor⁴⁴, L. Schoeffel¹³⁶,
 A. Schoening^{58b}, A.L.S. Schorlemmer⁵⁴, M. Schott³⁰, D. Schouten^{159a}, J. Schovancova¹²⁵,
 M. Schram⁸⁵, C. Schroeder⁸¹, N. Schroer^{58c}, M.J. Schultens²¹, J. Schultes¹⁷⁵,
 H.-C. Schultz-Coulon^{58a}, H. Schulz¹⁶, M. Schumacher⁴⁸, B.A. Schumm¹³⁷, Ph. Schune¹³⁶,
 C. Schwanenberger⁸², A. Schwartzman¹⁴³, Ph. Schwegler⁹⁹, Ph. Schwemling⁷⁸,
 R. Schwienhorst⁸⁸, R. Schwierz⁴⁴, J. Schwindling¹³⁶, T. Schwindt²¹, M. Schwoerer⁵,
 F.G. Sciacca¹⁷, G. Sciolla²³, W.G. Scott¹²⁹, J. Searcy¹¹⁴, G. Sedov⁴², E. Sedykh¹²¹,
 S.C. Seidel¹⁰³, A. Seiden¹³⁷, F. Seifert⁴⁴, J.M. Seixas^{24a}, G. Sekhniaidze^{102a},
 S.J. Sekula⁴⁰, K.E. Selbach⁴⁶, D.M. Seliverstov¹²¹, B. Sellden^{146a}, G. Sellers⁷³,
 M. Seman^{144b}, N. Semprini-Cesari^{20a,20b}, C. Serfon⁹⁸, L. Serin¹¹⁵, L. Serkin⁵⁴,
 R. Seuster^{159a}, H. Severini¹¹¹, A. Sfyrla³⁰, E. Shabalina⁵⁴, M. Shamim¹¹⁴, L.Y. Shan^{33a},
 J.T. Shank²², Q.T. Shao⁸⁶, M. Shapiro¹⁵, P.B. Shatalov⁹⁵, K. Shaw^{164a,164c},
 D. Sherman¹⁷⁶, P. Sherwood⁷⁷, S. Shimizu¹⁰¹, M. Shimojima¹⁰⁰, T. Shin⁵⁶,
 M. Shiyakova⁶⁴, A. Shmeleva⁹⁴, M.J. Shochet³¹, D. Short¹¹⁸, S. Shrestha⁶³, E. Shulga⁹⁶,
 M.A. Shupe⁷, P. Sicho¹²⁵, A. Sidoti^{132a}, F. Siegert⁴⁸, Dj. Sijacki^{13a}, O. Silbert¹⁷²,
 J. Silva^{124a}, Y. Silver¹⁵³, D. Silverstein¹⁴³, S.B. Silverstein^{146a}, V. Simak¹²⁷,
 O. Simard¹³⁶, Lj. Simic^{13a}, S. Simion¹¹⁵, E. Simioni⁸¹, B. Simmons⁷⁷,
 R. Simoniello^{89a,89b}, M. Simonyan³⁶, P. Sinervo¹⁵⁸, N.B. Sinev¹¹⁴, V. Sipica¹⁴¹,
 G. Siragusa¹⁷⁴, A. Sircar²⁵, A.N. Sisakyan^{64,*}, S.Yu. Sivoklov⁹⁷, J. Sjölin^{146a,146b},
 T.B. Sjursen¹⁴, L.A. Skinnari¹⁵, H.P. Skottowe⁵⁷, K. Skovpen¹⁰⁷, P. Skubic¹¹¹,
 M. Slater¹⁸, T. Slavicek¹²⁷, K. Sliwa¹⁶¹, V. Smakhtin¹⁷², B.H. Smart⁴⁶, L. Smestad¹¹⁷,
 S.Yu. Smirnov⁹⁶, Y. Smirnov⁹⁶, L.N. Smirnova⁹⁷, O. Smirnova⁷⁹, B.C. Smith⁵⁷,
 D. Smith¹⁴³, K.M. Smith⁵³, M. Smizanska⁷¹, K. Smolek¹²⁷, A.A. Snesarev⁹⁴,
 S.W. Snow⁸², J. Snow¹¹¹, S. Snyder²⁵, R. Sobie^{169,k}, J. Sodomka¹²⁷, A. Soffer¹⁵³,
 C.A. Solans¹⁶⁷, M. Solar¹²⁷, J. Solc¹²⁷, E.Yu. Soldatov⁹⁶, U. Soldevila¹⁶⁷,
 E. Solfaroli Camillocci^{132a,132b}, A.A. Solodkov¹²⁸, O.V. Solovyanov¹²⁸, V. Solovyev¹²¹,
 N. Soni¹, V. Sopko¹²⁷, B. Sopko¹²⁷, M. Sosebee⁸, R. Soualah^{164a,164c}, A. Soukharev¹⁰⁷,
 S. Spagnolo^{72a,72b}, F. Spanò⁷⁶, R. Spighi^{20a}, G. Spigo³⁰, R. Spiwoks³⁰, M. Spousta^{126,ag},
 T. Spreitzer¹⁵⁸, B. Spurlock⁸, R.D. St. Denis⁵³, J. Stahlman¹²⁰, R. Stamen^{58a},
 E. Stanecka³⁹, R.W. Stanek⁶, C. Stanescu^{134a}, M. Stanescu-Bellu⁴², M.M. Stanitzki⁴²,
 S. Stapnes¹¹⁷, E.A. Starchenko¹²⁸, J. Stark⁵⁵, P. Staroba¹²⁵, P. Starovoitov⁴²,
 R. Staszewski³⁹, A. Staude⁹⁸, P. Stavina^{144a,*}, G. Steele⁵³, P. Steinbach⁴⁴, P. Steinberg²⁵,
 I. Stekl¹²⁷, B. Stelzer¹⁴², H.J. Stelzer⁸⁸, O. Stelzer-Chilton^{159a}, H. Stenzel⁵², S. Stern⁹⁹,
 G.A. Stewart³⁰, J.A. Stillings²¹, M.C. Stockton⁸⁵, K. Stoerig⁴⁸, G. Stoicea^{26a},
 S. Stonjek⁹⁹, P. Strachota¹²⁶, A.R. Stradling⁸, A. Straessner⁴⁴, J. Strandberg¹⁴⁷,
 S. Strandberg^{146a,146b}, A. Strandlie¹¹⁷, M. Strang¹⁰⁹, E. Strauss¹⁴³, M. Strauss¹¹¹,
 P. Striznec^{144b}, R. Ströhmer¹⁷⁴, D.M. Strom¹¹⁴, J.A. Strong^{76,*}, R. Stroynowski⁴⁰,
 B. Stugu¹⁴, I. Stumer^{25,*}, J. Stupak¹⁴⁸, P. Sturm¹⁷⁵, N.A. Styles⁴², D.A. Soh^{151,u},
 D. Su¹⁴³, HS. Subramania³, R. Subramaniam²⁵, A. Succurro¹², Y. Sugaya¹¹⁶, C. Suhr¹⁰⁶,
 M. Suk¹²⁶, V.V. Sulin⁹⁴, S. Sultansoy^{4d}, T. Sumida⁶⁷, X. Sun⁵⁵, J.E. Sundermann⁴⁸,
 K. Suruliz¹³⁹, G. Susinno^{37a,37b}, M.R. Sutton¹⁴⁹, Y. Suzuki⁶⁵, Y. Suzuki⁶⁶, M. Svatos¹²⁵,
 S. Swedish¹⁶⁸, I. Sykora^{144a}, T. Sykora¹²⁶, J. Sánchez¹⁶⁷, D. Ta¹⁰⁵, K. Tackmann⁴²,

A. Taffard¹⁶³, R. Tafirout^{159a}, N. Taiblum¹⁵³, Y. Takahashi¹⁰¹, H. Takai²⁵,
 R. Takashima⁶⁸, H. Takeda⁶⁶, T. Takeshita¹⁴⁰, Y. Takubo⁶⁵, M. Talby⁸³,
 A. Talyshev^{107,f}, M.C. Tamsett²⁵, K.G. Tan⁸⁶, J. Tanaka¹⁵⁵, R. Tanaka¹¹⁵, S. Tanaka¹³¹,
 S. Tanaka⁶⁵, A.J. Tanasijczuk¹⁴², K. Tani⁶⁶, N. Tannoury⁸³, S. Tapprogge⁸¹, D. Tardif¹⁵⁸,
 S. Tarem¹⁵², F. Tarrade²⁹, G.F. Tartarelli^{89a}, P. Tas¹²⁶, M. Tasevsky¹²⁵, E. Tassi^{37a,37b},
 Y. Tayalati^{135d}, C. Taylor⁷⁷, F.E. Taylor⁹², G.N. Taylor⁸⁶, W. Taylor^{159b},
 M. Teinturier¹¹⁵, F.A. Teischinger³⁰, M. Teixeira Dias Castanheira⁷⁵, P. Teixeira-Dias⁷⁶,
 K.K. Temming⁴⁸, H. Ten Kate³⁰, P.K. Teng¹⁵¹, S. Terada⁶⁵, K. Terashi¹⁵⁵, J. Terron⁸⁰,
 M. Testa⁴⁷, R.J. Teuscher^{158,k}, J. Therhaag²¹, T. Theveneaux-Pelzer⁷⁸, S. Thoma⁴⁸,
 J.P. Thomas¹⁸, E.N. Thompson³⁵, P.D. Thompson¹⁸, P.D. Thompson¹⁵⁸,
 A.S. Thompson⁵³, L.A. Thomsen³⁶, E. Thomson¹²⁰, M. Thomson²⁸, W.M. Thong⁸⁶,
 R.P. Thun⁸⁷, F. Tian³⁵, M.J. Tibbetts¹⁵, T. Tic¹²⁵, V.O. Tikhomirov⁹⁴,
 Y.A. Tikhonov^{107.f}, S. Timoshenko⁹⁶, E. Tiouchichine⁸³, P. Tipton¹⁷⁶, S. Tisserant⁸³,
 T. Todorov⁵, S. Todorova-Nova¹⁶¹, B. Toggerson¹⁶³, J. Tojo⁶⁹, S. Tokár^{144a},
 K. Tokushuku⁶⁵, K. Tollefson⁸⁸, M. Tomoto¹⁰¹, L. Tompkins³¹, K. Toms¹⁰³,
 A. Tonoyan¹⁴, C. Topfel¹⁷, N.D. Topilin⁶⁴, E. Torrence¹¹⁴, H. Torres⁷⁸,
 E. Torró Pastor¹⁶⁷, J. Toth^{83,ac}, F. Touchard⁸³, D.R. Tovey¹³⁹, T. Trefzger¹⁷⁴,
 L. Tremblet³⁰, A. Tricoli³⁰, I.M. Trigger^{159a}, S. Trincaz-Duvoid⁷⁸, M.F. Tripiana⁷⁰,
 N. Triplett²⁵, W. Trischuk¹⁵⁸, B. Trocmé⁵⁵, C. Troncon^{89a}, M. Trottier-McDonald¹⁴²,
 P. True⁸⁸, M. Trzebinski³⁹, A. Trzupke³⁹, C. Tsarouchas³⁰, J.C-L. Tseng¹¹⁸,
 M. Tsiakiris¹⁰⁵, P.V. Tsiarehka⁹⁰, D. Tsiou^{5,ah}, G. Tsipolitis¹⁰, S. Tsiskaridze¹²,
 V. Tsiskaridze⁴⁸, E.G. Tskhadadze^{51a}, I.I. Tsukerman⁹⁵, V. Tsulaia¹⁵, J.-W. Tsung²¹,
 S. Tsuno⁶⁵, D. Tsybychev¹⁴⁸, A. Tua¹³⁹, A. Tudorache^{26a}, V. Tudorache^{26a},
 J.M. Tuggle³¹, M. Turala³⁹, D. Turecek¹²⁷, I. Turk Cakir^{4e}, E. Turlay¹⁰⁵, R. Turra^{89a,89b},
 P.M. Tuts³⁵, A. Tykhonov⁷⁴, M. Tylmad^{146a,146b}, M. Tyndel¹²⁹, G. Tzanakos⁹,
 K. Uchida²¹, I. Ueda¹⁵⁵, R. Ueno²⁹, M. Ugland¹⁴, M. Uhlenbrock²¹, M. Uhrmacher⁵⁴,
 F. Ukegawa¹⁶⁰, G. Unal³⁰, A. Undrus²⁵, G. Unel¹⁶³, Y. Unno⁶⁵, D. Urbaniec³⁵,
 P. Urquijo²¹, G. Usai⁸, M. Uslenghi^{119a,119b}, L. Vacavant⁸³, V. Vacek¹²⁷, B. Vachon⁸⁵,
 S. Vahsen¹⁵, J. Valenta¹²⁵, S. Valentinetti^{20a,20b}, A. Valero¹⁶⁷, S. Valkar¹²⁶,
 E. Valladolid Gallego¹⁶⁷, S. Vallecorsa¹⁵², J.A. Valls Ferrer¹⁶⁷, R. Van Berg¹²⁰,
 P.C. Van Der Deijl¹⁰⁵, R. van der Geer¹⁰⁵, H. van der Graaf¹⁰⁵, R. Van Der Leeuw¹⁰⁵,
 E. van der Poel¹⁰⁵, D. van der Ster³⁰, N. van Eldik³⁰, P. van Gemmeren⁶,
 I. van Vulpen¹⁰⁵, M. Vanadia⁹⁹, W. Vandelli³⁰, A. Vaniachine⁶, P. Vankov⁴²,
 F. Vannucci⁷⁸, R. Vari^{132a}, T. Varol⁸⁴, D. Varouchas¹⁵, A. Vartapetian⁸, K.E. Varvell¹⁵⁰,
 V.I. Vassilakopoulos⁵⁶, F. Vazeille³⁴, T. Vazquez Schroeder⁵⁴, G. Vegni^{89a,89b},
 J.J. Veillet¹¹⁵, F. Veloso^{124a}, R. Veness³⁰, S. Veneziano^{132a}, A. Ventura^{72a,72b},
 D. Ventura⁸⁴, M. Venturi⁴⁸, N. Venturi¹⁵⁸, V. Vercesi^{119a}, M. Verducci¹³⁸, W. Verkerke¹⁰⁵,
 J.C. Vermeulen¹⁰⁵, A. Vest⁴⁴, M.C. Vetterli^{142,d}, I. Vichou¹⁶⁵, T. Vickey^{145b,ai},
 O.E. Vickey Boeriu^{145b}, G.H.A. Viehhauser¹¹⁸, S. Viel¹⁶⁸, M. Villa^{20a,20b},
 M. Villaplana Perez¹⁶⁷, E. Vilucchi⁴⁷, M.G. Vincter²⁹, E. Vinek³⁰, V.B. Vinogradov⁶⁴,
 M. Virchaux^{136,*}, J. Virzi¹⁵, O. Vitells¹⁷², M. Viti⁴², I. Vivarelli⁴⁸, F. Vives Vaque³,
 S. Vlachos¹⁰, D. Vladoiu⁹⁸, M. Vlasak¹²⁷, A. Vogel²¹, P. Vokac¹²⁷, G. Volpi⁴⁷, M. Volpi⁸⁶,
 G. Volpini^{89a}, H. von der Schmitt⁹⁹, H. von Radziewski⁴⁸, E. von Toerne²¹, V. Vorobel¹²⁶,

V. Vorwerk¹², M. Vos¹⁶⁷, R. Voss³⁰, T.T. Voss¹⁷⁵, J.H. Vosseveld⁷³, N. Vranjes¹³⁶, M. Vranjes Milosavljevic¹⁰⁵, V. Vrba¹²⁵, M. Vreeswijk¹⁰⁵, T. Vu Anh⁴⁸, R. Vuillermet³⁰, I. Vukotic³¹, W. Wagner¹⁷⁵, P. Wagner¹²⁰, H. Wahlen¹⁷⁵, S. Wahrmund⁴⁴, J. Wakabayashi¹⁰¹, S. Walch⁸⁷, J. Walder⁷¹, R. Walker⁹⁸, W. Walkowiak¹⁴¹, R. Wall¹⁷⁶, P. Waller⁷³, B. Walsh¹⁷⁶, C. Wang⁴⁵, H. Wang¹⁷³, H. Wang^{33b,aj}, J. Wang¹⁵¹, J. Wang⁵⁵, R. Wang¹⁰³, S.M. Wang¹⁵¹, T. Wang²¹, A. Warburton⁸⁵, C.P. Ward²⁸, D.R. Wardrope⁷⁷, M. Warsinsky⁴⁸, A. Washbrook⁴⁶, C. Wasicki⁴², I. Watanabe⁶⁶, P.M. Watkins¹⁸, A.T. Watson¹⁸, I.J. Watson¹⁵⁰, M.F. Watson¹⁸, G. Watts¹³⁸, S. Watts⁸², A.T. Waugh¹⁵⁰, B.M. Waugh⁷⁷, M.S. Weber¹⁷, J.S. Webster³¹, A.R. Weidberg¹¹⁸, P. Weigell⁹⁹, J. Weingarten⁵⁴, C. Weiser⁴⁸, P.S. Wells³⁰, T. Wenaus²⁵, D. Wendland¹⁶, Z. Weng^{151,u}, T. Wengler³⁰, S. Wenig³⁰, N. Wermes²¹, M. Werner⁴⁸, P. Werner³⁰, M. Werth¹⁶³, M. Wessels^{58a}, J. Wetter¹⁶¹, C. Weydert⁵⁵, K. Whalen²⁹, A. White⁸, M.J. White⁸⁶, S. White^{122a,122b}, S.R. Whitehead¹¹⁸, D. Whiteson¹⁶³, D. Whittington⁶⁰, F. Wicek¹¹⁵, D. Wicke¹⁷⁵, F.J. Wickens¹²⁹, W. Wiedenmann¹⁷³, M. Wielers¹²⁹, P. Wienemann²¹, C. Wiglesworth⁷⁵, L.A.M. Wiik-Fuchs²¹, P.A. Wijeratne⁷⁷, A. Wildauer⁹⁹, M.A. Wildt^{42,r}, I. Wilhelm¹²⁶, H.G. Wilkens³⁰, J.Z. Will⁹⁸, E. Williams³⁵, H.H. Williams¹²⁰, W. Willis³⁵, S. Willocq⁸⁴, J.A. Wilson¹⁸, M.G. Wilson¹⁴³, A. Wilson⁸⁷, I. Wingerter-Seez⁵, S. Winkelmann⁴⁸, F. Winklmeier³⁰, M. Wittgen¹⁴³, S.J. Wollstadt⁸¹, M.W. Wolter³⁹, H. Wolters^{124a,h}, W.C. Wong⁴¹, G. Wooden⁸⁷, B.K. Wosiek³⁹, J. Wotschack³⁰, M.J. Woudstra⁸², K.W. Wozniak³⁹, K. Wraight⁵³, M. Wright⁵³, B. Wrona⁷³, S.L. Wu¹⁷³, X. Wu⁴⁹, Y. Wu^{33b,ak}, E. Wulf³⁵, B.M. Wynne⁴⁶, S. Xella³⁶, M. Xiao¹³⁶, S. Xie⁴⁸, C. Xu^{33b,y}, D. Xu¹³⁹, L. Xu^{33b}, B. Yabsley¹⁵⁰, S. Yacoob^{145a,al}, M. Yamada⁶⁵, H. Yamaguchi¹⁵⁵, A. Yamamoto⁶⁵, K. Yamamoto⁶³, S. Yamamoto¹⁵⁵, T. Yamamura¹⁵⁵, T. Yamanaka¹⁵⁵, T. Yamazaki¹⁵⁵, Y. Yamazaki⁶⁶, Z. Yan²², H. Yang⁸⁷, U.K. Yang⁸², Y. Yang¹⁰⁹, Z. Yang^{146a,146b}, S. Yanush⁹¹, L. Yao^{33a}, Y. Yao¹⁵, Y. Yasu⁶⁵, G.V. Ybeles Smit¹³⁰, J. Ye⁴⁰, S. Ye²⁵, M. Yilmaz^{4c}, R. Yoosoofmiya¹²³, K. Yorita¹⁷¹, R. Yoshida⁶, K. Yoshihara¹⁵⁵, C. Young¹⁴³, C.J. Young¹¹⁸, S. Youssef²², D. Yu²⁵, J. Yu⁸, J. Yu¹¹², L. Yuan⁶⁶, A. Yurkewicz¹⁰⁶, B. Zabinski³⁹, R. Zaidan⁶², A.M. Zaitsev¹²⁸, Z. Zajacova³⁰, L. Zanello^{132a,132b}, D. Zanzi⁹⁹, A. Zaytsev²⁵, C. Zeitnitz¹⁷⁵, M. Zeman¹²⁵, A. Zemla³⁹, C. Zender²¹, O. Zenin¹²⁸, T. Ženiš^{144a}, Z. Zinonos^{122a,122b}, D. Zerwas¹¹⁵, G. Zevi della Porta⁵⁷, D. Zhang^{33b,aj}, H. Zhang⁸⁸, J. Zhang⁶, X. Zhang^{33d}, Z. Zhang¹¹⁵, L. Zhao¹⁰⁸, Z. Zhao^{33b}, A. Zhemchugov⁶⁴, J. Zhong¹¹⁸, B. Zhou⁸⁷, N. Zhou¹⁶³, Y. Zhou¹⁵¹, C.G. Zhu^{33d}, H. Zhu⁴², J. Zhu⁸⁷, Y. Zhu^{33b}, X. Zhuang⁹⁸, V. Zhuravlov⁹⁹, A. Zibell⁹⁸, D. Zieminska⁶⁰, N.I. Zimin⁶⁴, R. Zimmermann²¹, S. Zimmermann²¹, S. Zimmermann⁴⁸, M. Ziolkowski¹⁴¹, R. Zitoun⁵, L. Živković³⁵, V.V. Zmouchko^{128,*}, G. Zobernig¹⁷³, A. Zoccoli^{20a,20b}, M. zur Nedden¹⁶, V. Zutshi¹⁰⁶, L. Zwalinski³⁰.

¹ School of Chemistry and Physics, University of Adelaide, Adelaide, Australia

² Physics Department, SUNY Albany, Albany NY, United States of America

³ Department of Physics, University of Alberta, Edmonton AB, Canada

⁴ (a) Department of Physics, Ankara University, Ankara; (b) Department of Physics, Dumlupinar University, Kutahya; (c) Department of Physics, Gazi University, Ankara; (d) Division of Physics, TOBB University of Economics and Technology, Ankara; (e) Turkish

Atomic Energy Authority, Ankara, Turkey

⁵ LAPP, CNRS/IN2P3 and Université de Savoie, Annecy-le-Vieux, France

⁶ High Energy Physics Division, Argonne National Laboratory, Argonne IL, United States of America

⁷ Department of Physics, University of Arizona, Tucson AZ, United States of America

⁸ Department of Physics, The University of Texas at Arlington, Arlington TX, United States of America

⁹ Physics Department, University of Athens, Athens, Greece

¹⁰ Physics Department, National Technical University of Athens, Zografou, Greece

¹¹ Institute of Physics, Azerbaijan Academy of Sciences, Baku, Azerbaijan

¹² Institut de Física d'Altes Energies and Departament de Física de la Universitat Autònoma de Barcelona and ICREA, Barcelona, Spain

¹³ ^(a) Institute of Physics, University of Belgrade, Belgrade; ^(b) Vinca Institute of Nuclear Sciences, University of Belgrade, Belgrade, Serbia

¹⁴ Department for Physics and Technology, University of Bergen, Bergen, Norway

¹⁵ Physics Division, Lawrence Berkeley National Laboratory and University of California, Berkeley CA, United States of America

¹⁶ Department of Physics, Humboldt University, Berlin, Germany

¹⁷ Albert Einstein Center for Fundamental Physics and Laboratory for High Energy Physics, University of Bern, Bern, Switzerland

¹⁸ School of Physics and Astronomy, University of Birmingham, Birmingham, United Kingdom

¹⁹ ^(a) Department of Physics, Bogazici University, Istanbul; ^(b) Division of Physics, Dogus University, Istanbul; ^(c) Department of Physics Engineering, Gaziantep University, Gaziantep; ^(d) Department of Physics, Istanbul Technical University, Istanbul, Turkey

²⁰ ^(a) INFN Sezione di Bologna; ^(b) Dipartimento di Fisica, Università di Bologna, Bologna, Italy

²¹ Physikalisches Institut, University of Bonn, Bonn, Germany

²² Department of Physics, Boston University, Boston MA, United States of America

²³ Department of Physics, Brandeis University, Waltham MA, United States of America

²⁴ ^(a) Universidade Federal do Rio De Janeiro COPPE/EE/IF, Rio de Janeiro; ^(b) Federal University of Juiz de Fora (UFJF), Juiz de Fora; ^(c) Federal University of Sao Joao del Rei (UFSJ), Sao Joao del Rei; ^(d) Instituto de Fisica, Universidade de Sao Paulo, Sao Paulo, Brazil

²⁵ Physics Department, Brookhaven National Laboratory, Upton NY, United States of America

²⁶ ^(a) National Institute of Physics and Nuclear Engineering, Bucharest; ^(b) University Politehnica Bucharest, Bucharest; ^(c) West University in Timisoara, Timisoara, Romania

²⁷ Departamento de Física, Universidad de Buenos Aires, Buenos Aires, Argentina

²⁸ Cavendish Laboratory, University of Cambridge, Cambridge, United Kingdom

²⁹ Department of Physics, Carleton University, Ottawa ON, Canada

³⁰ CERN, Geneva, Switzerland

³¹ Enrico Fermi Institute, University of Chicago, Chicago IL, United States of America

- ³² (a) Departamento de Física, Pontificia Universidad Católica de Chile, Santiago; (b) Departamento de Física, Universidad Técnica Federico Santa María, Valparaíso, Chile
- ³³ (a) Institute of High Energy Physics, Chinese Academy of Sciences, Beijing; (b) Department of Modern Physics, University of Science and Technology of China, Anhui; (c) Department of Physics, Nanjing University, Jiangsu; (d) School of Physics, Shandong University, Shandong, China
- ³⁴ Laboratoire de Physique Corpusculaire, Clermont Université and Université Blaise Pascal and CNRS/IN2P3, Clermont-Ferrand, France
- ³⁵ Nevis Laboratory, Columbia University, Irvington NY, United States of America
- ³⁶ Niels Bohr Institute, University of Copenhagen, Kobenhavn, Denmark
- ³⁷ (a) INFN Gruppo Collegato di Cosenza; (b) Dipartimento di Fisica, Università della Calabria, Arcavata di Rende, Italy
- ³⁸ AGH University of Science and Technology, Faculty of Physics and Applied Computer Science, Krakow, Poland
- ³⁹ The Henryk Niewodniczanski Institute of Nuclear Physics, Polish Academy of Sciences, Krakow, Poland
- ⁴⁰ Physics Department, Southern Methodist University, Dallas TX, United States of America
- ⁴¹ Physics Department, University of Texas at Dallas, Richardson TX, United States of America
- ⁴² DESY, Hamburg and Zeuthen, Germany
- ⁴³ Institut für Experimentelle Physik IV, Technische Universität Dortmund, Dortmund, Germany
- ⁴⁴ Institut für Kern- und Teilchenphysik, Technical University Dresden, Dresden, Germany
- ⁴⁵ Department of Physics, Duke University, Durham NC, United States of America
- ⁴⁶ SUPA - School of Physics and Astronomy, University of Edinburgh, Edinburgh, United Kingdom
- ⁴⁷ INFN Laboratori Nazionali di Frascati, Frascati, Italy
- ⁴⁸ Fakultät für Mathematik und Physik, Albert-Ludwigs-Universität, Freiburg, Germany
- ⁴⁹ Section de Physique, Université de Genève, Geneva, Switzerland
- ⁵⁰ (a) INFN Sezione di Genova; (b) Dipartimento di Fisica, Università di Genova, Genova, Italy
- ⁵¹ (a) E. Andronikashvili Institute of Physics, Iv. Javakhishvili Tbilisi State University, Tbilisi; (b) High Energy Physics Institute, Tbilisi State University, Tbilisi, Georgia
- ⁵² II Physikalisches Institut, Justus-Liebig-Universität Giessen, Giessen, Germany
- ⁵³ SUPA - School of Physics and Astronomy, University of Glasgow, Glasgow, United Kingdom
- ⁵⁴ II Physikalisches Institut, Georg-August-Universität, Göttingen, Germany
- ⁵⁵ Laboratoire de Physique Subatomique et de Cosmologie, Université Joseph Fourier and CNRS/IN2P3 and Institut National Polytechnique de Grenoble, Grenoble, France
- ⁵⁶ Department of Physics, Hampton University, Hampton VA, United States of America
- ⁵⁷ Laboratory for Particle Physics and Cosmology, Harvard University, Cambridge MA,

United States of America

⁵⁸ (a) Kirchhoff-Institut für Physik, Ruprecht-Karls-Universität Heidelberg, Heidelberg;

(b) Physikalisches Institut, Ruprecht-Karls-Universität Heidelberg, Heidelberg; (c) ZITI Institut für technische Informatik, Ruprecht-Karls-Universität Heidelberg, Mannheim, Germany

⁵⁹ Faculty of Applied Information Science, Hiroshima Institute of Technology, Hiroshima, Japan

⁶⁰ Department of Physics, Indiana University, Bloomington IN, United States of America

⁶¹ Institut für Astro- und Teilchenphysik, Leopold-Franzens-Universität, Innsbruck, Austria

⁶² University of Iowa, Iowa City IA, United States of America

⁶³ Department of Physics and Astronomy, Iowa State University, Ames IA, United States of America

⁶⁴ Joint Institute for Nuclear Research, JINR Dubna, Dubna, Russia

⁶⁵ KEK, High Energy Accelerator Research Organization, Tsukuba, Japan

⁶⁶ Graduate School of Science, Kobe University, Kobe, Japan

⁶⁷ Faculty of Science, Kyoto University, Kyoto, Japan

⁶⁸ Kyoto University of Education, Kyoto, Japan

⁶⁹ Department of Physics, Kyushu University, Fukuoka, Japan

⁷⁰ Instituto de Física La Plata, Universidad Nacional de La Plata and CONICET, La Plata, Argentina

⁷¹ Physics Department, Lancaster University, Lancaster, United Kingdom

⁷² (a) INFN Sezione di Lecce; (b) Dipartimento di Matematica e Fisica, Università del Salento, Lecce, Italy

⁷³ Oliver Lodge Laboratory, University of Liverpool, Liverpool, United Kingdom

⁷⁴ Department of Physics, Jožef Stefan Institute and University of Ljubljana, Ljubljana, Slovenia

⁷⁵ School of Physics and Astronomy, Queen Mary University of London, London, United Kingdom

⁷⁶ Department of Physics, Royal Holloway University of London, Surrey, United Kingdom

⁷⁷ Department of Physics and Astronomy, University College London, London, United Kingdom

⁷⁸ Laboratoire de Physique Nucléaire et de Hautes Energies, UPMC and Université Paris-Diderot and CNRS/IN2P3, Paris, France

⁷⁹ Fysiska institutionen, Lunds universitet, Lund, Sweden

⁸⁰ Departamento de Física Teórica C-15, Universidad Autónoma de Madrid, Madrid, Spain

⁸¹ Institut für Physik, Universität Mainz, Mainz, Germany

⁸² School of Physics and Astronomy, University of Manchester, Manchester, United Kingdom

⁸³ CPPM, Aix-Marseille Université and CNRS/IN2P3, Marseille, France

⁸⁴ Department of Physics, University of Massachusetts, Amherst MA, United States of America

- ⁸⁵ Department of Physics, McGill University, Montreal QC, Canada
- ⁸⁶ School of Physics, University of Melbourne, Victoria, Australia
- ⁸⁷ Department of Physics, The University of Michigan, Ann Arbor MI, United States of America
- ⁸⁸ Department of Physics and Astronomy, Michigan State University, East Lansing MI, United States of America
- ⁸⁹ ^(a) INFN Sezione di Milano; ^(b) Dipartimento di Fisica, Università di Milano, Milano, Italy
- ⁹⁰ B.I. Stepanov Institute of Physics, National Academy of Sciences of Belarus, Minsk, Republic of Belarus
- ⁹¹ National Scientific and Educational Centre for Particle and High Energy Physics, Minsk, Republic of Belarus
- ⁹² Department of Physics, Massachusetts Institute of Technology, Cambridge MA, United States of America
- ⁹³ Group of Particle Physics, University of Montreal, Montreal QC, Canada
- ⁹⁴ P.N. Lebedev Institute of Physics, Academy of Sciences, Moscow, Russia
- ⁹⁵ Institute for Theoretical and Experimental Physics (ITEP), Moscow, Russia
- ⁹⁶ Moscow Engineering and Physics Institute (MEPhI), Moscow, Russia
- ⁹⁷ Skobeltsyn Institute of Nuclear Physics, Lomonosov Moscow State University, Moscow, Russia
- ⁹⁸ Fakultät für Physik, Ludwig-Maximilians-Universität München, München, Germany
- ⁹⁹ Max-Planck-Institut für Physik (Werner-Heisenberg-Institut), München, Germany
- ¹⁰⁰ Nagasaki Institute of Applied Science, Nagasaki, Japan
- ¹⁰¹ Graduate School of Science and Kobayashi-Maskawa Institute, Nagoya University, Nagoya, Japan
- ¹⁰² ^(a) INFN Sezione di Napoli; ^(b) Dipartimento di Scienze Fisiche, Università di Napoli, Napoli, Italy
- ¹⁰³ Department of Physics and Astronomy, University of New Mexico, Albuquerque NM, United States of America
- ¹⁰⁴ Institute for Mathematics, Astrophysics and Particle Physics, Radboud University Nijmegen/Nikhef, Nijmegen, Netherlands
- ¹⁰⁵ Nikhef National Institute for Subatomic Physics and University of Amsterdam, Amsterdam, Netherlands
- ¹⁰⁶ Department of Physics, Northern Illinois University, DeKalb IL, United States of America
- ¹⁰⁷ Budker Institute of Nuclear Physics, SB RAS, Novosibirsk, Russia
- ¹⁰⁸ Department of Physics, New York University, New York NY, United States of America
- ¹⁰⁹ Ohio State University, Columbus OH, United States of America
- ¹¹⁰ Faculty of Science, Okayama University, Okayama, Japan
- ¹¹¹ Homer L. Dodge Department of Physics and Astronomy, University of Oklahoma, Norman OK, United States of America
- ¹¹² Department of Physics, Oklahoma State University, Stillwater OK, United States of America

- ¹¹³ Palacký University, RCPTM, Olomouc, Czech Republic
- ¹¹⁴ Center for High Energy Physics, University of Oregon, Eugene OR, United States of America
- ¹¹⁵ LAL, Université Paris-Sud and CNRS/IN2P3, Orsay, France
- ¹¹⁶ Graduate School of Science, Osaka University, Osaka, Japan
- ¹¹⁷ Department of Physics, University of Oslo, Oslo, Norway
- ¹¹⁸ Department of Physics, Oxford University, Oxford, United Kingdom
- ¹¹⁹ ^(a) INFN Sezione di Pavia; ^(b) Dipartimento di Fisica, Università di Pavia, Pavia, Italy
- ¹²⁰ Department of Physics, University of Pennsylvania, Philadelphia PA, United States of America
- ¹²¹ Petersburg Nuclear Physics Institute, Gatchina, Russia
- ¹²² ^(a) INFN Sezione di Pisa; ^(b) Dipartimento di Fisica E. Fermi, Università di Pisa, Pisa, Italy
- ¹²³ Department of Physics and Astronomy, University of Pittsburgh, Pittsburgh PA, United States of America
- ¹²⁴ ^(a) Laboratório de Instrumentação e Física Experimental de Partículas - LIP, Lisboa, Portugal; ^(b) Departamento de Física Teórica y del Cosmos and CAFPE, Universidad de Granada, Granada, Spain
- ¹²⁵ Institute of Physics, Academy of Sciences of the Czech Republic, Praha, Czech Republic
- ¹²⁶ Faculty of Mathematics and Physics, Charles University in Prague, Praha, Czech Republic
- ¹²⁷ Czech Technical University in Prague, Praha, Czech Republic
- ¹²⁸ State Research Center Institute for High Energy Physics, Protvino, Russia
- ¹²⁹ Particle Physics Department, Rutherford Appleton Laboratory, Didcot, United Kingdom
- ¹³⁰ Physics Department, University of Regina, Regina SK, Canada
- ¹³¹ Ritsumeikan University, Kusatsu, Shiga, Japan
- ¹³² ^(a) INFN Sezione di Roma I; ^(b) Dipartimento di Fisica, Università La Sapienza, Roma, Italy
- ¹³³ ^(a) INFN Sezione di Roma Tor Vergata; ^(b) Dipartimento di Fisica, Università di Roma Tor Vergata, Roma, Italy
- ¹³⁴ ^(a) INFN Sezione di Roma Tre; ^(b) Dipartimento di Fisica, Università Roma Tre, Roma, Italy
- ¹³⁵ ^(a) Faculté des Sciences Ain Chock, Réseau Universitaire de Physique des Hautes Energies - Université Hassan II, Casablanca; ^(b) Centre National de l'Énergie des Sciences Techniques Nucleaires, Rabat; ^(c) Faculté des Sciences Semlalia, Université Cadi Ayyad, LPHEA-Marrakech; ^(d) Faculté des Sciences, Université Mohamed Premier and LPTPM, Oujda; ^(e) Faculté des sciences, Université Mohammed V-Agdal, Rabat, Morocco
- ¹³⁶ DSM/IRFU (Institut de Recherches sur les Lois Fondamentales de l'Univers), CEA Saclay (Commissariat à l'Énergie Atomique), Gif-sur-Yvette, France
- ¹³⁷ Santa Cruz Institute for Particle Physics, University of California Santa Cruz, Santa Cruz CA, United States of America

- ¹³⁸ Department of Physics, University of Washington, Seattle WA, United States of America
- ¹³⁹ Department of Physics and Astronomy, University of Sheffield, Sheffield, United Kingdom
- ¹⁴⁰ Department of Physics, Shinshu University, Nagano, Japan
- ¹⁴¹ Fachbereich Physik, Universität Siegen, Siegen, Germany
- ¹⁴² Department of Physics, Simon Fraser University, Burnaby BC, Canada
- ¹⁴³ SLAC National Accelerator Laboratory, Stanford CA, United States of America
- ¹⁴⁴ ^(a) Faculty of Mathematics, Physics & Informatics, Comenius University, Bratislava; ^(b) Department of Subnuclear Physics, Institute of Experimental Physics of the Slovak Academy of Sciences, Kosice, Slovak Republic
- ¹⁴⁵ ^(a) Department of Physics, University of Johannesburg, Johannesburg; ^(b) School of Physics, University of the Witwatersrand, Johannesburg, South Africa
- ¹⁴⁶ ^(a) Department of Physics, Stockholm University; ^(b) The Oskar Klein Centre, Stockholm, Sweden
- ¹⁴⁷ Physics Department, Royal Institute of Technology, Stockholm, Sweden
- ¹⁴⁸ Departments of Physics & Astronomy and Chemistry, Stony Brook University, Stony Brook NY, United States of America
- ¹⁴⁹ Department of Physics and Astronomy, University of Sussex, Brighton, United Kingdom
- ¹⁵⁰ School of Physics, University of Sydney, Sydney, Australia
- ¹⁵¹ Institute of Physics, Academia Sinica, Taipei, Taiwan
- ¹⁵² Department of Physics, Technion: Israel Institute of Technology, Haifa, Israel
- ¹⁵³ Raymond and Beverly Sackler School of Physics and Astronomy, Tel Aviv University, Tel Aviv, Israel
- ¹⁵⁴ Department of Physics, Aristotle University of Thessaloniki, Thessaloniki, Greece
- ¹⁵⁵ International Center for Elementary Particle Physics and Department of Physics, The University of Tokyo, Tokyo, Japan
- ¹⁵⁶ Graduate School of Science and Technology, Tokyo Metropolitan University, Tokyo, Japan
- ¹⁵⁷ Department of Physics, Tokyo Institute of Technology, Tokyo, Japan
- ¹⁵⁸ Department of Physics, University of Toronto, Toronto ON, Canada
- ¹⁵⁹ ^(a) TRIUMF, Vancouver BC; ^(b) Department of Physics and Astronomy, York University, Toronto ON, Canada
- ¹⁶⁰ Faculty of Pure and Applied Sciences, University of Tsukuba, Tsukuba, Japan
- ¹⁶¹ Department of Physics and Astronomy, Tufts University, Medford MA, United States of America
- ¹⁶² Centro de Investigaciones, Universidad Antonio Narino, Bogota, Colombia
- ¹⁶³ Department of Physics and Astronomy, University of California Irvine, Irvine CA, United States of America
- ¹⁶⁴ ^(a) INFN Gruppo Collegato di Udine; ^(b) ICTP, Trieste; ^(c) Dipartimento di Chimica, Fisica e Ambiente, Università di Udine, Udine, Italy
- ¹⁶⁵ Department of Physics, University of Illinois, Urbana IL, United States of America

- ¹⁶⁶ Department of Physics and Astronomy, University of Uppsala, Uppsala, Sweden
- ¹⁶⁷ Instituto de Física Corpuscular (IFIC) and Departamento de Física Atómica, Molecular y Nuclear and Departamento de Ingeniería Electrónica and Instituto de Microelectrónica de Barcelona (IMB-CNM), University of Valencia and CSIC, Valencia, Spain
- ¹⁶⁸ Department of Physics, University of British Columbia, Vancouver BC, Canada
- ¹⁶⁹ Department of Physics and Astronomy, University of Victoria, Victoria BC, Canada
- ¹⁷⁰ Department of Physics, University of Warwick, Coventry, United Kingdom
- ¹⁷¹ Waseda University, Tokyo, Japan
- ¹⁷² Department of Particle Physics, The Weizmann Institute of Science, Rehovot, Israel
- ¹⁷³ Department of Physics, University of Wisconsin, Madison WI, United States of America
- ¹⁷⁴ Fakultät für Physik und Astronomie, Julius-Maximilians-Universität, Würzburg, Germany
- ¹⁷⁵ Fachbereich C Physik, Bergische Universität Wuppertal, Wuppertal, Germany
- ¹⁷⁶ Department of Physics, Yale University, New Haven CT, United States of America
- ¹⁷⁷ Yerevan Physics Institute, Yerevan, Armenia
- ¹⁷⁸ Centre de Calcul de l'Institut National de Physique Nucléaire et de Physique des Particules (IN2P3), Villeurbanne, France
- ^a Also at Laboratório de Instrumentação e Física Experimental de Partículas - LIP, Lisboa, Portugal
- ^b Also at Faculdade de Ciências and CFNUL, Universidade de Lisboa, Lisboa, Portugal
- ^c Also at Particle Physics Department, Rutherford Appleton Laboratory, Didcot, United Kingdom
- ^d Also at TRIUMF, Vancouver BC, Canada
- ^e Also at Department of Physics, California State University, Fresno CA, United States of America
- ^f Also at Novosibirsk State University, Novosibirsk, Russia
- ^g Also at Fermilab, Batavia IL, United States of America
- ^h Also at Department of Physics, University of Coimbra, Coimbra, Portugal
- ⁱ Also at Department of Physics, UASLP, San Luis Potosi, Mexico
- ^j Also at Università di Napoli Parthenope, Napoli, Italy
- ^k Also at Institute of Particle Physics (IPP), Canada
- ^l Also at Department of Physics, Middle East Technical University, Ankara, Turkey
- ^m Also at Louisiana Tech University, Ruston LA, United States of America
- ⁿ Also at Dep Física and CEFITEC of Faculdade de Ciências e Tecnologia, Universidade Nova de Lisboa, Caparica, Portugal
- ^o Also at Department of Physics and Astronomy, University College London, London, United Kingdom
- ^p Also at Department of Physics, University of Cape Town, Cape Town, South Africa
- ^q Also at Institute of Physics, Azerbaijan Academy of Sciences, Baku, Azerbaijan
- ^r Also at Institut für Experimentalphysik, Universität Hamburg, Hamburg, Germany
- ^s Also at Manhattan College, New York NY, United States of America

- ^t Also at CPPM, Aix-Marseille Université and CNRS/IN2P3, Marseille, France
- ^u Also at School of Physics and Engineering, Sun Yat-sen University, Guanzhou, China
- ^v Also at Academia Sinica Grid Computing, Institute of Physics, Academia Sinica, Taipei, Taiwan
- ^w Also at School of Physics, Shandong University, Shandong, China
- ^x Also at Dipartimento di Fisica, Università La Sapienza, Roma, Italy
- ^y Also at DSM/IRFU (Institut de Recherches sur les Lois Fondamentales de l'Univers), CEA Saclay (Commissariat à l'Energie Atomique), Gif-sur-Yvette, France
- ^z Also at Section de Physique, Université de Genève, Geneva, Switzerland
- ^{aa} Also at Departamento de Fisica, Universidade de Minho, Braga, Portugal
- ^{ab} Also at Department of Physics and Astronomy, University of South Carolina, Columbia SC, United States of America
- ^{ac} Also at Institute for Particle and Nuclear Physics, Wigner Research Centre for Physics, Budapest, Hungary
- ^{ad} Also at California Institute of Technology, Pasadena CA, United States of America
- ^{ae} Also at Institute of Physics, Jagiellonian University, Krakow, Poland
- ^{af} Also at LAL, Université Paris-Sud and CNRS/IN2P3, Orsay, France
- ^{ag} Also at Nevis Laboratory, Columbia University, Irvington NY, United States of America
- ^{ah} Also at Department of Physics and Astronomy, University of Sheffield, Sheffield, United Kingdom
- ^{ai} Also at Department of Physics, Oxford University, Oxford, United Kingdom
- ^{aj} Also at Institute of Physics, Academia Sinica, Taipei, Taiwan
- ^{ak} Also at Department of Physics, The University of Michigan, Ann Arbor MI, United States of America
- ^{al} Also at Discipline of Physics, University of KwaZulu-Natal, Durban, South Africa
- * Deceased